(4)

David Taylor Research Center

Bethesda, Maryland 20084-5000

DTRC/SME-89/27 April 1989

Ship Materials Engineering Department

Research & Development Report

EFFECTS OF HIGH RATE SHEAR ON THE MICROSTRUCTURE AND DEFORMATION AND FRACTURE BEHAVIOR OF TWO HIGH STRENGTH STEELS

by

E. M. Hackett

DTRC/SME-89/27 Effects of High Rate Shear on the Microstructure and Deformation and Fracture Behavior of Two High Strength Steels

DISCLAIMER NOTICE

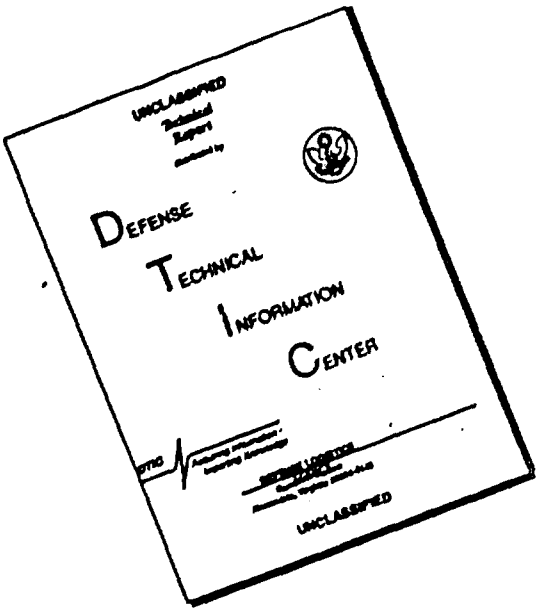

THIS DOCUMENT IS BEST QUALITY AVAILABLE. THE COPY FURNISHED TO DTIC CONTAINED A SIGNIFICANT NUMBER OF PAGES WHICH DO NOT REPRODUCE LEGIBLY.

MAJOR DTRC TECHNICAL COMPONENTS

CODE 011 DIRECTOR OF TECHNOLOGY, PLANS AND ASSESSMENT

12 SHIP SYSTEMS INTEGRATION DEPARTMENT

14 SHIP ELECTROMAGNETIC SIGNATURES DEPARTMENT

15 SHIP HYDROMECHANICS DEPARTMENT

16 AVIATION DEPARTMENT

17 SHIP STRUCTURES AND PROTECTION DEPARTMENT

18 COMPUTATION, MATHEMATICS & LOGISTICS DEPARTMENT

19 SHIP ACOUSTICS DEPARTMENT

27 PROPULSION AND AUXILIARY SYSTEMS DEPARTMENT

28 SHIP MATERIALS ENGINEERING DEPARTMENT

DTRC ISSUES THREE TYPES OF REPORTS:

1. **DTRC reports, a formal series,** contain information of permanent technical value. They carry a consecutive numerical identification regardless of their classification or the originating department.

2. **Departmental reports, a semiformal series,** contain information of a preliminary, temporary, or proprietary nature or of limited interest or significance. They carry a departmental alphanumerical identification.

3. **Technical memoranda, an informal series,** contain technical documentation of limited use and interest. They are primarily working papers intended for internal use. They carry an identifying number which indicates their type and the numerical code of the originating department. Any distribution outside DTRC must be approved by the head of the originating department on a case-by-case basis.

NDW-DTNSRDC 5602/51 (Rev 2-88)

Unclassified
SECURITY CLASSIFICATION OF THIS PAGE

REPORT DOCUMENTATION PAGE

1a. REPORT SECURITY CLASSIFICATION UNCLASSIFIED	1b. RESTRICTIVE MARKINGS
2a. SECURITY CLASSIFICATION AUTHORITY	3. DISTRIBUTION/AVAILABILITY OF REPORT APPROVED FOR PUBLIC RELEASE; DISTRIBUTION UNLIMITED
2b. DECLASSIFICATION/DOWNGRADING SCHEDULE	
4. PERFORMING ORGANIZATION REPORT NUMBER(S) DTRC/SME-89/27	5. MONITORING ORGANIZATION REPORT NUMBER(S)
6a. NAME OF PERFORMING ORGANIZATION David Taylor Research Center 6b. OFFICE SYMBOL (If applicable) Code 2814	7a. NAME OF MONITORING ORGANIZATION
6c. ADDRESS (City, State, and ZIP Code) Bethesda, MD 20084-5000	7b. ADDRESS (City, State, and ZIP Code)
8a. NAME OF FUNDING/SPONSORING ORGANIZATION ONT Materials Block 8b. OFFICE SYMBOL (If applicable) Code 011.5	9. PROCUREMENT INSTRUMENT IDENTIFICATION NUMBER
8c. ADDRESS (City, State, and ZIP Code) Bethesda, MD 20084-5000	10. SOURCE OF FUNDING NUMBERS PROGRAM ELEMENT NO. 62234N PROJECT NO. RS3490 TASK NO. WORK UNIT ACCESSION NO. DN 507603

11. TITLE (Include Security Classification)
Effects of High Rate Shear on The Microstructure and Deformation and Fracture Behavior of Two High Strength Steels

12. PERSONAL AUTHOR(S)
E.M. Hackett

13a. TYPE OF REPORT	13b. TIME COVERED	14. DATE OF REPORT (Year, Month, Day)	15. PAGE COUNT
RDT&E	FROM _____ TO _____	April, 1989	169

16. SUPPLEMENTARY NOTATION

17. COSATI CODES			18. SUBJECT TERMS (Continue on reverse if necessary and identify by block number)
FIELD	GROUP	SUB-GROUP	High Strength Steels, Dynamic Loading, Fracture, Shear, Micromechanisms of Fracture, Shear Banding

19. ABSTRACT (Continue on reverse if necessary and identify by block number)

The shear localization behavior of two high strength steels was evaluated at loading rates ranging from quasi-static to impact. The steels evaluated were similar in yield strength, but had different levels of toughness. The steel with superior toughness was direct quenched (DQ). The second steel was quenched and tempered (Q&T). Fatigue precracked Dual Notched Shear (DNS) specimens, loaded in mode II (in-plane shear), were employed. The objectives were to measure energy density variations with loading rate, estimate the temperatures achieved in the shear zones of the specimens and examine micromechanisms of localized shear deformation as related to the microstructures of the steels. Temperatures in the shear zones were estimated from energy absorption characteristics and compared with temperatures measured adjacent to the fatigue crack tips, to assess compliance with "adiabatic" conditions.

(CONTINUED ON REVERSE)

20. DISTRIBUTION/AVAILABILITY OF ABSTRACT	21. ABSTRACT SECURITY CLASSIFICATION	
☐ UNCLASSIFIED/UNLIMITED ☒ SAME AS RPT ☐ DTIC USERS	UNCLASSIFIED	
22a. NAME OF RESPONSIBLE INDIVIDUAL E.M. Hackett	22b. TELEPHONE (Include Area Code) 301-267-3755	22c. OFFICE SYMBOL Code 2814

DD FORM 1473, 84 MAR 83 APR edition may be used until exhausted
All other editions are obsolete

SECURITY CLASSIFICATION OF THIS PAGE

19. (CONTINUED FROM FRONT)

A loading apparatus was constructed which enabled shear loading of the DNS specimens and measurements of load, displacement and temperature. The shear localization behavior of the steels was quantified in terms of energy absorption characteristics, temperature increases in the shear zones, and widths of the shear zones. Post-test metallographic examinations were performed to determine the widths of the shear zones, examine the micromechanisms of localized shear deformation and evaluate for the presence of metallurgical transformations.

Energy density increased with increasing loading rate for both steels. The highest values for energy density were those for the impact rate tests of the DQ steel. Shear zone temperatures estimated from thermocouple measurements for the impact rate tests were in the range of 120°C (248°F). Evaluation of the impact rate test data using a dimensionless rate-thermal diffusivity parameter, indicated that adiabatic conditions were not achieved in the shear zones of specimens from either steel. Post-test metallurgical examinations of the shear zones of the DNS specimens showed both steels to exhibit deformed shear bands over the entire range of loading rates. Metallographic results from the impact rate tests of both steels suggested that a microvoid nucleation and growth mechanism controlled the shear localization process.

CONTENTS

LIST OF TABLES

LIST OF FIGURES

ABSTRACT

The shear localization behavior of two high strength steels was evaluated at loading rates ranging from quasi-static to impact. The steels evaluated were similar in yield strength, but had different levels of toughness. The steel with superior toughness was direct quenched (DQ). The second steel was quenched and tempered (Q&T). Fatigue precracked Dual Notched Shear (DNS) specimens, loaded in mode II (in-plane shear), were employed. The objectives were to measure energy density variations with loading rate, estimate the temperatures achieved in the shear zones of the specimens and examine micromechanisms of localized shear deformation as related to the microstructures of the steels. Temperatures in the shear zones were estimated from energy absorption characteristics and compared with temperatures measured adjacent to the fatigue crack tips, to assess compliance with "adiabatic" conditions.

A loading apparatus was constructed which enabled shear loading of the DNS specimens and measurements of load, displacement and temperature. The shear localization behavior of the steels was quantified in terms of energy absorption characteristics, temperature increases in the shear zones, and widths of the shear zones. Post-test metallographic examinations were performed to determine the widths of the shear zones, examine the micromechanisms of localized shear deformation and evaluate for the presence of metallurgical transformations.

Energy density increased with increasing loading rate for both steels. The highest values for energy density were those for the impact rate tests of the DQ steel. Shear zone temperatures estimated from thermocouple measurements for the impact rate tests were in the range of 120°C (248°F). Evaluation of the impact rate test data using a dimensionless rate-thermal diffusivity parameter, indicated that adiabatic conditions were not achieved in the shear zones of specimens from either steel. Post-test metallurgical examinations of the shear zones of the DNS specimens showed both steels to exhibit deformed shear bands over the entire range of loading rates. Metallographic results from the impact rate tests of both steels suggested that a microvoid nucleation and growth mechanism controlled the shear localization process.

ACKNOWLEDGEMENTS

I would like to thank Mike Vassilaros, Mark Kirk, Joe Waskey and Rick Link of the David Taylor Research Center (DTRC) for helpful discussions and suggestions regarding the experimental portions of this work. I am particularly indebted to Rick Link for additional advice and guidance on analytical aspects of the temperature estimations. The technical advice and assistance of Jill Nasso, Florence Connell and Fred Dersch of DTRC is also appreciated.

Discussions with Lee Magness of the Ballistics Research Laboratory, and Professor Ronald Armstrong of the University of Maryland on plastic wave theory were beneficial in developing the background section. Dr. Jacques Giovanola of the Stanford Research Institute provided helpful suggestions regarding estimation of shear zone temperatures. Professor Jacques Duffy of Brown University provided useful comments on design of the experiments.

I am grateful to Mike Frankowick of The Johns Hopkins University for his assistance in machining specimens and experimental fixtures, and to Professor Robert E. Green, Jr. for technical guidance.

Dr. John Gudas of DTRC was instrumental in helping to guide this effort and in providing motivation when it was needed. I am particularly thankful for his help in rigorously critiquing preliminary drafts of this work.

I would like to express my thanks to Professor Robert B. Pond, Sr., for his guidance and personal encouragement.

ADMINISTRATIVE INFORMATION

This report was prepared as part of the Ship and Submarine Materials Block (ND2B), under the sponsorship of Mr. Ivan Caplan, DTRC, Code 011.5. This effort was performed at this center under Program Element 62234N and was supervised by Dr. J.P. Gudas.

INTRODUCTION

Localization of plastic flow in metallic materials is a commonly observed phenomenon. Sometimes, the localization is intentional as in the case of extrusions, where the geometry of the die, physical and mechanical properties of the material, and the velocity of the piece being worked determine the degree of flow localization [Doyle, et al., 1969]. In other cases, flow localization is not intentional but is rather a naturally occurring result of a specific combination of material properties, strain rate, temperature and stress state. One example is the formation of Luder's bands in tension test specimens. Luder's bands are regions of inhomogeneous shear deformation in metals [Reed-Hill, 1973].

For steels which exhibit a sharp yield point, Luder's bands are formed in the region of the stress-strain diagram immediately following the lower yield point. These bands typically form at stress concentrations, such as the fillets, [Liss, 1957] and propagate at an almost constant stress through the gage length of the specimen. This type of shear deformation has been observed at strain rates ranging from 10^{-3}/sec to 10/sec [Winlock and Leiter, 1937] and is a function of geometry, temperature and the micromechanisms of the deformation process. Luder's bands are macroscopically observable and represent the contributions of microscopic slip in many grains. Temperature elevations due to localization of

plastic flow in Luder's bands at quasi-static loading rates have been shown to be small (18°C (64°F)), [Moss and Pond, 1975].

Unlike the case for Luder's bands, shear deformation under high rate loading is often more localized and associated with significant temperature increases due to deformation heating [Rogers, 1982]. When the applied strain rate is sufficiently high to cause the deformation to be constrained to a narrow band, near-adiabatic conditions can result in the band. For steels, these Adiabatic Shear Bands (ASB) typically occur under impact or ballistic loading [Hutchings, 1982].

While use of the term adiabatic is not rigorously correct in this instance, for purposes of the work described herein, adiabatic shearing will be defined as shear deformation confined to a narrow band that is associated with significant localized temperature increases resulting from high rate loading. For the case of high strength steels it has been postulated that the localized temperature increases can exceed the austenite transformation temperature for short durations, thereby producing metastable austenite which is then transformed to a martensitic phase by a rapid quench from the surrounding material. This theory was first proposed by Zener and Holloman [1944] who discovered "white-etching" bands in a high strength steel that had been subjected to impact loading. The material in the bands was found to have a very high

hardness leading to the conclusion that a transformation to martensite had occurred. White-etching bands in steels subjected to impact or explosive loading have subsequently been seen by many other investigators [E.G.: Glenn and Leslie, 1971; Manganello and Abbot, 1972] and are often referred to as "transformed" shear bands. It is generally accepted that the transformed phase in adiabatic shear bands in high strength steels has a structure and hardness similar to martensite but there is not a consensus on the exact nature of the sub-structure of the bands [Manion and Stock, 1970, Thornton and Heiser, 1971; Glenn and Leslie, 1971].

Shear localization under high rate loading, where transformations do not occur, results in the formation of "deformed" shear bands. While the temperatures achieved in the case of deformed shear bands may not equal those attained in transformed bands, the localized heating can still significantly affect the deformation and fracture behavior of the material [Rogers, 1982].

The scale of adiabatic shear banding in high strength steels varies, but is generally considered to be a localization of plastic flow crossing many grains. This is in contrast to slip bands or deformation bands which are microscopic regions of localized flow contained within single grains. Adiabatic shear bands have been shown to range from 1 micron to more than 100 microns in width [Wright, 1987] with lengths sometimes crossing

the entire section being considered.

Flow localization under predominantly adiabatic conditions has been shown to occur under conditions ranging from ballistic impact to orthogonal machining of metals. The brittle phase resulting from transformations due to adiabatic heating at shear bands in high strength steels can control the fragmentation behavior of armor [Staker, 1980] and is thus of great interest in ordnance problems. Similarly, machinability during high speed orthogonal cutting of high strength steels has been shown to depend, in certain cases, on the formation of adiabatic shear bands [Dao and Shockey, 1979; Semiatin, 1980].

Stress state has also been identified as a key variable in attainment of adiabatic shear bands. The stress state influences are coupled with those due to geometric factors. The tendency for shear band formation is greater in either torsion or compression since these states suppress fracture to greater overall strains [Rogers, 1982]. In testing notched specimens in dynamic shear, Kalthoff and Winkler [1986] and Winkler [1987] have shown a greater tendency for shear band formation with increasing notch acuity. They produced a deformation map for adiabatic shear band damage that showed the tendency for shear band formation to be greatest in specimens containing a fatigue precrack.

Recht, [1964], Semiatin, [1980] and Curran et al, [1985], have developed models to attempt to predict the occurrence of shear bands based on physical and mechanical properties. It is generally agreed that the controlling influences are strain hardening capacity, strain rate sensitivity, and the temperature dependence of the flow stress. The formation of an adiabatic shear band is thought to occur at the instability when thermal softening overcomes the capacity for strain hardening. This serves to explain the frequently observed case of higher strength (higher hardness) materials exhibiting a greater tendency to form adiabatic shear bands [Staker, 1980]. Giovanola [1988] concluded that adiabatic shear localization in a 4340 steel occurred in two sequential stages; the first localization was consistent with the above thermomechanical instability model while the second localization involved microvoid nucleation and growth. Giovanola [1988] concluded that microvoid nucleation and growth was the mechanism leading to shear band fracture and that transformations occurring in the shear bands may be a consequence rather than the cause of the final shear band fracture. That is, frictional heating due to internal surfaces of the band rubbing against one another, was the cause of the observed temperature increase.

Phase transformations associated with adiabatic shear banding have been the subject of much research. A possible alternative to the mechanism suggested by Zener and Holloman [1944], is the

formation of the new phase by a simple shear or other atomic re-arrangement, similar to that occurring for deformation twinning, not requiring the attainment of the austenite transformation temperature [Bridgman, 1935]. In order to establish what actually occurs, it is necessary to observe the band formation and record its' temperature simultaneously. As these simultaneous measurements are extremely difficult, they have been attempted by only a few investigators. Moss [1980] has shown evidence which refutes the attainment of the austenite transformation temperature in adiabatic shear bands produced by explosive loading in a high strength steel. He suggested that a lower temperature magnetic state change might have been responsible for the phase change. More recently, Marchand and Duffy [1988] have concluded that the austenite transformation temperature could be achieved. They measured temperatures approaching this level in shear bands formed in a thin-walled tubular specimen loaded dynamically in torsion. Giovanola [1988] has also reported temperatures in shear bands which exceeded the austenite transformation temperature. Giovanola [1988] was also able to show good correlations between shear band temperatures estimated from thermocouple measurements, and calculated shear band temperatures from energy absorption considerations.

The previously cited investigations of Kalthoff and Winkler [1986], Winkler [1987], and Giovanola [1988] used very high

strength (greater than 1241 MPa (180 ksi) yield strength) steels which were loaded at extremely high rates (strain rates in the range 10^4 - 10^6/sec). Marchand and Duffy [1988] used a 690 MPa (100 ksi) yield strength steel but also used a very high loading rate. Temperatures were measured or inferred in the case of the thin-walled torsional testing experiments [Marchand and Duffy, 1988; Giovanola, 1988], but not in the case of the specimens containing fatigue precracks [Kalthoff and Winkler, 1986; Winkler, 1987]. The experiments conducted by Kalthoff and Winkler [1986] and Winkler [1987] did not incorporate measurements of the load-displacement behavior of their material and hence local energy absorption characteristics could not be determined.

The experiments performed for this investigation were designed to expand on some of the features of the above work, in evaluating the shear localization behavior of two medium-to-high strength steels at loading rates likely to be encountered in structural applications (strain rates of 10^2/sec to 10^3/sec). Fatigue precracked Dual Notched Shear (DNS) specimens were employed. The objectives of this work were to measure energy density variations with loading rate, estimate temperatures achieved in the shear zones of the specimens and examine the micromechanisms of localized shear deformation as related to the microstructures of the steels. Shear zone temperatures calculated from measurements of absorbed energy were compared with temperatures measured by thermocouples near

the fatigue crack tips. As mentioned previously, Giovanola [1988], was able to show good correlations between measured and calculated shear band temperatures but did not establish strain rate bounds for these correlations. For the lower strain rates used in this investigation, the energy concentrated near a crack tip and the resulting temperature rise, are not known. Both are significant as regards the fracture behavior of steels and will be quantified in this investigation. Two steel alloys were chosen to evaluate the effects of toughness and microstructural differences on the respective shear localization behaviors.

The approach to achieving the objective was to develop a technique for characterization of high rate shear deformation and fracture behavior, and employ this technique to quantify the high rate shear behavior of two steels with similar yield strength levels but different microstructures and levels of toughness. The steel with the higher level of toughness was direct quenched (DQ), while the second steel was conventionally quenched and tempered (Q&T). The deformation and fracture behavior of these steels under in-plane shear (mode II) loading was examined in the presence of fatigue cracks. The loading rates were varied from quasi-static through impact conditions. The shear localization behavior of the steels was quantified in terms of energy absorption characteristics, temperature rise in the shear zone and width of the shear zone.

Measurements were made of load and displacement to enable estimation of the energy input to the specimens. Temperature increases near the tips of the fatigue cracks were monitored during testing to determine both the magnitude of the temperature rise and the position, in time, of the maximum temperature elevation relative to the ongoing deformation. The measured temperatures were used in conjunction with assumptions based on transient heat flow, to estimate the temperatures in the shear zone. Estimated temperatures were compared with temperatures calculated from energy absorption characteristics. Post test metallographic examinations were performed to determine the widths of the shear zones, evaluate micromechanisms of the shear localization process and to evaluate for the presence of metallurgical transformations.

BACKGROUND

Adiabatic shearing is most often associated with elevated loading rates. It is therefore appropriate to begin this review by examining work performed in the area of high strain rate deformation. The second part of the background will examine development of plastic wave theory and the relation to localization of plastic flow in metallic materials. The final section will review the mechanical and material aspects of adiabatic shear banding (ASB). Work concerning the temperature rise associated with adiabatic shearing from both an experimental and analytical viewpoint will be examined.

High Rate Deformation

The following is a chronology of work dealing with the effects of high rate loading on the mechanical behavior of metals and theories and experiments concerned with plastic deformation in general.

The practical goal of eliminating localized inhomogeneous deformation in the form of Luder's bands ("stretcher strains") from steels used in deep drawing processes formed the basis for an investigation by Winlock and Leiter [1937]. They tested tensile specimens of low carbon sheet steel with the goal of examining the effects of testing speed, grain size and prior cold work on the yield point and yield point elongation. Their

data showed that the yield point elongation increased with increasing test speed or decreasing grain size. The yield point was also shown to increase with increasing test speed. Small amounts of prior cold work were shown to eliminate both the yield point and the occurrence of Luder's bands. Winlock and Leiter concluded that the occurrence of Luder's bands was directly related to a delay in the initiation of plastic slip noted for iron and iron-carbon alloys. The nature of this delay was examined in detail later by Kramer and Maddin [1952].

Clark and Datwyler [1938] expanded on the work of Winlock and Leiter by developing a method for determining force-elongation diagrams from steels loaded dynamically in tension. The dynamic force-elongation diagrams for several steels were determined and compared with those for the static cases. In all of these cases it was found that the yield and maximum forces were higher with dynamic than with static loading. They also concluded that there was an indication that the the elongation and in some cases, reduction in area, of cold worked materials in dynamic tension were superior to those in static tension. This last point was questioned in a subsequent discussion of the paper by Mann [1936] who argued that the ductility measured in the static and dynamic tests should have been identical.

In reviewing data on yield strength and loading rate effects in tension tests, MacGregor [1940] noted that discontinuous

yielding, associated with the formation of Luder's bands in steels, also occurred for certain aluminum alloys, brasses, and zinc and cadmium crystals. Later, it was proposed [Cottrell and Bilby, 1949] that the yield point and further discontinuous yielding in steels were due to dislocations breaking away from solute atmospheres. MacGregor presented a summary of data on effects of testing speed on yield and tensile strengths of steels and showed that large changes in strain rate (several orders of magnitude) were necessary to cause significant changes in the mechanical properties.

A method for determining the true stress-true strain behavior for impact loaded tension specimens was described by DeForest, MacGregor and Anderson [1942]. Briefly, this method consisted of scribing fine circumferential scratches on a tapered tensile specimen at different axial locations, measuring the diameters of the bar at these locations before and after the test, and recording only the ultimate and fracture loads during the test. Their results, for three steels and an annealed brass, are consistent with the trends previously observed by Clark and Datwyler [1938] and Winlock and Leiter [1937]. That is, the effect of increasing the testing speed was in most cases to increase the fracture strains and stresses at the maximum loads, although in this case true stress-strain behavior was determined.

It has been shown that approximately 85% - 95% of the energy expended in plastic deformation of metals is evolved as heat [Taylor and Quinney, 1933]. In static tension testing the heat generated from the mechanical work is conducted away rapidly enough to prevent specimen heating. In high speed tests however, sufficient time does not exist for this conduction and the heat is retained locally for a short duration. Nadai and Manjoine [1941] were the first to attempt to measure this local temperature rise during high speed tensile tests. A series of tests on pure iron were performed using chromel-alumel thermocouples to measure the temperature at specific locations on the gage sections of the specimens. The time to fracture for these specimens was less than 2 milliseconds. The temperature rise at the minimum section just prior to fracture was determined to be approximately 50°C (122°F). The average temperature rise computed from the energy absorbed to fracture was 25°C (77°F).

Macgregor and Fisher [1944] demonstrated an equivalence between notched bar impact tests and static tension tests on the basis of energy absorbed per unit of deformed volume. To obtain the energy per unit deformed volume for Charpy V-notch (CVN) specimens, a fine grid was inscribed on the specimens prior to testing. Material having a strain of greater than 1% was defined as the deformed volume. The energy absorbed per unit deformed volume in the tension tests was determined from the true stress-true strain behavior. Good correlations

between the two types of tests were found to be present on this basis when notched tensile specimens were used. Differences in results between CVN specimens and conventional tension test specimens were attributed primarily to the notch effect rather than to the difference in testing speed.

The internal inertia of specimens subjected to high rate loading was discussed by Holloman and Zener [1944]. They concluded that the lack of uniformity of the stress over the gage length in high rate tests can be so great that the measurement of the stress at either end of the specimen is of little significance. In examining the published data on high rate testing, they concluded that at a velocity of 30 m/sec (100 ft/sec), the error introduced by the inertial effects would be a large percentage of the measured stress. For a tensile specimen with a 25 mm (1 inch) gage section, this velocity translates to a strain rate of approximately 1200/sec.

From the standpoint of flow localization in tension, Holloman and Zener [1944] suggested that a critical strain rate exists above which a steel tensile specimen will fail by shear along the first Luder's band formed and homogeneous deformation will not occur. For pure shear it was suggested that a critical velocity would not exist due to the flattening of the force-elongation curve for shear deformation. It was pointed out however, that "when the yield point elongation in the material is so large that the temperature rise of the material

in the band is several hundred degrees centigrade, the "static" stress-strain curve will be lowered. In this case the deformation to fracture may likewise be confined to a narrow band." This last issue, which is a description of adiabatic shearing, was investigated experimentally in a separate paper by Zener and Holloman [1944] which will be discussed in a subsequent section.

The effects of testing machine rigidity and loading rate on the initiation and propagation of the plastic zone in tension tests of a mild steel was investigated by Miklowitz [1947]. It was shown that the yield point elongation increased with increasing test speed as noted previously by Clark and Datwyler [1938] and MacGregor and Anderson [1941]. Stresscoat patterns on the tension specimens revealed more uniformity and greater line spacing for the slow (.0635 mm/min (.0025 in./min.)) tests as opposed to the rapid (381 mm/min (15 in/min)) tests. In the rapid tests it was found that many more disturbances can form in the gage section because the load was high and therefore only small concentrations at random locations were required to initiate yielding. The slope of the load drop from the upper yield point was found to be steeper as machine rigidity was increased. Also, the upper yield stress was found to increase and the yield point elongation to decrease with greater machine rigidity.

Kolsky [1949] developed a method for minimizing or eliminating inertial effects in high rate testing by several modifications to the original Hopkinson bar approach. As noted previously by Holloman and Zener [1944] and Taylor [1946], the inertia of both the apparatus used for loading and the specimens themselves contribute significantly to the forces involved in high rate loading. Often, it is impossible to separate forces due to inertia and those due to the mechanical properties of the material being investigated. Kolsky overcame these obstacles by using very thin specimens and a simple pressure bar system for which the inertia effects could be calculated in terms of the propagation of elastic stress waves. Using this system, he examined the dynamic stress-strain behavior of copper and lead. In the case of lead he concluded that the mechanical behavior was similar to that of a viscous fluid. This was similar to the previous observations of Bridgman [1935] for certain metals under combined shearing and hydrostatic pressure and those of Taylor [1946] for lead projectiles impacting hardened steel plates.

Clark and Wood [1949] identified a delay time for plastic deformation in rapid-load tests of an annealed mild steel. In the context of their work, rapid loading implied a uniform stress distribution along the gage section of a specimen. This condition is not achieved for impact loading. The loading device used for the tests was able to apply tensile loads of 5 milliseconds or greater in duration and maintain the load

achieved at the end of the test for a given time. Specimens were loaded rapidly to a point beyond the static elastic limit and the delay time for the start of plastic deformation was noted. This delay time varied from 5 milliseconds at 352 MPa (51 ksi) to 6 seconds at 255 MPa (37 ksi). Similar tests on a stainless steel, two quenched and tempered steels and two aluminum alloys showed no delay time for plastic deformation. It was concluded that the time delay for the initiation of plastic deformation is associated only with materials exhibiting a definite yield point in the static stress-strain diagram.

The influence of temperature on the delay time for plastic deformation in a mild steel was investigated by Wood and Clark [1951]. The mild steel exhibited two regions of behavior in the relationship between applied stress and the delay time for plastic deformation at a given temperature. At higher stresses the delay time was shown to increase exponentially with increasing stress. At a lower critical stress, corresponding to the static upper yield point, a second region of behavior was observed where the delay time for plastic deformation was indeterminate. It was also found that the temperature dependence of the delay time at stresses above the lower critical value could not be represented by a thermal activation function of the Arrhenius form. In general, however, the delay time was found to increase with decreasing temperature.

Expanding on the work of Clark and Wood [1951], Kramer and Maddin [1952] identified a delay time for slip in tests on single crystal specimens of body centered cubic (BCC) beta brass. A delay time for slip was not observed however for face centered cubic (FCC) alpha brass or aluminum. The fact that a delay time for slip was found in a BCC metal and not in the FCC metals led the authors to propose this delay time as a basis for an explanation of the well-known transition temperature behavior of BCC metals. They proposed that the existence of a delay time for slip will permit a specimen to be loaded at a rate sufficiently rapid such that the delay time is not exceeded. In such a case, plastic deformation cannot occur and the fracture must occur by cleavage. It was also pointed out that the use of strain rate as a characterizing parameter for describing plastic flow behavior can be misleading since even at a constant strain rate the stress rate will vary continuously.

Vreeland, Wood and Clark [1953] examined the effects of time and temperature on yielding in rapid tension tests of an annealed steel. It was found that aging of the specimens for a sufficient time at a given temperature between above-yield stress pulses produced recovery in the material such that yielding did not occur in repeated cycles of stressing and aging. The proposed mechanism for this effect is that due to Cottrell and Bilby [1949] where carbon and nitrogen are assumed

to tie up dislocations in atmospheres. To support this view the authors found that the activation energy for the recovery process roughly corresponded to the activation energies for carbon and nitrogen diffusion in steel.

In the Campbell Memorial lecture to the 35th annual convention of the American Society for Metals (ASM), Clark [1953] provided an excellent review of many aspects of the mechanical behavior of metals under high rate loading. In particular, he showed how the delay time for yielding in BCC metals was consistent with a dislocation model based on the work of Frank and Read [1950] and that of Cottrell [1948 and 1950]. This model had three components including, solute atmospheres (carbon and nitrogen) pinning dislocations on a slip plane, the interaction of dislocations and grain boundaries, and dislocation generation by the Frank-Read mechanism. In a steel, dislocations anchored by solute atmospheres will not begin to move when a stress is applied, but must wait for thermal fluctuations of sufficient magnitude to break away from the atmospheres. The time required for the release of the dislocations decreases with increasing stress and temperature in a manner similar to that observed for the delay time for slip as proposed by Kramer and Maddin [1952].

Campbell and Duby [1956] in an examination of the yield behavior of mild steel in compression, showed less hardening caused by dynamic strain as opposed to static strain. They

concluded that the mechanism of plastic flow at high strain rates differs from that at ordinary strain rates. No coarse slip bands were formed in the dynamic case although there was evidence of grain boundary movement and fine slip. They attributed this behavior to the increased number of dislocation sources activated at the high strain rates and the possibility that there would be insufficient time for complete slip bands to form.

Cooper and Campbell [1967] avoided the wave mechanics problems associated with very high loading rates by restricting their experimental work to "medium" rates of strain (10/sec to 10^2/sec). At such rates it was assumed that forces due to inertia of the testing machine and the specimen were negligible. This is in good agreement with the previous work of Holloman and Zener [1944], who concluded that significant errors would be introduced by inertia considerations in tensile testing at a strain rate of 1200/sec. Cooper and Campbell did, however, emphasize the importance of the loading machine compliance and specimen design in maintaining a constant strain rate throughout a test. A hydraulic loading machine was described which was capable of testing at nearly constant strain rates up to 10^2/sec.

Lindholm and Yeakley [1968] presented details of a split Hopkinson pressure bar method for obtaining complete stress strain curves, in either tension or compression, at strain

rates on the order of 1000/sec, This essentially followed the earlier work of Kolsky [1949], who first proposed use of the split Hopkinson bar technique for compression loading. The Hopkinson bar technique assumes that, at very high loading rates, stress can only be measured by an elastic element in series with the test specimen. Stress waves are generated at the dynamic strain rates achieved in Hopkinson bar tests. The elastic element therefore, usually takes the form of a long bar so that the loading duration of the specimen is less than the wave transit time in the bar. This avoids the occurrence of complicating reflected waves in the recorded signals.

Lindholm and Yeakley proposed a unique tensile specimen and tensile loading arrangement for the Hopkinson bar which eliminated complicating features (threaded connections, complex bar configurations) that tended to add uncertainties to the wave mechanics of the problem. For measurement of diametral changes in compression specimens, a novel non-contacting, coaxial capacitance gage was designed and used successfully at high strain rates.

Dowling, Harding and Campbell [1970] evaluated the dynamic punching behavior of annealed aluminum, copper, annealed and hard drawn brass and mild and high-tensile steels. Punch load-displacement curves were developed for these materials at punching speeds between 1.3×10^{-6} m/sec and 23 m/sec (5×10^{-5} in/sec and 900 in/sec). Effects of loading rate on the energy

required for punching were determined from the load-displacement curves. An increase in the energy absorbed with increased speed of punching was found for the aluminum and copper while the reverse was true for the high-tensile steel and hard drawn brass. There was no significant effect of punching speed on the absorbed energy for annealed brass and mild steel. Estimates of the shear zone widths were made for all of the materials using metallography and microhardness measurements. An examination of the punched specimens revealed that the widths of the sheared zones greatly exceeded the radial clearance of the dies, especially for the more ductile materials. In general, no marked effect of loading rate on the widths of the sheared zones was observed for the materials in this investigation. An earlier investigation by Dowling and Harding [1967] on mild steel had shown a decrease in the sheared zone widths at the highest punching speeds.

The temperature and strain rate dependence of the shear strength of mild steel was investigated by Campbell and Ferguson [1970]. A unique double shear specimen with an active gage length of 0.84 mm (0.031 inches) was employed to increase the maximum strain rates attainable. Consistent with the above results of Dowling, Harding and Campbell [1970], the width of the sheared zone in the double shear specimens was greater than the effective gage section defined by the slot width. The rate sensitivity of the flow stress was found to be a decreasing

function of temperature, except at the highest strain rates where a large increase in rate sensitivity was observed.

The vast majority of studies on high rate deformation of metallic materials in the 1970's and 1980's have used variations of the Hopkinson bar approaches described previously by Kolsky [1949] and Lindholm and Johnson [1968]. Frantz and Duffy [1972] used a torsional Kolsky bar to examine the effects of sharp increases in strain rate on the dynamic stress-strain behavior of 1100 aluminum. Eleiche and Campbell [1975] used a similar apparatus to study the effects of high rate loading and unloading on the deformation behavior of a magnesium alloy. Senseny, et al [1986] used a torsional Kolsky bar to evaluate the influence of strain rate and strain rate history on the flow stress of several metals including OFHC copper, and commercially pure zinc. Several authors (Costin, et al, [1979]; Hartley, et al [1987]; Giovanola, [1988] and Marchand and Duffy, [1988]) have used modified torsional Kolsky bars to examine the shear localization behaviors of various materials. These papers will be described in more detail in a later section.

As described above, Hopkinson bar approaches were designed to overcome wave interaction complications in the analysis of high rate mechanical tests, by using an elastic element in series with the test specimen to estimate loads and strains. Wave interactions within a specimen are however, modified

during the deformation process as the specimen is plastically strained. The analysis of "plastic wave" propagation in a specimen tested at high strain rates is essential to account for certain aspects of the mechanical behavior, and is the subject of the subsequent section.

Plastic Wave Theory

Limitations in high rate testing such as those discussed previously by Holloman and Zener [1944] provided the impetus both for the development of the Hopkinson bar approaches, and for development of plastic wave theory. Plastic wave theory regards the propagation of plastic waves in high rate testing in a manner analogous to the propagation of elastic waves. That is, the local modulus ($d\sigma/d\epsilon$) of the stress strain curve is used in place of the elastic modulus to calculate the wave speeds. A key feature of plastic wave theory is the prediction of a "critical velocity" where the stress strain relation becomes horizontal. The "critical velocity" is the velocity at which instantaneous failure is predicted at the impact location before the remainder of the test piece has had a chance to respond. The following recounts the development of plastic wave theory and its relation to shear localization behavior.

In discussing impact at very high speeds, Taylor [1946] was essentially in agreement with the previous conclusions of Holloman and Zener [1944]. He stated that "When attempts are

made to increase the rate of strain by increasing the relative velocity of the two ends of a specimen beyond a certain limit, the inertia forces within its' own length produce variations in stress which are of the same order as those applied at the end." To obtain an estimate of this critical velocity he suggested the formula:

$$V = (\sigma_y/\rho)^{1/2} \qquad (1)$$

Where σ_y denotes the materials' yield strength and ρ denotes its' density. Taylor noted that any attempt to force a material to a higher velocity would be likely to make the metal flow like a liquid. He cited as an example his experience with a lead bullet fired at 305 m/sec (1000 ft/sec) which produced a thin spray of lead on striking a steel target, just as a jet of water would have. Taylor also cited the work of Mann [1936] with a high velocity tension impact machine in the support of a critical velocity. Mann found that at a certain critical speed, the energy, as determined by his method, decreased while the elongation remained constant or even increased.

The concept of a critical impact velocity was also suggested independently, by von Karman and Duwez [1950]. The actual work on this concept was performed by the authors in 1941 and 1942, but was classified due to its relation to national defense issues. This work was later presented by von Karman in 1946 but was not published until 1950. The principle contribution

of this work was to demonstrate the existence of a critical impact velocity beyond which a material would break near the impacted end with negligible plastic strain. The investigation presented a theoretical derivation for the critical impact velocity based on the propagation of a stress wave in a cylindrical bar where the impact velocity was large enough to produce plastic strain. The critical velocity was determined from:

$$V = \int_{o}^{\epsilon(uts)} [(d\sigma/d\epsilon)/\rho)]^{1/2}\, d\epsilon \qquad (2)$$

Where $d\sigma/d\epsilon$ is the slope of the stress-strain curve at a given strain, ρ is the density and ϵ(uts) is the strain at the ultimate tensile stress. Von Karman reasoned that the slope of the stress strain curve ($d\sigma/d\epsilon$) approaches zero for large values of strain. It is obvious then, that the plastic wave speed goes to zero at this strain, which indicates that the integral relation for impact velocity (equation 2) will produce a singular (critical) velocity at this point. The theoretical analysis was verified with experiments on annealed copper wire which demonstrated the existence of a critical velocity at 46 m/sec (150 ft/sec). It was found that to have a drop in both absorbed energy and elongation at the critical velocity, it was necessary to have specimens with a length to width ratio of at least 20.

The theory of strain propagation developed in the work of Von Karman and Duwez [1950], showed that for impact velocities greater than approximately 3 m/sec (10 ft/sec), the assumption of uniform strain along the specimen during impact is not reasonable. Determination of stress-strain diagrams from load-time traces in impact tests, where the load is recorded at the fixed end of the specimen, depend on this assumption being valid. This led the authors to conclude that it was "not logical to utilize tension impact tests to study the influence of the rate of strain on the properties of metals." This conclusion was similar to that arrived at by Holloman and Zener [1944] and Taylor [1946].

Duwez and Clark [1947] presented a more complete discussion of the von Karman theory and experimental verification. They also addressed the special case of the application of the theory to metals exhibiting a yield point. In such cases the von Karman theory would not rigorously apply due to multi-valued functions for the velocity of strain propagation around the yield point. Duwez and Clark [1947] conducted experiments on wire specimens of annealed low carbon steel (165 MPa (24 ksi) yield, 296 MPa (43 ksi) ultimate) at velocities up to 46 m/sec (150 ft/sec) to observe rate effects in a material with a yield point. It was found that the plastic strain along the specimen did not change progressively, as was the case with copper, but was concentrated at certain portions of the gage

length while other sections exhibited no strain at all. An interesting result was that up to an impact velocity of 13 m/sec (42 ft/sec), no plastic strain occurred near the moving end of the wire and the strain resulting from impact was purely elastic. From elastic wave theory, this implied that an elastic stress almost 3 times the static yield strength could be sustained. This was confirmed experimentally. It was postulated that this increased stress could be sustained for 2 to 3 milliseconds after the passage of the wave.

Hoppmann [1947] used a guillotine impact tester to demonstrate the existence of a critical velocity for hard drawn copper in accordance with the von Karman/Taylor theory. He achieved good agreement between the predicted and experimental critical velocities but pointed out that the dynamic stress strain curve, rather than the static one, should be used in determining the critical velocity.

Clark and Wood [1950], continuing work on the von Karman theory, concluded that the critical velocity can be obtained within an order of magnitude from the static stress-strain diagram. For cold-worked metals and alloys they showed that the percentage elongation increased to a maximum with increasing loading rate and then declined rapidly. The maximum in elongation was attained at the critical velocity.

The original von Karman/Taylor theory for the determination of a critical velocity depended on the use of a static stress-strain diagram which is known to be velocity dependent. Pond and Glass [1961] improved on this approach by using the true stress-strain behavior of the material for the calculation of the critical velocity. One proposed method involved using an elastic-perfectly plastic constitutive behavior which was justified on the basis of the yield and ultimate stresses approaching the same value with increasing loading rate [Winlock and Leiter, 1937]. Using this approach, the authors successfully computed critical velocities of wave propagation for several polycrystalline materials.

To facilitate the determination of von Karman critical velocities, Pond and Winter [1980] suggested that the dynamic modulus of resilience, which represents the area under the elastic portion of the stress strain curve, provided the necessary input for the calculation of critical velocities. The dynamic modulus of resilience can be obtained from scleroscope hardness and it was shown that such hardness measurements ranked the critical velocities in a reproducible manner.

Investigations, such as those cited above, which were focused on plastic wave theory and the determination of material "critical" velocities, formed the basis for many evaluations of flow localization behavior in metallic

materials. In most instances, however, the flow behavior of metals under high rate loading is affected by localized deformation heating. In such cases, the competing effects of strain hardening and thermal softening, along with other experimental variables, control localization of plastic flow, which in many cases can be confined to narrow bands. The concepts of plastic wave theory and material critical velocities, modified to account for thermal softening effects, are thus directly relateable to evaluations of localized shearing in metals at high velocities (adiabatic shear banding). The following section traces the development of understanding of adiabatic shear banding in metallic materials.

Adiabatic Shear Banding

Perhaps the first work to carefully examine the effects of large shearing stresses on metallic materials was that of Bridgman [1935, 1937]. This work examined the effects of high shearing stresses combined with high hydrostatic pressures on mechanical behavior. It was found that the shearing stress was not independent of hydrostatic pressure for the high hydrostatic pressures (4895 MPa (710 ksi)) imposed. This is contrary to the view held under the more limited range of normal pressures encountered in engineering practice. For certain materials it was found that, under the above conditions, a detonation or instability would occur at specific values of shearing stress. In some cases this was attributed to a polymorphic transition in the material being studied.

In his experiments, Bridgman measured the shearing force for thin disks of material as a function of the mean normal pressure. Distinct "breaks" in such a curve were taken to be an indication of a polymorphic transition. An analysis of the thermal conditions for these tests indicated negligible overall heat rise during a test. Bridgman therefore suggested that the transition could be of a type produced by shear alone, without high temperatures being necessary. He further suggested that under the conditions imposed, the material would be so disordered that crystallographic slip would not play a role in the deformation and that the metal would in fact behave more

like a liquid. He concluded however, in the 1937 paper, that even under the severe conditions imposed in the experiments, the material did not become amorphous and the most conspicuous difference in liquid versus solid behavior was in the relative independence of the shearing force on the speed of slip in the solid.

Also in the 1937 paper, Bridgmann described a phenomena that he called "snapping" which was probably the first description of what is today called adiabatic shearing. During his experiments, certain metals and other materials, including graphite and quartz, were found to emit snapping noises when sheared under the high hydrostatic pressures. The most notable structural metal involved was titanium. He concluded that "During the snapping there must be a rather large intensely localized generation of heat, which will undo the hardening effect ....." If the tests had been performed in load control, he suggested that the system would have suffered a complete internal rupture. The tendency for snapping was found to be the least in the cubic metals and higher for the hexagonal metals such as titanium.

Bridgman's investigations were an early look at the phenomena of localized constrained flow producing phase transitions in a manner similar to what is attributed to adiabatic shear banding in high strength steels. The important difference between Bridgman's work and subsequent

investigations, is the suggestion that high temperatures may not be necessary to achieve the phase transitions.

As a follow-up to their 1944 work on inertial effects in high rate loading, Zener and Holloman [1944] conducted tests to verify a proposed equivalence between changes in strain rate and changes in temperature on the stress-strain relation in steels. They concluded that the behavior of the steels examined at very high deformation rates could be obtained by tests at moderate rates performed at low temperatures. It was noted that for a 690 MPa (100 ksi) yield strength steel, large changes in the strain rate produced very little effect on the isothermal stress-strain relation. An increase in strain rate however, tended to change the conditions from isothermal to adiabatic. The adiabatic stress-strain relations were calculated for the steels used in the test program and showed negative slopes in certain cases at lower temperatures. These negative slopes were said to be the result of the local temperature rise being more than sufficient to overcome the rise in stress due to strain hardening. The negative stress-strain curve implied an intrinsic instability of the material, where deformation could not be homogeneous.

Zener and Holloman [1944] performed an experiment designed to produce such an instability with the 690 MPa (100 ksi) yield strength steel. The highly localized shear was produced with a punch at a velocity of 3 m/sec (10 ft/sec) producing a strain

rate on the order of 2000/sec (clearance on the die was approximately 1.6 mm (0.0625 in)). The result was a concentration of the shear deformation into a narrow (approximately 30 micron) band which etched white and that they concluded was martensite. It was reasoned that the localized temperature in the band exceeded the austenite transformation temperature and a rapid quench to martensite was provided by the surrounding material. This was the first documented case of what is conventionally known as adiabatic shear banding.

Bourne [1950] examined the effects of dynamic compressive loading on the microstructure of a 0.7% Carbon steel. The microstructure of the steel prior to testing was reported to be pearlitic. The strength level was not reported. Rectangular plates of the steel were impacted at approximately 12 m/sec (40 ft/sec), causing a reduction in thickness of 50% and fracture across the section thickness in most cases. Microscopic examination of the fractures revealed that white layers were present at the fractured faces. Examination of the white layers with X-ray diffraction showed retained austenite and martensite. Lack of clear evidence of tetragonal martensite in the X-ray results led the author to conclude that some tempering of the martensite had occurred, altering the tetragonality of the matrix in the white layers.

McIntire and Manning [1958] observed white-etching bands in a 0.8% carbon hammer steel which had been subjected to impact.

They concluded that sharp blows can produce hard, brittle martensite in hammer heads when the edges break off. Subsequent use of the tool was likely to result in further chipping due to the presence of the untempered martensite. X-ray examination revealed the presence of some austenite in the hard layers leading the authors to conclude that the material had locally been heated above the austenite transformation temperature. This is the identical conclusion reached by Zener and Holloman [1944].

Recht [1964] presented criteria for the prediction of catastrophic shear in metallic materials. Catastrophic shear was shown to result when the local temperature gradients exceeded the strain hardening capacity of the material. The shear was shown to localize into very narrow (1 micron) regions where the local strain rate could be as high as 10^8/second. When the localized shear zone became established, the dynamic shear strength tended to become insensitive to the strain rate. Titanium and titanium alloys were found to be particularly susceptible to the localized shearing. To achieve similar states of localization in a mild steel required approximately 1300 times the velocity needed for localization in titanium. Computations of shear zone temperatures were made using a model based on an infinitely thin shear band which generated heat at a constant rate within an infinite medium. Recht found that for such a band the temperature attained should

depend on the plastic strain (γ), the plastic strain rate ($\dot{\gamma}$) and the rate at which heat is conducted away from the band. This is expressed in the following equation:

$$T = \tau_y/J \; [(\dot{\gamma}(\gamma-\gamma_y))/\pi K\rho C]^{1/2} \quad (3)$$

where

T = Temperature
K = Thermal Conductivity
C = Specific Heat
γ = Plastic Strain
$\dot{\gamma}$ = Plastic Strain Rate
γ_y = Yield Strain in Shear
τ_y = Yield Stress in Shear
J = Mechanical Equivalent of Heat
ρ = Density

Calculated temperatures in the sheared zones in titanium were shown to approach 1000°F for machining speeds of over 0.5 m/sec (1.7 ft./sec).

Manion and Stock [1970] performed a metallographic examination of white-etching shear bands in a 0.6% C - 0.5% Cr steel. The steel was in sheet form, quenched and tempered at 600°C (1112°F) and the bands were produced by punching plugs from the sheet. To determine if the bands were martensite, specimens containing the bands were tempered at 300°C (572°F) for 30 minutes. This heat treatment would have tempered any martensite present in the bands and caused the bands to darken. It was observed that only portions of the bands darkened after the above heat treatment. The remaining material remained white, leaving questions as to the nature of the microstructure.

Adiabatic shear in explosively loaded cylinders of a modified 4337 steel was examined by Thornton and Heiser [1971]. Microhardness measurements showed an increase in hardness for the shear bands (Rc 50-56) versus the matrix (Rc 30-38). X-ray diffraction revealed the structure to be characteristic of body centered tetragonal martensite with no evidence of retained austenite. SEM examination of the bands revealed a microstructure characteristic of fine-grained untempered martensite with no evidence of carbide precipitate particles. Attempts to discover chemical segregation within the bands using an electron microprobe revealed no concentration gradients for any of the constituent elements.

In a similar investigation, Glenn and Leslie [1971] examined "white streaks" in a Ni-Cr-Mo armor plate which had been subjected to ballistic impact. Hardness measurements showed the sheared regions to be harder (HV 1025) than the unaffected bulk of the plate (HV 777). Transmission electron microscopy (TEM) examination of the structure of the sheared regions indicated a BCC structure with a very fine (0.1 micron) grain size. It was concluded that the streaks were formed by the Zener-Holloman [1944] mechanism and were a form of martensite which was formed in heavily deformed austenite. Due to the unusual characteristics of this transformation, the resulting structure did not resemble conventional tetragonal martensite, a conclusion also reached previously by Bourne [1950].

Adiabatic instabilities in the orthogonal machining of an Fe-18.5 Ni-0.52 C tempered martensitic steel were examined by Lemaire and Backofen [1972]. A reversion of the tempered martensitic structure to austenite was observed during machining which produced discontinuous chips as a result of adiabatic instability in the shear zone. Calculation of the temperature rise during cutting predicted that continuous plastic deformation during chip formation could not heat the material to its' reversion temperature (426°C, (800°F)). It was predicted that the additional heat required for the reversion was obtained from rapid shearing during the instability.

Manganello and Abbott [1972] discussed an alternative adiabatic shear band formation mechanism to that of Zener-Holloman [1944]. This mechanism involved severe local plastic deformation and heating of tempered martensite (containing carbides and a high dislocation density) which caused carbides to dissolve (at sub critical temperatures) and to migrate to new dislocation sites. Such a mechanism could operate at much lower temperatures than required by the Zener-Holloman [1944] mechanism.

A theoretically determined thermal instability strain was used by Culver [1973] to examine dynamic plastic deformation in a number of alloys. The thermal instability strain represented the strain at which thermal softening caused an instability in

the stress strain curve. It was found that the thermal instability strain was lowest for titanium alloys and highest for FCC materials such as copper, aluminum and stainless steel. The lower values for this parameter implied an increased susceptibility to thermal instability during high rate loading. The use of this parameter in predicting dynamic instabilities in titanium, mild steel and aluminum was investigated using a torsional impact apparatus.

Culver [1973] found that the theoretical and experimental values for the thermal instability strain agreed closely only in the case of titanium. For the steel and aluminum, localization of plastic flow occurred in wider zones than in the titanium and continued strain was obtained with falling stress up to strains approximately equal to the theoretical instability strains, at which point failure occurred. The failure therefore, could not be directly linked with a thermal instability, although it was suggested that a secondary instability in the severely necked material could have caused failure. A two stage model for adiabatic shear instability in 4340 was later proposed by Giovanola [1988], however the secondary localization was believed to be due to microvoid nucleation and growth and not the consequence of thermal effects.

Backman and Finnegan [1973] cited evidence of recrystallization surrounding an adiabatic shear band in a mild

steel as evidence of the high temperatures achieved during deformation. They concluded that adiabatic shearing initiated at flaws, pits and inhomogeneities in the material.

The majority of investigations concerning adiabatic heating in machining have concentrated on the primary shear zone of the machining operation. The primary shear zone is formed at the interface between the tool and the workpiece. Wright [1973] investigated adiabatic heating in the secondary shear zone along the tool-workpiece interface and concluded that "seizure" along this interface could cause very high rates of deformation within the chip flow zone and considerable adiabatic heat generation. Wright [1973] proposed that the highest temperatures achieved during machining were located in the center of the secondary shear zone and not where the tool first contacts the workpiece. Using methods relying on the hardness and etching response of the tool steel involved, a temperature of approximately 1000°C (1832°F) was predicted for the tool-workpiece interface. The low carbon steel used was machined at 3 m/sec (10 ft/sec) and a feed rate of 7.8×10^{-4} mm/rev (0.02 in/rev). Depth of cut was not specified.

Winter and Hutchings [1975] examined the role of adiabatic shear in solid particle erosion of steel and titanium targets. Specimens were impacted by angular particles which were oriented such that a micro-machining action occurred on the target surface. Localization of the surface deformation was

much more intense in the case of the titanium, which produced chips that detached as they formed.

Lindholm and Hargreaves [1976] were the first to report occurrence of adiabatic shear bands in high rate torsion experiments which enabled direct measurement of applied load and deformation. An AMS 6418 steel was tested in torsion at three shear strain rates. At 0.01/sec, the deformation was stable to large strains. At 10/sec, initial effects of thermal softening on the deformation were observed. A catastrophic adiabatic shear localization was produced at 98/sec along with formation of the typical white etching transformation bands at the fracture plane. Dynamic torsion testing was subsequently used by several investigators (E.G.; Costin, et al, 1979; Hartley, et al, 1987; Marchand and Duffy, 1987; and Giovanola, 1988) to examine shear band behavior in various materials.

Dao and Shockey [1979] measured temperatures accompanying the formation of shear bands during orthogonal machining of 4340 steel and 2014 aluminum. An infrared microscope was focused on the chip near the cutting tool to record temperature variations as the bands were formed. Peak temperature changes of 180°C (356°F) for the steel and 100°C (212°F) for the aluminum were recorded. It was suggested that the peak temperatures in the shear bands were greater than these estimates due to the relatively wide 0.175mm (0.007 in) circular area over which the microscope was focused. The

average measured width of the shear bands for the 4340 steel was 0.02 mm (0.0008 in).

Staker [1980] conducted experiments with explosively-loaded hollow cylinders of 4340 steel which were tempered to achieve two different hardness levels (Rc 43 and Rc 27). The harder material was observed to form white etching adiabatic shear bands as a result of the explosive loading, while the softer material failed by a ductile shear cracking mode. Both modes of cracking were observed to appear similar if only the surfaces of the specimens were considered. Sectioning and metallographic examination were required to reveal the differences in the fracture modes.

Moss [1980], conducted experiments which used an explosively driven punch to shear plugs from a Cr-Ni steel, creating adiabatic shear bands. Regions of chemical inhomogeneity, originally present in the steel, were deformed next to the shear bands and served as reference lines to determine the amount of shear strain in the bands. Shear strains of 572 and shear strain rates as large as 9×10^7/sec were attained in the bands. Estimations of the temperature rise in the shear bands from the material properties, shear strain and shear strain rate, showed that attainment of the austenite transformation temperature was not possible. It was suggested that a carbide and lath morphology change or a magnetic transformation were responsible for the resulting structure in the shear bands.

Metallurgical influences on shear band activity were examined by Shockey and Ehrlich [1980]. Their experiments were performed with an exploding cylinder test which eliminated macroscopic stress concentration sites to allow the observation of the influence of microstructural features on shear band initiation and propagation. For a 4340 steel, increasing hardness was found to increase the number and sizes of the bands produced. A high carbon (1.5%) tool steel however, was found to exhibit homogeneous plastic flow at Rc 27 (annealed) and brittle fracture at Rc 55 (hardened). Mechanical fibering was found to be secondary to the macroscopic state of strain in terms of influencing shear band activity. Shockey and Ehrlich were unable to identify microstructural features (E.G. grain boundaries, inclusions, precipitates and voids) that might have been responsible for shear band initiation.

Costin [1982] used a torsional Kolsky bar to examine the conditions of strain and temperature for the formation of adiabatic shear bands in 1018 cold rolled steel. A series of fine lines, parallel to the specimen axis, were scribed on the inner surfaces of the tubular specimens used in the investigation. Post-test examinations of these lines enabled measurement of the strain distribution along the gage length of the specimen, and assessment of whether the deformation was homogeneous or restricted to a narrow band. It was found that

the critical strain at which localization occurs depends on the energetics of the loading scheme which, in turn, vary with the strain rate. Localization was found to begin at or near the point of maximum shear stress in the adiabatic stress-strain curve. However, in the low strain rate regime (90/sec < 700/sec) there is insufficient energy available to drive the growth of a perturbation which would lead to a shear band.

A torsional hydraulic machine and a torsional kolsky bar were employed by Lindholm and Johnson [1985] to study the shear localization behavior of a wide range of materials, including several steel and aluminum alloys, and depleted uranium. General features of the shear behavior of all of the alloys included: (1) positive strain hardening to large strains at low (< 10/sec) strain rates; (2) positive strain hardening for all strains at the low strain rates; (3) the rate of strain hardening was overcome by thermal softening for strain rates in the transition (adiabatic shear) region (> 10/sec); and (4) significant loss of ductility in some alloys (E.G., steels) at high strain rates due to thermally induced shear instabilities. A finite element code was employed to solve the transient heat conduction problem in the torsionally-loaded specimens. For a relatively low conductivity material such as steel, it was found that the transition from isothermal to adiabatic conditions occurs at strain rates between 10/sec and 100/sec.

Observations on the effects of the temperature rise at

fracture in two titanium alloys were performed by Bryant, Makel and Wilsdorf [1986]. Investigation of the fracture surfaces of rapidly strained (strain rate = 28/sec) tensile specimens revealed droplet-like features at the edges of dimples which they concluded were the remnants of molten pieces of the micro-ligaments. The heat required to produce this localized melting was rationalized in terms of three mechanisms: (1) uniform straining to necking, (2) energy dissipation at the crack tip and (3) deformation to fracture of the micro-ligaments. The largest temperature rise was that for the energy dissipation at the crack tip which was calculated from a model attributed to Rice and Levy [1969]. The low thermal conductivity and high yield stresses (1172 MPa (170 ksi) and 1379 MPa (200 ksi)) of the titanium alloys were thought to be conducive to the localized melting.

Kalthoff and Winkler [1986] investigated the loading rate dependence of the mode II (in-plane shear) fracture toughness, K_{IID}, for a high strength Ni-Co-Mo steel. They used a double cracked shear specimen which was loaded by ballistic impact at rates ranging from 12 m/sec (39 ft/sec) to 33 m/sec (108 ft/sec). The specimens were unsupported and hence were loaded inertially by their own mass. It was observed that these loading rates were more than one order of magnitude greater than those achievable in drop weight tests. The shadow optical method of caustics in reflection was employed to determine the stress intensities at the crack tips.

Kalthoff and Winkler [1986] evaluated the effects of notch tip acuity on the type of "damage" occurring (i.e. tensile fracture damage or shear band damage. They constructed a "deformation map" in terms oi the parameter $Vo/\sqrt{\rho}$, where Vo is the impact velocity and ρ is the notch tip radius. A threshold value of this parameter was established beyond which the failure mode was always by shear banding. Increasing notch acuity was found to enhance the tendency for shear band damage at the same impact velocity, hence fatigue precracked specimens showed the greatest tendency for shear band damage.

The expected "white bands" were not observed in the Ni-Co-Mo steel. It was speculated that this was due to the fact that this steel had a martensitic structure and hence the transformed shear bands would be more difficult to visualize. For this reason an experiment was performed using a Cr-Mo steel with a notch tip radius of 1 mm (0.040 inches), impacted at 40 m/sec (131 ft/sec). The "white bands" were observed to form under these conditions and the metallographic observations supported the speculation that "the phenomenon of shear crack propagation observed under conditions of very high rates of loading, are a result of the formation of adiabatic shear bands which subsequently fail by brittle fracture processes".

In a follow-on investigation, Winkler [1987] conducted more detailed metallographic and fractographic analyses of several shear band fractures in the Cr-Mo steel. It was observed that

the fracture surfaces of the straight propagating shear cracks did not show shear lips. The flat fracture surfaces were shiny in appearance and it was postulated that melting temperatures may have occurred at these surfaces. This postulate was unsupported by experimental measurements or analysis. Examination of the fractures with scanning electron microscopy was not able to reveal the fine structure internal to the white bands. Several instances of fragmentation of the transformed material in the bands were observed.

Strain distributions and temperature increases during plane strain compression testing of AISI 316L stainless steel were examined by Colas and Sellars [1987]. Plane strain compression tests were performed on a servo-hydraulic test machine at strain rates ranging from 0.5/sec to 50/sec. Certain specimens were separated along the centerline of the test section and grid lines were scribed on the mating surfaces. Coordinates of the grid were measured before bolting the two halves together prior to testing. Temperature increases were measured by means of embedded 1.5mm (0.06 in) diameter chromel-alumel thermocouples. It was found that the strain distribution patterns were determined by the geometrical configuration of the specimen during testing and not by the nominal strain rate. The variation of local strains within a specimen was however, found to increase with strain rate. This was attributed to localized increases in temperature. The embedded thermocouples

recorded temperature changes as high as 120°C (248°F) for the 50/sec strain rate tests.

Estimates of temperature increases in the vicinity of a propagating crack tip in a viscoplastic material were conducted by Sung and Achenbach [1987]. It was shown that rupture processes and the dissipation of mechanical energy in the vicinity of a crack tip can give rise to substantial temperature increases. While some of the dissipated energy is converted into surface energy of the new crack faces, the remainder is converted into heat. It was shown that under certain conditions, near the center of the source region around the crack tip, the effects of heat conduction are negligible and an adiabatic approximation provides an acceptable approximation to the local temperature fields. The conditions under which the adiabatic approximation applies were defined in terms of a dimensionless parameter (V^*) which involved the velocity of the source region, a characteristic length parameter of the source region, and the thermal diffusivity. This parameter is given by

$$V^* = (L/2k)V \qquad (4)$$

where, L = a characteristic length, k = thermal diffusivity and V = velocity of the source. It was shown that when $V^* > 10$, the adiabatic approximation is adequate for calculation of the transient temperature at the moving source (crack tip).

Using a mechanical behavior model proposed by Bodner and Partom [1975], Sung and Achenbach also provided estimates of the maximum temperature increases expected at a propagating crack tip under specific conditions. For a crack propagating in steel under mode I (opening) loading conditions, with a velocity of 300 m/sec (984 ft/sec), their predicted temperature increase at the crack tip was 730°C (1346°F). A characteristic length of 1 mm (0.040 in) was assumed.

A non-contacting infrared detector system was employed by Hartley, et al [1987] to determine the temperature history of points lying across the projected path of shear bands in torsional Kolsky bar tests of 1018 cold rolled steel and 1020 hot rolled steel. The observed shear bands were relatively wide, about 250 microns in 1018 and 150 microns in 1020. The bands were not observed to etch white in metallographic examinations. Temperature increases as high as 450°C (842°F) at the band centers were measured. The shear strain rates achieved ranged from 1000/sec to 5000/sec.

Giovanola [1988] examined adiabatic shear banding in a 4340 steel (HRC 40) under dynamic torsional loading. The results were presented in two parts; (1) strain localization and energy dissipation measurements, and (2) Fractographic and metallographic observations.

For part one of the Giovanola [1988] investigation, shear banding in the dynamic torsion tests was directly observed

using high speed photography. The stress-strain curve for the shear banded material and estimates of the energy dissipated in the shear band were also obtained. It was found that the shear localization progressed in two distinct stages and it was suggested that these stages corresponded to the occurrence of deformed bands and transformed bands, respectively. Energy dissipation was found to occur primarily during the second stage of localization. At the onset of the second localization the estimated temperature in the shear band from energy dissipation measurements is only about 200°C (392°F). This is well below the austenite transformation temperature (723°C (1340°F)). At the end of the second localization, however, the estimated temperature was 1100°C (2012°F). Hence, from the standpoint of temperature elevation, it was concluded that a phase transformation was possible. Part 2 of the investigation provided metallographic evidence of transformed shear bands. Values of the energy dissipation in the bands determined from the stress-strain behavior were correlated with energy dissipation values calculated using experimental temperatures from thermocouples on the specimens. Simple one dimensional heat flow calculations were employed and the correlations were found to be excellent.

Part 2 of the Giovanola [1988] investigation was focused on metallographic and fractographic examinations of the experiments performed for part 1. SEM observations of the

fracture surfaces indicated that microvoid nucleation and growth was the mechanism leading to shear band fracture. Transformed shear bands were present only over a small part of the fracture surfaces. This led to the conclusion that these transformed regions were a consequence of frictional heating after separation and were not necessarily an integral part of the failure process. Frictional heating and "re-welding" of the fracture surfaces was cited as more likely to occur in experiments involving combined shear and compressive loading.

Using an improved version of the temperature measurement system employed by Hartley [1987], Marchand and Duffy [1988] studied the formation process of adiabatic shear bands in a structural steel. A torsional Kolsky bar apparatus was used for the tests. Simultaneous measurements of temperature, stress and strain were coupled with high speed photographs of the shear band area, to provide a complete history of the shear band development. An examination of a grid pattern deposited on the specimen surface revealed that the plastic deformation process of shear localization proceeds in three stages. The first stage involves homogeneous straining over the specimen gage section. In the second stage the deformation is observed to become generally inhomogeneous, finally localizing into a narrow (20 micron) shear band in stage three, where catastrophic failure of the test section occurs. The shear bands produced were observed to etch white. Temperatures as high as 590°C (1094°F) were measured in the shear bands.

Microvoid formation during shear deformation of several ultra-high strength steels (4340, 4130, AF1410) was examined by Cowie, et al [1989]. Tests were conducted using both torsional shear specimens and a unique double linear shear specimen. The linear shear tests spanned seven orders of magnitude in strain rate, from isothermal to adiabatic test conditions. The resulting instability strains for the 4340 steel (Rc 56) were almost identical over the range of strain rates. This data implied little effect of thermal softening on the instability strain at these high strength levels. A dominant role of microstructural instability in the shear localization was suggested instead of thermal softening. Their experimental evidence strongly suggested that strain localization in these steels was driven by microvoid softening controlled by nucleation at 100 nm scale particles. The tests emphasized void nucleation rather than void growth as the event leading to shear localization. Enhanced resistance to shear instability was observed with particle dissolution.

The majority of the work described above examined very high strength materials at extreme strain rates ($>10^4$/sec). Only Cowie, et al, examined shear localization over several orders of magnitude in strain rate, and their work did not examine the effects of fatigue cracks on shear localization. While most of the investigations were focused on evaluating models for thermomechanical instability, the more recent investigations

[Giovanola, 1988; and Cowie, et al, 1989] suggest a dominant role of microvoid nucleation in controlling the onset of shear instabilities in high strength steels. Giovanola [1988] has shown that the highest temperatures in dynamic torsion tests were achieved only after the onset of the shear localization and that the classic "white-etching bands" may be an artifact of the shear instability and not an integral part of the process as was originally suggested by Zener and Holloman [1944].

The experiments performed for this investigation were designed to expand on some of the features of the above work, in evaluating the shear localization behavior of two medium-to-high strength steels at loading rates likely to be encountered in structural applications (strain rates of 10^2/sec to 10^3/sec). The objectives of this work were measurement of energy density variations with loading rate, estimation of the temperatures achieved in the sheared zones of fatigue precracked, Dual Notched Shear (DNS) specimens and examination of the micromechanisms of localized shear deformation as related to the microstructures of the steels. Shear zone temperatures calculated from measurements of absorbed energy were compared with temperatures measured by thermocouples near the fatigue crack tips. As mentioned previously, Giovanola [1988], was able to show good correlations between measured and calculated shear band temperatures but did not establish strain rate bounds to these correlations. For the lower strain rates

used in this investigation, the energy concentrated near a crack tip and the resulting temperature rise, are not known. Both are significant as regards the fracture behavior of steels and will be quantified in this investigation. Two steel alloys were chosen to evaluate the effects of toughness and microstructural differences on the respective shear localization behaviors.

The approach to achieving the objective was to develop a technique for characterization of high rate shear deformation and fracture behavior, and employ this technique to quantify the high rate shear behavior of two steels with similar yield strength levels but different microstructures and levels of toughness. The deformation and fracture behavior of these steels under in-plane shear (mode II) loading was examined in the presence of fatigue cracks. The loading rates were varied from quasi-static through impact conditions. The shear localization behavior of the steels was quantified in terms of energy absorption characteristics, temperature rise in the shear zone and width of the shear zone.

Measurements were made of load and displacement to enable estimation of the energy input to the specimens. Temperature increases near the tips of the fatigue cracks were monitored during testing to determine both the magnitude of the temperature rise and the position, in time, of the maximum temperature elevation relative to the ongoing deformation.

The measured temperatures were used in conjunction with assumptions based on transient heat flow, to estimate the temperatures in the shear zone. Estimated temperatures were compared with temperatures calculated from energy absorption characteristics. Post test metallographic observations were performed to determine the widths of the shear zones, evaluate the micromechanisms of localized shear deformation and to evaluate for the presence of metallurgical transformations.

MATERIALS

The chemical compositions and room temperature mechanical properties for the two steels used in this investigation are presented in Tables 1 and 2 respectively. The steels investigated were a Quenched and Tempered processed steel (Q&T Steel) and a Direct Quenched processed steel (DQ Steel). The principle difference in chemical composition is in the increased Nickel content of the Q&T steel, as compared with the DQ steel. Other differences are principally due to the material processing. The Q&T steel is a conventional quenched and tempered martensitic steel (see Figure 1), while the DQ steel is a direct quenched and tempered steel displaying a martensitic-bainitic microstructure (see Figure 2). Direct quenching refers to quenching that is performed on-line with the rolling process to take advantage of the transformation characteristics of the deforming austenite. This process, in conjunction with controlled-rolling [Hamburg and Wilson, 1987] has been shown to produce steel plate with superior combinations of strength and toughness when compared to conventionally processed material [DeArdo, 1983].

Mechanical properties of the two steels are compared in Table 2. Tensile properties were obtained using standard 12.8 mm (0.505 in) diameter tensile specimens. Tests were conducted in accordance with ASTM E8. While the steels have similar yield strengths, the ultimate strength for the DQ steel is

greater, indicating a greater strain hardening capacity. The DQ steel was also shown to have superior ductility in comparison to the Q&T steel.

Table 2 also presents fracture toughness (J_{IC}, and T material) data for the two steels. The fracture toughness data for the Q&T steel was that of Vassilaros, et al [1982]. Fracture toughness data for the DQ steel was generated for the present investigation using the elastic compliance procedure for determination of J-R curves as described in ASTM E1152-87. J_{IC} is the elastic plastic fracture toughness determined in accordance with ASTM E813-81, and represents the resistance of the material to ductile crack initiation. T material is the slope of the J integral resistance curve and represents the incremental resistance of the material to ductile tearing. For calculation of T material, the slope of the J-R curve over the range of crack extensions from 0.15 mm to 1.5 mm (0.06 in to 0.060 in) was used. The J-integral was calculated in accordance with the crack growth corrected equation of Ernst [1981]. Values for T material were calculated from the expression:

$$T \text{ material} = dJ/da \times (E/\sigma_o^2) \qquad (5)$$

where dJ/da is the slope of the J-R curve, E is the elastic modulus and σ_o is the material flow stress. Flow stress was defined as an average of the yield and ultimate strengths. The

DQ steel was shown to exhibit superior J_{IC} fracture toughness and T material in comparison with the Q&T steel.

The above steels were chosen for this investigation primarily due to the differences in their strain hardening capacities, ductilities and levels of toughness at the same nominal yield strength level. The competition between strain hardening capacity and thermal softening characteristics of steels is thought to be a controlling influence in the occurrence of adiabatic shear [Recht, 1964].

EXPERIMENTAL PROCEDURE

Expanding on the previous work of Kalthoff and Winkler [1986] and Winkler [1987], a dual notched shear (DNS) specimen was employed to study the influence of fatigue pre-cracks on the shear localization behavior of the high strength steels. This specimen is illustrated in Figure 3. The specimen contains two parallel edge notches separated by a distance of 25 mm (1 inch). The edge notches were inserted to a depth of approximately half the specimen width, using electrical discharge machining (EDM). The slots were machined in the T-L (ASTM E399) orientation for all specimens.

The resulting slots were 0.25 mm (0.010 inches) inches in width. The specimen surfaces in the central region of the DNS specimens were ground and polished to a 1 micron diamond finish prior to fatigue precracking. Fatigue pre-cracking was accomplished by alternately loading each slot in three-point bending with a total span of four inches. The stress intensity for precracking was maintained below 27 MPa$\sqrt{m}$ (25 ksi$\sqrt{in}$) throughout the range of fatigue crack growth. The stress intensity was calculated using the formulae for three-point bend specimens in ASTM E399. The influence of the second notch was not taken into account since this would only lower the effective stress intensity.

A loading apparatus was constructed to allow shear loading of the central section of the DNS specimen. This apparatus is illustrated schematically in Figure 4. The DNS specimen is located between the upper and lower support platens. The upper support platen was bolted to the lower support platen to rigidly restrain the two outer sections of the DNS specimen. Four bolts torqued to 267 J (60 ft-lbs) provided the restraint on each end of the specimen. The central section of the DNS specimen was rigidly restrained in a similar fashion with two bolts on either side of the specimen connecting upper and lower loading platens. The clearance between the lower loading platen and the lower support platen was 0.25 mm (0.010 in) on either side. This clearance was checked prior to each test with a feeler gage to ensure repeatability among the tests.

The apparatus incorporated a piezo-electric load cell and an eddy current transducer for measurements of load and displacement, respectively. Quasi-static, dynamic and impact tests of DNS specimens were conducted using this apparatus. Quasi-static tests were conducted by placing the apparatus in a Tinius Olsen, LOCAP 269 kN (60,000 lb), screw-type tensile machine and taking the specimen to the desired displacement. Quasi-static tests were performed at a displacement rate of approximately 0.51 mm/minute (0.020 inches/minute). Dynamic tests were performed using an MTS Model 810, 222 kN (50,000 lb) closed loop servo-hydraulic test machine operating at a

displacement rate of approximately 38 mm/sec (1.5 inches/sec).

For the impact tests, the apparatus was placed in a Dynatup Model 5100, drop tower where the loading was applied by a falling crosshead. The crosshead was dropped from a height of 0.91 m (3 ft) with a resulting impact velocity of 4.3 m/sec (14 ft/sec). The applied energy for the impact tests was 2020 joules (1490 ft-lbs). The resulting displacement rates for these tests ranged from 0.69 m/sec (27 in/sec) to 0.91 m/sec (36 in/sec). Additional features of the impact tests included the use of "stop blocks" in the apparatus to control the overall displacement of the sheared section; "stop columns" in the drop tower to limit excessive loading of the apparatus after displacement of the test section; and use of crossed triangular "absorbers" of annealed 5086 aluminum to smooth out initial load transients which inhibit data analysis.

A key feature of DNS specimen testing at all three test rates was measurement of specimen temperature in the region ahead of one of the fatigue cracks in each specimen. Temperature in all of the tests was measured using thin film Type K (chromel-alumel) thermocouples. The junction regions of these thermocouples were approximately 0.127 mm (0.005 in) in thickness and were in direct contact with the specimen surface at the regions of interest. The nominal location points for the thermocouples on the DNS specimens are shown, schematically, in Figure 5. Measurements of the actual

thermocouple positions on each specimen were performed following test completion. The thermocouple signals were routed through differential amplifiers set to a gain of 10X.

The thin film thermocouples were calibrated in an ice-water bath and at boiling water temperature and compared with the output of conventional Type K thermocouples at these temperatures. A DNS specimen half was used for these calibrations. The thin film thermocouple was mounted to the surface, while the conventional thermocouple was inserted to the mid thickness of the specimen. The thermocouple readings were taken one half hour after exposure of the specimens to the known temperature sources. To evaluate the response of the thermocouples under conditions more closely approximating those to be encountered during testing, a soldering iron was used to provide a point heat source and was brought into close proximity to the tips of the thermocouples. The output of the thermocouples was monitored simultaneously on a digital oscilloscope and a calibrated digital Type K thermocouple read-out. The maximum voltage obtained from the oscilloscope trace was converted into a temperature using calibration tables for Type K thermocouples. This temperature was compared with the maximum temperature obtained on the calibrated digital read-out. This procedure was performed on each specimen prior to testing to ensure that the thermocouples were functioning properly.

Load and displacement were calibrated statically against known measures. The piezo-electric load cell (PCB Piezotronics, Model 226A) was calibrated against a calibrated strain-gauge load cell up to 179 kN (40,000 lbs). The calibration slope for the load cell was 38 kN/volt (8532 lbs/volt). The eddy current displacement transducer (Kaman Industries, Model KD2300-6C) was calibrated in a micrometer against a metal target. The calibration slope for the eddy current transducer was 7.57 mm/volt (0.298 in/volt).

The load and displacement transducers had limiting frequency responses of 100 kHz and 20 kHz respectively, which were more than adequate for the test durations involved in the impact tests. As an example, a 20 kHz frequency response implies that the transducer and associated electronics will not resolve events occurring faster than 1/20,000 or 10 microseconds. The test durations for the impact tests were on the order of several milliseconds and hence were over 100 times the resolvable limit of the transducer with the lowest frequency response. The response time of the thermocouples was in the range of 0.5 milliseconds.

All data from the tests were acquired using a Nicolet model 4094 digital oscilloscope with 12 bit (1 part in 4096) high rate analog to digital converters. For the quasi-static tests the time base used was 13 minutes, while that for the dynamic

tests was 173 milliseconds. A dual time base was used for the impact tests. Load and displacement were recorded on a 20 millisecond time base, while the two temperature channels were recorded on a 173 millisecond time base. The digital test records were transferred to a Zenith Model 248 microcomputer for analysis and plotting of the data.

All tests were conducted at room temperature. Following testing, measurements were made of the actual precrack depths across the specimen cross sections. These measurements were made at five equally-spaced points across the fracture surfaces, including the specimen edges. The five values were averaged to determine the overall precrack depth. The precrack depths were subtracted from measurements of the specimen widths (W) to obtain the remaining ligament (b_o) dimensions.

The test sections of each specimen were removed and mounted for metallographic examination. The metallographic sections were plated using Buehler EDGEMET compound (Rc 50), prior to mounting, to provide edge retention at the fracture surfaces. The metallographic sections examined were approximately 1.27 mm (0.050 in) below the original surface of the specimen. All of the metallographic sections were ground and polished to a 0.25 micron finish and were etched in a 2% nital solution. The specimens were examined metallographically using a Zeiss AXIOMAT metallograph, to reveal the deformed microstructures, widths of the sheared zones and general geometric outline of

the deformed test sections. Measurements of the widths of the shear zones were performed on the metallograph at a magnification of 250X, where an accuracy of $\pm$ 2 microns was obtained. The measured widths were from the edge of the fracture surface to where the microstructure (martensite laths) was unaffected by the shear deformation.

Examinations of the deformed microstructures of specific specimens were also performed with a JEOL Model 35, scanning electron microsope (SEM). SEM examinations of the fracture surfaces of specific specimens were also performed. Microhardness measurements were made on certain metallographic cross sections through the specimens to compare hardness in the shear zones with that of the bulk material. A LECO, Model 400 microhardness tester was used for these measurements. A diamond pyramid (Vickers) indenter was used with 10 g loading to provide indentations small enough to fit within the shear zones. A test matrix for the investigation is presented in Table 3.

RESULTS and DISCUSSION

Calibration and Measurements

Results of calibrations performed on a thin film thermocouple in an ice water bath and at boiling water temperature are presented in Table 4. The thin film thermocouple accurately indicated the temperatures of the known sources within 0.3% at 0°C (32°F) and 0.05% at 100°C (212°F) and compared well with the output of a conventional Type K thermocouple. As mentioned in the previous section, the responses of the thin film thermocouples on each specimen were checked prior to testing by exposing them to a point heat source. A soldering iron was used to provide the point source. A typical temperature-time record for response of a thin film thermocouple to point heating with a soldering iron is provided in Figure 6. The output shown in Figure 6 was recorded as a voltage on a digital oscilloscope and was converted to temperature using a linear fit to voltage-calibration tables for Type K thermocouples. The output was also monitored on a calibrated Type K thermocouple digital read-out. The digital read-out indicated a maximum temperature of 70°C (158°F). This was in excellent agreement with the maximum temperature calculated from the recorded trace 71°C (160°F). Similar levels of agreement were found for all of the thermocouples tested.

Results of physical measurements of the specimens performed both before and after testing, are presented in Table 5. One of the objectives in fatigue precracking the specimens was to obtain a remaining ligament (b_o) dimension of approximately 3.8 mm (0.150 in) for all of the specimens. This was to ensure, as closely as possible, geometric similarity among the specimens to allow direct comparison of the energy absorbed during testing. As shown in Table 5, the b_o dimensions for all of the specimens, except DQ steel specimen GOA-9, were in the range of 3.81 mm (0.150 in) to 4.06 mm (0.160 in), indicating excellent agreement between the specimens. The b_o dimension for GOA-9 was significantly shorter than the other specimens, invalidating comparisons with the other specimens on a strict absorbed energy basis. Comparison of all specimens on the basis of energy absorbed per unit fracture surface area and on the basis of energy absorbed per total deformed volume (energy density) was also performed. These calculations will be presented in the following section.

Table 6 presents post-test measurements of the thermocouple positions on each DNS specimen relative to the fatigue precrack tip ("y" dimension) and the fracture surface ("x" dimension). The relevant dimensions are illustrated in Figure 5. Variations from both the nominal "x" and "y" dimensions shown in Figure 5 were observed for both thermocouples. These variations were due to errors in initial placement and, in the

case of "x" dimension variations, also due to crack movement outside of the predicted fracture path. The actual positions of the thermocouples, recorded in Table 6, were used in estimations of the shear zone temperatures from heat flow considerations to be presented in a later section.

Dual Notched Shear (DNS) Specimen Testing

Results of the DNS specimen tests at all three rates (quasi-static, dynamic and impact) are presented in Tables 7 and 8. Delta T(i) and delta T(o) are the maximum temperatures achieved at the inner and outer thermocouple locations shown in Figure 5. The maximum displacement is the displacement that was achieved at catastrophic failure of the test section. The absorbed energy for each specimen was determined by integrating the area under the load-displacement curve up to the point of catastrophic failure of the test section. The energy per unit area was obtained by dividing the total absorbed energy by the total area area of the specimen remaining ligaments, using the measurements provided in Table 5.

At the quasi-static test rate, the DQ steel specimen (GOA-11) achieved a higher maximum load and greater maximum displacement than the the comparable Q&T steel specimen (FKS-6) as shown in Table 7 and Figures 7 through 10. Integration of the areas under the load-displacement curves for the two specimens (Figures 8 and 10) showed that the DQ steel specimen

(GOA-11) absorbed a greater amount of energy than Q&T steel specimen, FKS-6 (Table 7). The temperatures reported for these tests (Table 7) were recorded from a digital read-out device connected to the thin film thermocouples at the inner location. Temperatures at the outer thermocouple location were not monitored for the quasi-static tests. As expected for these slow displacement rate tests, conditions were almost completely isothermal, with only very small temperature elevations observed. These elevations were observed to coincide with the catastrophic failure of the test sections.

A large elevation (24%) in maximum load was observed for the dynamic DQ steel specimen (GOA-10) in comparison with the quasi-static DQ steel specimen (GOA-11) as shown in Table 7. A lesser elevation (13% - 17%) was shown in a comparison of the dynamic Q&T steel specimens (FKS-4,8) with the quasi-static Q&T steel specimen (FKS-6). The maximum displacements achieved for all three dynamic rate tests were slightly greater than those for the quasi-static tests. As for the quasi-static tests, The DQ steel specimen (GOA-10) was shown to absorb a greater amount of energy than the Q&T steel specimens (FKS-4,8). Dynamic DQ steel specimen GOA-10 was observed to absorb 32% more energy than quasi-static DQ steel specimen, GOA-11. For the Q&T steel, the average absorbed energy for the dynamic tests (FKS-4,8) was 20% greater than that for the quasi-static case (FKS-6).

The results for both the quasi-static and dynamic test rates are consistent with expectations from the mechanical property and fracture tests. That is, the tougher, more ductile DQ steel absorbed more energy in the DNS specimen tests and exhibited a greater test rate dependence of the maximum load and absorbed energy than did the Q&T steel. This is consistent with the general observed trend for static versus dynamic tension [Winlock and Leiter, 1937] and mode 1 (opening) ductile fracture behavior [Hasson and Joyce, 1981] of steels.

Plots of load-time and temperature-time for the three dynamic tests are shown in Figures 11 - 16. The temperature-time plots are for the inner thermocouple location. For all three tests, the temperature elevation was observed to begin near the maximum in the load-time trace and to reach a peak only after the central test section of the DNS specimen had failed catastrophically. The times between maximum load and maximum temperature were similar for DQ steel specimen GOA-10 and Q&T steel specimen FKS-4 (65 ms and 68 ms, respectively), but significantly longer for Q&T steel specimen FKS-8 (113 ms). The maximum temperature increase at the inner thermocouple location was that for Q&T steel specimen FKS-4 (17°C (30°F)). The DQ steel specimen (GOA-10) exhibited a temperature increase of 14°C (26°F).

The temperature-time records for DQ steel specimen GOA-10 (Figure 12) and Q&T steel specimen FKS-4 (Figure 14) exhibited a small (1.1°C (2°F)) temperature decrease just prior to the attainment of maximum load. A possible explanation for this decrease is the thermoelastic effect [Dieter, 1976]. The thermoelastic effect predicts small changes in temperature with rapid straining. Rapid elastic tension is expected to cause small temperature decreases, while rapid compression should cause small temperature increases. While this effect could account for the minor temperature variations observed. the sign of the temperature change appears to be contrary to that discussed above. The region of the DNS specimen where the thermocouples are located should experience compressive loading, and hence a small temperature increase. Relaxation of the compressive loading as plastic flow begins could, however, result in a small temperature decrease due to thermoelastic effects.

Results of the DNS specimen tests conducted at the impact loading rate are shown in Table 8 and in Figures 17 - 26. The Q&T steel specimens exhibited a very large (31%) increase in average maximum load as compared with the dynamic Q&T steel specimens. The DQ steel specimens exhibited only a 7% average increase in maximum load when compared with the dynamic loading rate. Maximum displacement values for all of the impact rate specimens, except DQ steel specimen GOA-8, were observed to

fall below those for the dynamic rate tests. The impact Q&T steel specimens absorbed an average of 11% more energy than the dynamic Q&T specimens, while the average absorbed energy for the impact DQ steel specimens (GOA-7, 8) was actually 29% less than that measured for the dynamic DQ steel specimen. This is opposite the trend observed for the quasi-static and dynamic tests and is indicative of a greater tendency for shear flow localization in the DQ steel at the impact loading rate.

In terms of energy absorption over all three test rates, the Q&T steel displayed a continuously increasing trend with increasing test rate. Allowing for the single dynamic rate DQ steel specimen test (GOA-10) being somewhat anomalous, one would conclude that either no distinct effect of test rate on the energy absorption values for the DQ steel was observed; or a decreasing trend was actually observed. The same trend was observed when comparisons among the specimens were made on the basis of absorbed energy per unit area (Tables 7 and 8). DQ steel specimen GOA-9 can not be directly compared to the other DNS specimens due to its smaller remaining ligament (b_o) dimension. Evaluations of the shear localization behaviors based on energy absorbed per deformed volume will be presented in a later section.

Load-time and temperature time plots for the impact rate tests are shown in Figures 17 - 26. The temperature plots are for the inner thermocouple location. As with the dynamic

tests, the temperature rise in all cases was observed to begin near the maximum in the load-time records. The temperature and load signals however, had to be recorded on separate time scales due to the short duration (less than 3 ms) of the impact rate tests and the longer time evolution of the temperatures at the thermocouples. This is similar to the trend observed by Giovanola [1988] for temperature measurements using thermocouples in dynamic torsion experiments. The time window used to record temperatures for specimen FKS-3 was set for too short a duration, hence maximum temperatures at the thermocouple locations were not obtained for this specimen.

The times between maximum load and maximum temperature recorded at the inner thermocouple location (delta T(i)) were similar for DQ steel specimens GOA-8 and GOA-9 (37.4 ms and 32.1 ms, respectively). The corresponding time for DQ steel specimen GOA-7 was significantly less (17.4 ms). This is due to the much closer proximity of the thin film thermocouple to the fracture plane in this specimen (see Table 6). The times between maximum load and maximum delta T(i) were significantly longer for the impact Q&T steel specimens (67.4 ms for FKS-5 and 57.3 ms for FKS-2). The thermocouple locations for these specimens were similar to those for the impact rate DQ steel specimens and hence can not be used to explain the time difference. The thermal conductivities for the two steels are primarily a function of chemical composition and therefore

should be approximately equivalent. The increased nickel content of the DQ steel would actually yield a higher thermal conductivity than the Q&T steel and hence this also, can not be used to explain the time difference.

The most probable cause of the difference in the time evolution of the temperatures between the DQ and Q&T impact tests is the shear localization behavior. A more rapid temperature evolution at the thermocouples would be expected if the deformation in one steel localized more rapidly than the other. This appears to be the case for the DQ steel as is also evidenced by the inability of this steel to continue to absorb more energy with increasing loading rate. An examination of the temperature-time records for the impact rate tests of both steels (Figures 18, 20, 22, 24 and 26) shows similar initial rates of heating, but different curvatures to the maximum temperature and pre- and post-maximum temperature regions of the plots. The impact DQ steel specimen temperature records peak early and begin to decline over the observed time window. The temperature plots for the impact Q&T steel specimens peak later with more of a curvature to the region just prior to maximum temperature. This behavior is consistent with heat flow being delayed due to less of a tendency for shear localization in the case of the Q&T steel.

The apparent enhanced tendency for shear localization with increased loading rate in the DQ steel with respect to the Q&T

steel can only be partly explained in terms of the mechanical properties of the materials. The DQ steel has both a higher ultimate tensile strength and capacity for strain hardening than the Q&T steel. In accordance with the shear localization model of Recht [1964], the slightly higher yield strength of the DQ steel would tend to promote localization, while the greater strain hardening capacity would tend to limit localization. The higher strength, in this case, appears to be the dominant factor. The temperature sensitivity of the flow behaviors of the two steels was not evaluated for this study and could have an effect on the overall shear localization if high temperatures were achieved in the shear zones. As will be shown in a subsequent section however, the predicted temperature increases in the shear zones were not very high and hence effects on the flow behaviors of the steels should be minimal.

Metallographic Evaluation of Shear Zone Dimensions and Correlation of Experimental and Analytical Results

The objectives of the metallurgical examinations of the shear zones of the DNS specimens were to measure the widths of the sheared zones and to evaluate changes (if any) in the microstructures due to the shear deformation. Metallographic measurements of the shear zone widths were used in conjunction with DNS specimen test data to calculate shear strains, strain rates and absorbed energy per deformed volume (energy density).

Measurements of the DNS specimen shear zone widths determined by metallographic observations are presented in Tables 9 and 10. Figure 27 shows a typical fracture profile which illustrates the width of the shear zone for DQ steel specimen GOA-9 (impact rate). The shear zone widths were measured from the edge of the fracture surfaces to where the microstructure was unaffected by the shear deformation (see Figure 27). The measured shear zone widths were based on an average of five measurements along the fracture surface of each specimen. The DNS specimens were fractured during testing into three sections with four mating fracture surfaces. Measurements of the shear zone widths along all of these surfaces was performed. The widths reported in Table 9 were the combined totals for the mating halves of the fracture surfaces adjacent to the thermocouple measurement locations (Side A, Figure 5). Widths reported in Table 10 were for the mating halves of the other fracture surfaces (Side B, Figure 5).

Tables 9 and 10 also show the shear zone volumes calculated from the shear zone widths and measurements of the specimen remaining ligaments presented in Table 5. Shear strains were calculated by dividing the displacements at failure of the test sections by the shear zone widths. Shear strain rates were calculated by dividing the displacement rates by the shear zone widths.

The shear zone widths for both steels were observed to decrease with increasing loading rate. This was similar to the trend observed by Dowling and Harding [1967] in high rate punch tests of a mild steel. The shear zones were also observed to be narrower than the clearance on the loading apparatus (0.25 mm (0.010 in)). This is contrary to the results obtained by Dowling, Harding and Campbell [1970], and Campbell and Ferguson [1970]. The narrower shear zones obtained in this study were likely the result of the use of fatigue precracked specimens. Shear strains at maximum displacement for both steels were shown to increase only slightly with loading rate from the quasi-static to the dynamic rate and almost not at all in going from the dynamic to the impact rate. An exception was Q&T steel impact rate specimen, FKS-2 which achieved a shear strain of 6.2 at test section failure for the A side shear zones. The shear strain rates for the DNS specimen tests were shown to span five orders of magnitude in strain rate. The highest strain rates achieved in the impact tests were in the range of 10^3/sec to 10^4/sec.

The DNS specimens, being loaded under a combined state of stress (shear and bending), also exhibited plastic deformation associated with bending of the central sections of the specimens. This bending deformation of the central sections of the DNS specimens adjacent to the thermocouple locations (Side A, Figure 5) is illustrated in Figures 28 through 33 for

specimens of both steels over the complete range of loading rates. The deformed volumes of material associated with this deformation were estimated by assuming a triangular region with the "x" and "y" dimensions as shown in Figure 29. This procedure was necessitated by the fact that there was not a clear microstructural delineation between the deformed and undeformed areas in this region. The "y" dimensions for the bending deformation region were tabulated and are reported in Table 11 for both the A and B side shear zones. A tabulation of the "y" dimension components (see Figures 28 through 33) of the bending deformation shown in Figures 28 through 33 is provided in Table 12.

The extent of the bending deformation in the DNS specimens, documented in Figures 28 through 33 and Table 12, provides further evidence of the enhanced tendency for shear localization in the DQ steel as compared with the Q&T steel. Particularly noteworthy is the comparison of impact rate DQ steel specimen GOA-8 (Figure 32) with dynamic rate DQ steel specimen GOA-10. The difference in the extent of the deformation is significant, with the impact rate specimen exhibiting a greatly reduced "y" dimension for the bending deformation in comparison with the dynamic rate specimen (0.13 mm (0.0052 in) versus 0.72 mm (0.0284 in), respectively). A similar comparison for the Q&T steel (Figures 31 and 33, Table 12) showed a trend for increasing the "y" dimension of the bending deformation with increased loading rate.

Table 13 presents calculations of shear zone energy densities and temperatures calculated from energy absorption considerations for the shear zones on the A side fracture surfaces. Partitioning of the energy was performed on the basis of a ratio of the deformed volumes at the A and B side fracture surfaces (Tables 9 and 10). Temperatures were calculated assuming adiabatic conditions using the defining equation for heat capacity [Sears, 1983] given by

$$Q = m \int_{T1}^{T2} C \, dT \qquad (6)$$

where

Q = Energy
T = Temperature
m = mass
C = specific heat

Solving this equation for temperature (T), recognizing that mass (m) = density (ρ) x volume (V), and assuming that the heat capacity (C) remains constant over the expected range of temperatures gives

$$\Delta T = Q/(\rho C V) \qquad (7)$$

where

Q = absorbed energy
ρ = density = 7.801 g/cm^3
C = specific heat = 0.473 J/g ^{o}C
V = deformed volume

Values for the specific heat (C) and density (ρ) were those for a 0.1% carbon steel as reported by Holman [1981]. The total energies reported in Table 13 were obtained by integrating the areas under the specimen load-displacement records up to the point of test section failure. It was assumed that 90% of the energy of plastic work would be evolved as heat [Taylor and Quinney, 1933]. The total energy, multiplied by 0.9 and partitioned to the A side shear zone by a ratio of the deformed volumes on both the A and B sides, was reported in the column entitled energy associated with side A zone. This was the energy used to calculate temperature in the shear zone from equation (7). To obtain the energy density, the energy for side A was divided by the total deformed volume (sum of volumes in Tables 9 and 11) associated with the A side fracture surfaces.

The energy densities for specimens of both steels were observed to increase with increased loading rate. The increases were greatest in the case of the DQ steel, with specimen GOA-8 (impact rate) exhibiting the highest value for energy density. Among the Q&T steel specimens, specimen FKS-2 (impact rate) exhibited the highest value for energy density.

For calculation of shear zone temperatures using equation (7) it was assumed that all of the energy for side A was converted to heat over the total deformed volume and that

adiabatic conditions prevailed. Adiabatic conditions imply that the deformation is occurring rapidly enough such that heat is retained locally and, for a short duration, there is almost no conduction to the surrounding matrix. Compliance with this adiabatic assumption for the DNS specimen tests will be examined later. The estimated maximum temperatures from equation (7) were greatest for the impact tests with a range from 543°C (1010°F) to 870°C (1598°F).

Temperatures in the Side A shear zones of the specimens were also estimated from thermocouple measurements using an equation which described one-dimensional transient heat flow from a planar source [Holman, 1981]. The equation describing this condition is,

$$(T(x) - T_o)/(T_i - T_o) = \text{erf}\ (x/(2\sqrt{kt}) \qquad (8)$$

where

$T(x)$ = thermocouple temperature
T_i = initial temperature
T_o = temperature in shear zone
t = time
k = thermal diffusivity
x = distance from the edge of the planar source (shear zone) to the thermocouple

and the Gauss error function is defined by

$$\text{erf}\ (x/(2\sqrt{kt}) = 2/\sqrt{\pi} \int_o^{x/2\sqrt{kt}} e^{\eta}\ d\eta \qquad (9)$$

where it is noted that in this definition η is a dummy variable and the integral is a function of its upper limit.

Thermal diffusivity was calculated from $k = K/\rho C$, where K = thermal conductivity, ρ = density, and C = specific heat. The thermal conductivity (K) used was 0.43 J/(sec cm ^{o}C) as reported by Holman [1981] for a 0.1% carbon steel. Equation (8) assumes that the plane source (edge of the shear zone) is instantaneously heated to temperature T_o and maintained at this temperature thereafter. While this equation does not apply in the strict adiabatic case, strict adiabatic conditions were not expected to apply at the strain rates achieved in the impact rate DNS specimen tests. This equation should therefore provide an upper bound estimate of the temperatures achieved in the specimen shear zones.

Estimates of the shear zone temperatures from the thermocouple measurements are presented in Table 14. The times (t) used in equation (8) were the difference between the time at which each specimen achieved maximum load and the time at which the maximum temperature at the thermocouple position was attained. This differential time was used due to the fact that the shear zone would only begin to be established near the maximum load achieved by the specimens. The distance (x) used in equation (8) was the difference between the measured distance from the shear band to the fracture surface (Table 6) and the measured shear zone width on the thermocouple side of

the fracture surface. The two quasi-static specimen tests (GOA-11 and FKS-6) were essentially isothermal and were not evaluated using equation (8).

As shown in Table 14, the maximum temperatures estimated in the shear zones were those for the impact rate tests, GOA-8 and FKS-2 (120°C (248°F)) and 121°C (250°F), respectively). No clear trend was observed between the temperature achieved and the type of steel (Q&T or DQ). Such temperatures would not be expected to significantly influence the mechanical properties of the steels [ASM Metals Handbook, 1978]. These temperatures were observed to fall significantly below those estimated from energy absorption considerations (Table 13). The most probable explanation for the disagreement is the assumption of adiabatic conditions in the estimation of the shear zone temperatures from energy absorption considerations. Equation (7), which was used for this estimation, assumes that the plastic work in the shear zone was instantly converted to heat over the entire shear volume. For the relatively low strain rate tests (compared to the majority of the literature) performed for this study, it was postulated that the adiabatic assumption may not be reasonable.

To ascertain to what degree the DNS specimen tests approached adiabatic conditions, a dimensionless thermal diffusivity-rate parameter [Sung and Achenbach, 1987] described previously in equation (4), (page 48), was employed. This

parameter (V^*)is based on thermal diffusivity (k), displacement rate (V) and a characteristic dimension (L) of the deformation, in the equality, $V^* = (L/2k)V$. This expression was derived to assess whether adiabatic conditions would exist at the tip of a rapidly propagating crack in a mechanical test specimen. Sung and Achenbach [1987] found that adiabatic conditions prevailed for $V^* > 10$.

Values of V^*, calculated for the DNS specimen tests performed in the present study, are presented in Table 15. The characteristic length used in equation (4) for calculation of V^*, was the shear zone width. It was shown that, even at the impact rate, conditions were not adiabatic when assessed using equation (4). The maximum value for V^* that was achieved (4.35) was for Q&T steel specimen FKS-2, tested at the impact rate. To achieve adiabatic conditions would require a higher loading rate. As an example, using equation (4) and assuming that the other factors (L and k) remained constant, specimen FKS-2 would not be characterized as achieving adiabatic conditions until a displacement rate of 2.1 m/sec (6.9 ft/sec) was attained. This displacement rate is approximately 2.3 times the rate actually achieved by specimen FKS-2 in the impact rate test conducted for this study.

An evaluation of this parameter (V^*) where adiabatic conditions were known to have been achieved, was performed by calculating V^* for the tests conducted by Kalthoff and Winkler

[1986] and Winkler [1987]. These authors reported adiabatic (transformed) shear bands in shear tests of a high strength steel impacted at approximately 40 m/sec (131 ft/sec). The measured shear zone width from this work was 0.0285 mm (0.00112 in). The thermal diffusivity used in the present study (k = 11.65 mm^2/sec) was used. The calculation showed V^* = 49 and hence, the parameter (V^*) would have correctly predicted adiabatic conditions for their tests.

Metallographic and Fractographic Characterization of Shear Zone Regions in DNS Specimens

In addition to the metallography performed for measurement of the shear zone widths and other specimen deformations, selected specimens were examined in greater detail using both light optical and scanning electron microscopy (SEM), and microhardness measurements. Both metallographic cross sections through the shear zones and the actual fracture surfaces of the specimens were examined.

Deformed shear zones, similar to that shown for DQ steel impact specimen, GOA-9, in Figure 27, were found adjacent to the fracture surfaces of all of the DNS specimens over the entire range of loading rates. As discussed in the previous section, the shear zone widths for both steels were observed to decrease with increased loading rate. Metallographic cross sections through the shear zone regions of two of the impact

rate specimens (DQ steel specimen, GOA-8 and Q&T steel specimen, FKS-2), were examined in greater detail. Figures 34 through 36 present optical and SEM micrographs of a cross section through Q&T steel specimen, FKS-2. This specimen, which exhibited the highest calculated energy density of the Q&T steel impact specimens, was observed to form deformed shear zones which displayed microvoids and microvoid coalescence in the region just below the fracture surface. This evidence suggests that microvoid nucleation and growth may have played an important role in the shear localization process. This is consistent with previous observations by Giovanola [1988], and Cowie, et al [1989].

Similar evidence, but to a much greater extent, was shown for DQ steel impact specimen, GOA-8, in Figures 37 through 40. In the optical micrograph (Figure 37), this specimen exhibited a different etching response from that observed for the bulk, in the region immediately adjacent to the fracture surface. This region was observed to etch darkly in the 2% nital solution which was employed. This response is contrary to that typically seen for "transformed" shear bands in the literature, which are most frequently shown to etch white in response to nital solutions. The higher magnification/resolution SEM micrographs of this region, shown in Figures 38 through 40, show a very dense array of microvoids with diameters generally less than 1 micron. The dense microvoid region was observed to gradually blend into a typical deformed zone region as shown in

Figure 38. The presence of the dense microvoid region immediately below the specimen fracture surface provides strong evidence that microvoid nucleation was a controlling factor in the shear localization process.

SEM fractographs of DNS specimens of both steels, representing the complete range of loading rates, are presented in Figures 41 through 54. For each specimen presented, a relatively low magnification fractograph of the fatigue precrack/shear fracture interface is followed by higher magnification fractographs of the shear fracture region just ahead of the fatigue precrack. In most cases, damage to the fracture surfaces due to the in-plane loading was evident.

At the quasi-static and dynamic test rates, specimens of both steels (Figures 41 trough 48) exhibited shear fracture on multiple surfaces in the "z" dimension (out of the page). The dynamic rate specimens (GOA-10 and FKS-4) displayed a greater number of small microvoids than did the quasi-static specimens as shown in a comparison of Figures 42 and 44, with Figures 46 and 48, respectively. At the impact rate, the fracture surfaces of both DQ steel specimen GOA-8, and Q&T steel specimen FKS-2 (Figures 50, 51, 53 and 54), revealed dense arrays of microvoids similar to those seen in the metallographic cross section of DQ steel specimen GOA-8. The microvoids observed for Q&T steel specimen FKS-2 were generally larger than those observed for DQ steel specimen GOA-8, and

were observed to coalesce into larger holes elongated in the direction of shear loading. The fractographic evidence again suggests a strong role of microvoid nucleation and growth in the high rate shear localization behavior of both the DQ and Q&T steels. The Q&T steel shear localization behavior appears to be controlled by microvoid nucleation and growth while nucleation alone appears to be the dominant factor controlling the shear localization behavior of the DQ steel.

Microhardness measurements were performed on metallographic cross sections through DNS specimens of both steels representing the complete range of loading rates. The microhardness measurements were performed using a Vickers diamond pyramid indenter and 10 g loading. Due to the very small indents produced with 10 g loading, accurate measurements of the Vickers microhardness number were difficult. Differences between microhardness numbers in the range HV 30 - HV 40 were therefore considered to be insignificant as these differences could result from small errors in measurement of the mean diagonals of the indents.

The results of the microhardness tests are presented in Table 16. No significant increases in hardness for the deformed shear zone regions, compared with the bulk, were found for the quasi-static or dynamic rate specimens. A minor average hardness increase (HV 364) was observed for the shear zone region of impact rate Q&T specimen FKS-2, in comparison

with the bulk (HV 310). A significant hardness increase was observed for both the deformed shear zone and dense microvoid regions of impact rate DQ steel specimen GOA-8 (HV 454 and HV 477, respectively) in comparison with the bulk (HV 338). The hardness increase in the dense microvoid region is most probably the result of the severe localized shear strains in that region.

The observed differences in the micromechanisms of deformation leading to shear localization in the two steels can be used to help explain differences in mechanical behavior as documented in the results of the DNS specimen tests. In the impact rate DNS tests, the DQ steel demonstrated an inability to continue to absorb more energy with increased loading rate. This was attributed to an enhanced tendency for shear localization at the impact rate which was reinforced by the observations of narrower shear zones and decreased bending deformation with increased loading rate. The region of dense microvoids with approximately equal diameters, observed in the shear zone of DQ steel impact rate specimen GOA-8, suggests that a massive nucleation of voids occurred over a short time period of time and was, at least in part, responsible for the enhanced tendency for shear localization at the impact loading rate.

The Q&T steel demonstrated the ability to continue to absorb more energy with increasing loading rate over the range

investigated. Examinations of the fracture surface of Q&T steel impact rate specimen FKS-2, also revealed a dense array of microvoids. These microvoids were however, generally larger and more varied in diameter than those observed in the DQ steel and were observed to coalesce into holes which were elongated in the direction of the shear loading. The observed microvoid coalescence and growth in the Q&T steel, as opposed to nucleation only, was consistent with the ability of this steel to continue to absorb more energy with increasing loading rate.

The differing void nucleation and growth conditions in the two steels are of course, attributable to the sizes and distributions of second phase particles such as carbides. The DQ steel which was thermomechanically processed (controlled rolled, and direct quenched) would be expected to have a finer dispersion of generally smaller carbides than the Q&T steel. This, in turn, would be expected to cause microvoid nucleation on a finer scale. Cowie, et al [1989] suggested that 100 nm alloy carbides of the $M_{23}C_6$ variety were responsible for microvoid nucleation controlled, shear localization in several ultrahigh strength steels.

To check the validity of the above hypothesis, high resolution SEM metallography was performed on metallographic sections through both the DQ and Q&T steels. SEM micrographs of the microstructures of both steels are presented in Figures 55 through 58. The microstructure of the DQ steel (Figures 55

and 56) can be characterized as a mixed martensite-bainite structure with a fine dispersion of carbides with less than 1 micron diameters in the matrix, and a network of fine carbides decorating prior austenite grain boundaries. For the DQ steel, the carbides within the prior austenite grains were aligned with the direction of growth of bainite needles. The Q&T steel (Figures 57 and 58) displayed a tempered martensitic structure with a random dispersion of carbides in the matrix, and carbides at prior austenite grain boundaries.

The principle difference, therefore, in carbide morphology and dispersion between the two steels lies in the more ordered dispersion of carbides in the DQ steel as opposed to the Q&T steel. The carbides in both steels appeared to be of similar size. Those in the DQ steel generally appeared slightly elongated in the direction of growth of the bainite needles, while those in the Q&T steel appeared to be more equiaxed. The critical stress for microvoid nucleation has been shown to depend on the interparticle spacing to particle radius ratio [Argon, Im and Safoglu, 1975]. The carbide particles in both steels were shown to be of similar size, however, those in the DQ steel, being aligned in the direction of growth of the bainite needles, tended to have local interparticle spacings which were closer than those in the Q&T steel. In accordance with the above, this would tend to argue for microvoid nucleation on a finer scale in the DQ steel, which was

consistent with the metallographic and fractographic evidence obtained for the present study. More conclusive evidence would require transmission electron microscopy (TEM) examinations of the carbide particles and dislocation sub-structures of the two steels.

An alternative rationale for the observation of enhanced shear localization in the DQ steel, relative to the Q&T steel, could be based on the difference in Nickel (Ni) content between the steels. As shown in Table 1, the Q&T steel had 5% Ni while the DQ steel had only 1% Ni. Nickel in alpha iron has been shown to enhance the capability for cross-slip [Jolley, 1967; Floreen, Hayden and Devine, 1970], thereby providing increased resistance to localization of plastic flow. The DQ steel, with a decreased Ni content relative to the Q&T steel, would therefore be predicted to have less cross-slip and hence an increased tendency for localization of plastic flow.

SUMMARY and CONCLUSIONS

This work examined the shear localization behavior of two medium-to-high strength steels over several orders of magnitude in loading rate. The steels evaluated were similar in yield strength level, but had different levels of toughness and capacities for strain hardening. These differences in mechanical and fracture properties were largely the result of different processing techniques. The tougher steel with greater strain hardening capacity was direct quenched (DQ) and exhibited a martensitic-bainitic microstructure. The second steel was conventionally quenched and tempered (Q&T) and displayed a martensitic microstructure. Dual Notched Shear (DNS) specimens incorporating fatigue precracks were used. The objectives of this investigation were measurement of energy density variations with loading rate, estimation of the temperatures achieved in the shear zones of the specimens, and examination of the micromechanisms of localized shear deformation as related to the microstructures of the steels.

The focus of this work was on evaluating the mechanism(s) of the shear localization processes in the two steels. The majority of literature on the topic of shear localization in steels maintains that the localization is driven by the competing effects of strain hardening and thermal softening due to localized deformation heating. This thermo-mechanical model predicts that shear localization will occur at the instability

where thermal softening overcomes the materials' capacity for strain hardening. It is further predicted that if the deformation heating is great enough, phase transformations may occur in the shear zone leading to development of a "transformed" shear band. Such models have, at least in part, been verified by very high rate testing of high strength steels, where transformed shear bands have been observed experimentally and thermal conditions were assumed to be adiabatic.

This work has examined the lower strain rate regime which is more applicable to the response of structures to mechanical impact. Fatigue cracks, another feature commonly encountered in engineering structures, were incorporated in the DNS specimens used to evaluate the shear localization behavior. This study, for the first time, examined the shear localization process in steels with fatigue cracks in the lower strain rate regime, while assessing compliance with adiabatic conditions through temperature measurements.

A significant portion of this investigation was devoted to the development of a test procedure that could be successfully employed in the evaluation of the shear localization behavior of steels containing fatigue cracks. Essential features of the loading apparatus included: (1) a rigid test specimen support structure which was designed to minimize bending of the DNS specimens; (2) high frequency response transducers for load and

displacement measurements and; (3) employment of thin film thermocouples for temperature measurement.

It was found that energy density increased with increasing loading rate for both steels. The highest values for energy density were those for the impact rate tests of the DQ steel. Shear zone temperatures estimated from thermocouple measurements for the impact rate tests were shown to be in the range of 120°C (248°F). Evaluation of the test data using a dimensionless rate-thermal diffusivity parameter [Sung and Achenbach, 1987], indicated that adiabatic conditions were not achieved in the shear zones of specimens from both steels, even at the impact test rate. Detailed post-test metallurgical examinations of the shear zone regions of the DNS specimens provided no evidence of transformed shear bands. Both steels were observed to exhibit deformed shear bands over the the entire range of loading rates. Metallographic results from the impact rate tests of the both steels suggest that a microvoid nucleation mechanism controlled the shear localization process in these steels.

The following conclusions can be drawn from this study:

(1) Shear zone widths in the fatigue precracked DNS specimens of both the Q&T and DQ steels were shown to decrease with increased test rate. The shear zone widths were found to be less than the clearance between the specimen and the shear

loading apparatus. This was attributed to the presence of the fatigue cracks as similar studies performed without precracks [Dowling and Harding 1970, Campbell and Ferguson, 1970], have shown shear zone widths exceeding the clearance of the test die. This result suggests that the presence of the fatigue cracks enhanced the tendency for shear localization in both steels which is in agreement with the conclusions of Kalthoff and Winkler [1986] for higher rate shear tests on high strength steels containing fatigue cracks.

(2) Measurement of the energy densities in the shear zones of the DNS specimens indicated an increasing trend with loading rate for both steels. The highest values for energy density were those for the impact rate tests of the DQ steel. Maximum loads achieved in the DQ steel impact rate tests were observed to be only slightly greater than those for the dynamic case; while maximum loads for the Q&T steel tests continued to increase throughout the range of loading rates. The higher values for energy density and the limiting trend observed for the maximum load behavior, suggests that the DQ steel has an enhanced tendency for shear localization with increased loading rate.

(3) The enhanced tendency for shear localization with increased loading rate for the DQ steel is supported by metallographic examinations showing greatly reduced bending deformation in the central sections of the DNS specimens for the impact rate tests

in comparison with the quasi-static and dynamic tests. Bending deformation in the impact rate Q&T steel tests was shown to increase with loading rate.

(4) A well defined shear band with a different etching response than the bulk material, was obtained with the DQ steel tested at the impact rate. This band was not a "transformed" band commonly described in the literature, but was found to consist largely of microvoids with diameters in the range of 0.1 micron. This observation suggests that the shear localization process in this steel, under the conditions imposed, is controlled by nucleation of microvoids, rather than a thermo-mechanical instability. SEM fractographs of the Q&T steel tested at the impact rate also exhibited microvoids which were generally larger and more varied in diameter than those observed in the DQ steel and were observed to coalesce into larger elongated holes. This observation suggests that the shear localization behavior of the Q&T steel is controlled by nucleation and growth of microvoids.

(5) Estimations of shear zone temperatures from thermocouple measurements indicated that the maximum temperatures achieved in the impact rate tests of both steels were in the range of 120°C (248°F). This also suggests that the shear localization was not driven by a thermo-mechanical instability process as such temperatures would not significantly influence the deformation behavior of high strength steels.

(6) Shear zone temperatures estimated from energy absorption considerations were found to significantly exceed those predicted from thermocouple measurements. This is due to the assumption of adiabatic conditions in the calculations for obtaining shear zone temperatures from absorbed energy. Adiabatic conditions were demonstrated not to exist in either the dynamic or impact rate tests for both steels. A dimensionless rate-thermal diffusivity parameter [Sung and Achenbach, 1987] was employed to make this determination.

SUGGESTIONS FOR FUTURE WORK

Adiabatic conditions were not achieved even at the highest loading rates employed in this study. Higher loading rate tests, in closer proximity to the adiabatic limit, would yield useful information on the nature of what are called "transformed" shear bands. Neither this work nor other work in the literature, has produced direct conclusive evidence of phase transformations occurring in white-etching (transformed) shear bands.

This work produced evidence suggesting that microvoid nucleation was the controlling mechanism in the shear localization behavior of the DQ steel that was examined. A more detailed metallurgical investigation, involving transmission electron microscopy, would define which microstructural features (E.G., carbides, dislocation cell structure) affect the void nucleation mechanism.

BIBLIOGRAPHY

ASM Metals Handbook, Ninth Edition, Volume 1, American Society for Metals, pp. 403 - 445, 1978

Backman, M.E. and Finnegan, S.A., "The Propagation of Adiabatic Shear," in Metallurgical Effects at High Strain Rates, edited by R.W. Rohde, B.M. Butcher, J.R. Holland and C.H. Karnes, TMS/AIME, pp. 531 - 544, 1973

Bodner, S.R. and Partom, Y., "Constitutive Equations for Elastic-Viscoplastic Strain-Hardening Materials," J. Appl. Mech., Vol. 42, pp. 385 - 389, 1975

Bourne, L., "Effect of High Speed Deformation on Steel," Journal of the Iron and Steel Institute, pp. 374 - 376, August, 1950

Bridgman, P.W., "Effects of High Shearing Stresses Combined with High Hydrostatic Pressures", Physical Review, Vol. 48, pp. 825 - 847, November, 1935

Bridgman, P.W., "Flow Phenomena in Heavily Stressed Metals", Journal of Applied Physics, Vol. 8, pp. 328 - 336, May, 1937

Bryant, J.D., Makel, D.D. and Wilsdorf, H.G.F., "Observations on the Effect of Temperature Rise at Fracture in Two Titanium Alloys", Materials Science and Engineering, Vol. 77, pp. 85 - 93, 1986

Campbell, J.D. and Duby, J., "The Yield Behavior of Mild Steel in Dynamic Compression," Proc. Roy. Soc. A, Vol. 236, pp. 24 - 40, 1956

Campbell, J.D. and Ferguson, W.G., "The Temperature and Strain-rate Dependence of the Shear Strength of Mild Steel," Phil. Mag., Vol. 21, pp. 63 - 82, 1970

Clark, D.S. and Datwyler, G., "Stress-Strain Relations Under Tension Impact Loading", Proceedings of ASTM, 38, pp. 98 - 111, 1938

Clark, D.S. and Wood, D.S., "The Time Delay for the Initiation of Plastic Deformation at Rapidly Applied Constant Stress," Proc., ASTM, Vol. 49, pp. 717 - 737, 1949

Clark, D.S. and Duwez, P.E., " The Influence of Strain Rate on Some Tensile Properties of Steel", Proceedings of ASTM, Vol. 50, pp. 560 - 576, 1950

Clark, D.S. and Wood, D.S., "The Tensile Impact Properties of Some Metals and Alloys", Transactions of ASM, Vol. 42, pp. 45 - 74, 1950

Clark, D.S., "The Behavior of Metals Under Dynamic Loading", Transactions of ASM, Vol. 46, pp. 34 - 62, 1953

Colas, R. and Sellars C.M., "Strain Distribution and Temperature Increase During Plane Strain Compression Testing," Journal of Testing and Evaluation, Vol. 15, No. 6, pp. 342 - 349, Nov., 1987

Cooper, R.H. and Campbell, J.D., "Testing of Materials at Medium Rates of Strain," Journal of Mechanical Engineering Science, Vol. 9, No. 4, pp. 278 - 284, 1967.

Costin, L.S., Crisman, E.E., Hawley, R.H. and J. Duffy, "On the Localization of Plastic Flow in Mild Steel Tubes Under Dynamic Torsional Loading," Inst. Phys. Conf. Ser. No. 47, pp. 90 - 101, 1979

Costin, L.S., A Study of The Formation of Adiabatic Shear Bands in Mild Steel Under Dynamic Loading," Proceedings of The Joint Conference on Experimental Mechanics, Oahu-Maui, Hawaii, pp. 662 - 667, May, 1982

Cottrell, A.H., "Affect of Solute Atoms on the Behavior of Dislocations," Conference on Strength of Solids, Phys. Soc. of London, p. 30, 1948

Cottrell, A.H. and Bilby, B.A., "Dislocation Theory of Yielding and Strain Aging of Iron," Proc. Phys. Soc. of London, A, Vol. 62, Pt. 1, p. 49, 1949

Cottrell, A.H., "The Yield Point in Single Crystal and Polycrystalline Metals," Symposium on the Plastic Deformation of Crystalline Solids, Mellon Institute, Pittsburgh, p. 60, May, 1960

Cowie, J.G., Azrin, M. and Olson, G.B., "Microvoid Formation During Shear Deformation of Ultrahigh Strength Steels," Metallurgical Transactions A, Vol. 20A, pp. 143 - 153, January, 1989

Culver, R.S., "Thermal Instability Strain in Dynamic Plastic Deformation," in Metallurgical Effects at High Strain Rates, edited by R.W. Rohde, B.M. Butcher, J.R. Holland and C.H. Karnes, TMS/AIME, pp. 519 - 530, 1973

Curran, D.R., Seaman, L. and Shockey, D.A., "Dynamic Failure of Solids", Physics Reports, Vol. 147, Nos. 5 and 6, pp. 253 - 338, March, 1987

Dao, K.C. and Shockey D.A., "A Method for Measuring Shear band Temperatures", Journal of Applied Physics, Vol. 50, pp. 8244 - 8247, December, 1979

DeArdo, A.J., "Accelerated Cooling: A Physical Metallurgy Perspective," Canadian Metallurgical Quarterly, Vol. 27, No. 2, pp. 141 - 154, 1988

DeForest, A.V., MacGregor, C.W.and Anderson, A.R., "Rapid Tension Tests Using The Two Load Method", Transactions of AIME, 150, pp. 301 - 308, 1942

Doyle, et al., Manufacturing Processes and Materials for Engineers, 2nd. Ed., Prentice-Hall Inc., Inglewood Cliffs, N.J., pp. 266 - 274, 1969

Dowling, A.R., and Harding, J., in Proc. 1st Intl. Conf. of Center for High Energy Forming, University of Denver, Denver, Colorado, 1967

Dowling, A.R, Harding, J. and Campbell, J.D., The Dynamic Punching of Metals, Journal of The Institute of Metals, Vol. 98, pp. 215 - 224, 1970

Duwez, P.E. and Clark, D.S., "An Experimental Study of the Propagation of Plastic Deformation Under Conditions of Longitudinal Impact", Proceedings, ASM, Vol. 47. pp. 502 - 531, 1947

Eleiche, A.M. and Campbell, J.D., "Strain-rate Effects During Reverse Torsional Shear," Exp. Mech., Vol. 16, pp. 281 - 290, 1975

Ernst, H.A., Paris, P.C., and Landes, J.D., "Estimations on J-Integral and Tearing Modulus (T) from a Single Specimen Test Record," ASTM STP 743, American Society for Testing and Materials, pp. 476 - 502, 1981

Floreen, S., Hayden, H.W. and Devine, T.M., "Cleavage Initiation in Fe-Ni Alloys," Met. Trans., Vol. 2, pp. 1403 - 1406, May 1971

Frank, F.C. and Read, W.T., "Multiplication Processes for Slow Moving Dislocations," Physics Review, Vol. 79, p. 722, 1950

Frantz, R.A. and Duffy, J., "The Dynamic Stress-Strain Behavior in Torsion of 1100-0 Aluminum Subjected to a Sharp Increase in Strain Rate," J. Appl. Mech., Vol. 39, pp. 939 - 945, 1972

Giovanola, J.H., "Adiabatic Shear Banding Under Pure Shear Loading. Part I: Direct Observation of Strain Localization and Energy Dissipation Measurements", Mechanics of Materials, Vol. 7, pp. 59 - 71, 1988

Giovanola, J.H., "Adiabatic Shear Banding Under Pure Shear Loading. Part II: Fractographic and Metallographic Observations", Mechanics of Materials, Vol. 7, pp. 73 - 87, 1988

Glenn, R.C. and Leslie, W.C., "The Nature of White Streaks in Impacted Steel Armor Plate", Metallurgical Transactions, Vol. 2, pp. 2945 - 2947, October, 1971

Hamburg, E. and Wilson, A.D., "Production and Properties, of Copper, Age Hardened Steels," in Processing, Microstructure and Properties of HSLA Steels, Edited by A.J. De Ardo, The Minerals, Metals & Materials Society, 1988

Hartley, K.A, J. Duffy and R.H. Hawley, "Measurement of the Temperature Profile During Shear Band Formation in Steels Deforming at High Strain Rates," J. Mech. Phys. Solids, Vol. 35, No. 3, pp. 283 - 301, 1987

Hasson, D.F. and Joyce, J.A., J. Eng. Mat. Tech., Vol. 103, pp. 133 -141, (1981)

Holman, J.P., Heat Transfer, McGraw-Hill Inc, 1981

Holloman, J.H. and Zener, C., "High Speed Testing of Mild Steel", Transactions of ASM, 32, pp. 111 - 122, 1944

Hoppmann, W.H., "The Velocity Aspect of Tension-Impact Testing", Proceedings of ASTM, Vol. 47, pp. 533 - 544, 1947

Hutchings, I.M., "The Behavior of Metals Under Ballistic Impact at Sub-Ordnance Velocities," in Material Behavior Under High Stress and Ultrahigh Loading Rates, Sagamore Army Materials Research Conference, 29th, Lake Placid, N.Y., pp. 161 - 196, 1982

Jolley, W., "Influence of a 3.28 pct Nickel Addition on the Yield and Fracture Behavior of Alpha Iron," Trans. Met. Soc. of AIME, Vol. 242, pp. 306 - 314, February, 1968

Kalthoff, J.F. and Winkler, S., "Fracture Behavior Under Impact", prepared for the European Research Office of the U.S. Army, London, Contract Number DAJA 45-85-C-0047, Approved for Public Release, Distribution Unlimited, 1986

Kolsky, H., "An Investigation of the Mechanical Properties of Materials at Very High Rates of Loading", Proceedings of the Physical Society, Vol. 62, pp. 676 - 699, 1949

Kramer, I.R. and Maddin, R., "Delay Time for the Initiation of Slip in Metal Single Crystals", Transactions of AIME, Journal of Metals, pp. 197 - 203, February, 1952

Lemaire, J.C. and Backofen, W.A., "Adiabatic Instability in the Orthogonal Machining of Steel", Metallurgical Transactions, Vol.3. pp. 477 - 481, February, 1972

Lindholm, U.S. and L.M. Yeakley, "High Strain Rate Testing: Tension and Compression," Exp. Mech., Vol. 8, No. 1, pp. 1 - 9, 1968

Lindholm, U.S. and Hargreaves, C.R., "Dynamic Testing of High Strength Steels and Their Susceptibility to Inhomogeneous Shear," Proc. 2nd Intl. Conf. on Mechanical Behavior of Materials, Boston, Massachusetts, American Society for Metals, Library of Congress Catalog Card Number: 76-27115, 1976

Lindholm, U.S. and Johnson, G.R., "Strain-Rate Effects in Metals at Large Shear Strains," in Material Behavior Under High Stress and Ultrahigh Loading Rates, Sagamore Army Materials Research Conference, 29th, Lake Placid, N.Y., pp. 61 - 79, 1982

Liss, R.B., Acta Metallurgica, Vol. 5, p. 342, 1957

MacGregor, C.W., "A Two Load Method of Determining the Average True Stress-True Strain Curve in Tension", Journal of Applied Mechanics, V. 61, pp. A156 - A158, December, 1939

MacGregor, C.W., "The Tension Test", Proceedings of ASTM, Vol. 40, pp. 508 - 534, 1940

MacGregor C.W. and Fisher, J.C., "Relations Between the Notched Beam Impact Test and The Static Tension Test", Journal of Applied Mechanics, pp. A-28-A-34, March, 1944

Manion, S.A. and Stock, T.A.C., "Adiabatic Shear Bands in Steel," Int. Journ. of Fracture Mech., Vol. 6, pp. 106 - 107, 1970

Mann, H.C., "High Velocity Tension Impact Test," Proc. ASTM, Vol. 36, p. 85, 1936

Marchand, A. and Duffy, J., "An Experimental Study of the Formation Process of Adiabatic Shear Bands in a Structural Steel", J. Mech. Phys. Solids, Vol. 36, No. 3, pp. 251 - 283, 1988

Manganello, S.J. and Abbott, K.H., "Metallurgical Factors Affecting The Ballistic Behavior of Steel Targets", Journal of Materials, JMLSA, Vol.7, pp. 231 - 239, June, 1972

McIntire, H.O. and Manning, G.K., "Producing Martensite by Impact", Metals Progress, Vol. 74, pp. 94 - 95, 1958

Miklowitz, J., "The Initiation and Propagation of the Plastic Zone in a Tension Bar of Mild Steel as Influenced by the Speed of Stretching and Rigidity of Testing Machine", Journal of Applied Mechanics, Vol. 14, pp. A-31-A-38, 1947

Moss, G.L., "Shear Strains, Strain Rates and Temperature Changes in Adiabatic Shear Bands", U.S. Army Ballistics Research Laboratory, Technical Report ARBRL-TR-02242, Approved for Public Release, Distribution Unlimited, May, 1980

Moss, G.L. and Pond, R.B., Sr., "Inhomogeneous Thermal Changes in Copper During Plastic Elongation", Metallurgical Transactions A, Vol. 6A, June, pp. 1223 - 1235, 1975

Nadai, A. and Manjoine, M.J., "High Speed Tension Tests at Elevated Temperatures - Parts I and II", Transactions of ASME, 63, pp. A-77-A-91, 1941

Pond, R.B. and Glass, C.M., "Crystallographic Aspects of High Velocity Deformation of Aluminum Single Crystals", in Response of Metals to High Velocity Deformation, Interscience Publishers, N.Y., pp. 145 - 161, 1961

Pond, R.B. and Winter, J.M., "A Simple Determination of Von Karman Critical Velocities", Mechanics of Nondestructive Testing, edited by W.W. Stinchcomb, Plenum Press, pp. 187 - 196, 1980

Recht, "Catastrophic Thermoplastic Shear", Journal of Applied Mechanics, paper No. 63-WA-67, pp. 1 - 5, November, 1963

Reed-Hill, R.E., Physical Metallurgy Principles, 2nd Ed., D. Van Nostrand Company, New York, N.Y., pp. 343 - 346, 1973

Rice, J.R. and Levy, N. in Physics of Strength and Plasticity, Edited by A.S. Argon, Massachusetts Institute of Technology Press, Cambridge, MA, p. 177, 1969

Rogers, H.C., "Adiabatic Shearing - General Nature and Material Aspects", in Material Behavior Under High Stress and Ultrahigh Loading Rates, Sagamore Army Materials Research Conference, 29th, Lake Placid, N.Y., pp. 101 - 119, 1982

Sears, F.W., Zemansky, M.W., and Young, H.D., University Physics, Addison-Wesley Publishing, pp. 297 - 317, 1983

Semiatin, S.L., Lahoti, G.D. and Oh, S.I., "The Occurrence of Shear Bands in Metalworking", in Material Behavior Under High Stress and Ultrahigh Loading Rates, Sagamore Army Materials Research Conference, 29th, Lake Placid, N.Y., pp. 119 - 159, 1982

Senseny, P.E., Duffy, J. and Hawley, R.H., "Experiments on Strain Rate History and Temperature Effects During The Plastic Deformation of Close-Packed Metals," Transactions of the ASME, Vol. 45, pp. 60 - 66, March, 1978

Shockey, D.A. and Ehrlich, D.C., "Metallurgical Influences on Shear Band Activity", in Shock Waves and High Strain Rate Phenomena in Metals: Concepts and Applications, Albuquerque, N.M., 22-26 June, pp. 249 - 261, 1980

Staker, M.R., "On Adiabatic Shear Band Determinations by Surface Observations", Scripta Metallurgica, Vol. 14, pp. 677 - 680, 1980

Sung, J.C. and Achenbach, J.D., "Temperature at a Propagating Crack Tip in a Viscoplastic Material," Journal of Thermal Stresses, Vol. 10, pp. 243 - 262, 1987

Taylor, G.I. and Quinney, M.A., "The Latent Energy Remaining in a Metal After Cold Work", Proceedings of the Royal Society, 143, pp. 307 - 326, 1934

Taylor, G.I., "The Testing of Materials at High Rates of Loading", Journal of the Institute of Civil Engineers, 26, pp. 486 - 518, 1946

Thornton, P.A. and Heiser, F.A., "Observations on Adiabatic Shear Zones in Explosively Loaded Thick-Wall Cylinders", Metallurgical Transactions, Vol. 2, pp. 1496-1499, May, 1971

Vassilaros, M.G., Gudas, J.P. and Joyce, J.A., "Experimental Investigation of Tearing Instability Phenomena for Structural Materials," U.S. Nuclear Regulatory Commission Report, NUREG/CR-2570, REV.1, USNRC, Washington, D.C. 20555, (1982)

Von Karman, T. and Duwez, P.E., "The Propagation of Plastic Deformation in Solids", Journal of Applied Physics, Vol. 21, pp. 987-994, 1950

Vreeland, T., Wood, D.S. and Clark, D.S., "A Study of The Delayed Yield Phenomenon", Transactions of ASM, Vol. 45, pp. 620-637, 1953

Winkler, S., "Fracture Behavior Under Impact II," Final Report, prepared for the European Research Office of the U.S. Army, London under Contract Number DAJA45-85-C-0047, Approved for Public Release, Distribution Unlimited, 1987

Winlock, J. and Leiter, W.E., "Some Factors Affecting the Plastic Deformation of Sheet and Strip Steel and Their Relation to the Deep Drawing Properties", Transactions of ASM, Vol. 25, No. 1, pp. 163 - 205, March, 1937

Winter, R.E. and Hutchings, I.M.,"The Role of Adiabatic Shear in Solid Particle Erosion," Wear, Vol. 34, pp. 141 - 148, 1975

Wood, D.S. and Clark, D.S., "The Influence of Temperature Upon the Time Delay for Yielding in Annealed Mild Steel", Transactions of ASM, Vol. 43, pp. 571 - 586, 1951

Wright, P.K., "Metallurgical Effects at High Strain Rates in the Secondary Shear Zone of the Machining Operation," in Metallurgical Effects at High Strain Rates, edited by R.W. Rohde, B.M. Butcher, J.R. Holland and C.H. Karnes, TMS/AIME, pp. 547 - 558, 1973

Wright, T.W., "Some Aspects of Adiabatic Shear Bands", U.S. Army Ballistics Research Laboratory, Technical Report BRL-TR-2785, Approved for Public Release, Distribution Unlimited, March, 1987

Zener, C. and Holloman, J.H., "Effects of Strain Rate Upon Plastic Flow of Steel", Journal of Applied Physics, 15, pp. 22-32, 1944

Table 1 - Chemical Composition (wt%) of Quenched and Tempered (Q&T) and Direct Quenched (DQ) Steels

STEEL	C	Mn	Si	S	P	Cu	Ni	Cr	Mo	V
Q&T (FKS)	0.11	0.76	0.03	0.004	0.005	0.022	5.00	0.42	0.53	0.043
DQ (GOA)	0.11	0.91	0.25	0.001	0.003	0.25	1.04	0.56	0.45	0.05

Table 2 - Room Temperature Mechanical and Fracture Properties of Quenched and Tempered (Q&T) and Direct Quenched (DQ) Steels

Steel	Ultimate Tensile Strength (MPa) (ksi)	0.2% Yield Strength (MPa) (ksi)	Elongation in 2 in. (%)	Reduction of Area (%)	J_{IC} (kJ/m^2) [$in\text{-}lbs/in^2$]	T Material
Q&T (FKS)	(1048) [152]	(952) [138]	21	55	(150) [857]	12
DQ (GOA)	(1124) [163]	(979) [142]	23	68	(188) [1075]	17

Table 3 - Test Matrix for Dual Notched Shear (DNS) Specimens

Specimen	Material	Loading Rate
GOA-11	DQ Steel	Quasi-Static
FKS-6	Q&T Steel	Quasi-Static
GOA-10	DQ Steel	Dynamic
FKS-4	Q&T Steel	Dynamic
FKS-8	Q&T Steel	Dynamic
GOA-7	DQ Steel	Impact
GOA-8	DQ Steel	Impact
GOA-9	DQ Steel	Impact
FKS-3	Q&T Steel	Impact
FKS-5	Q&T Steel	Impact
FKS-2	Q&T Steel	Impact

Table 4 - Thin Film Thermocouple Calibration Results

Condition	Temperature Conventional Type K (°C) [°F]	Temperature Thin Film Type K (°C) [°F]
Ice-water Bath	(0.17°) [32.3°]	(0.06°) [32.1°]
Boiling Water	(99.89°) [211.8°]	(99.94°) [211.9°]

Table 5 - Results of Measurements of Dual Notched Shear (DNS) Specimens

Specimen I.D.	Material	Loading Rate	Width W (mm) [in]	Thickness B (mm) [in]	Remaining Ligament b_o (A) (mm) [in]	b_o (B) (mm) [in]
GOA-11	DQ Steel	Quasi-Static	(23.4) [0.923]	(10.2) [0.400]	(3.89) [0.153]	(3.91) [0.154]
FKS-6	Q&T Steel	Quasi-Static	(22.9) [0.900]	(10.1) [0.399]	(3.86) [0.152]	(3.81) [0.150]
GOA-10	DQ Steel	Dynamic	(23.4) [0.923]	(10.2) [0.401]	(3.89) [0.153]	(3.86) [0.152]
FKS-4	Q&T Steel	Dynamic	(23.3) [0.918]	(10.1) [0.398]	(3.93) [0.155]	(4.01) [0.158]
FKS-8	Q&T Steel	Dynamic	(23.4) [0.920]	(10.1) [0.398]	(3.99) [0.157]	(3.91) [0.154]
GOA-7	DQ Steel	Impact	(23.4) [0.922]	(10.1) [0.398]	(3.91) [0.154]	(3.79) [0.149]
GOA-8	DQ Steel	Impact	(23.4) [0.920]	(10.1) [0.398]	(3.99) [0.157]	(3.96) [0.156]
GOA-9	DQ Steel	Impact	(23.8) [0.924]	(10.2) [0.400]	(3.51) [0.138]	(3.53) [0.139]
FKS-3	Q&T Steel	Impact	(23.3) [0.919]	(10.2) [0.400]	(4.14) [0.163]	(4.04) [0.159]
FKS-5	Q&T Steel	Impact	(23.3) [0.918]	(10.1) [0.398]	(3.89) [0.153]	(3.99) [0.157]
FKS-2	Q&T Steel	Impact	(23.4) [0.920]	(10.1) [0.398]	(3.99) [0.157]	(3.99) [0.157]

Table 6 - Post-Test Measurements of Thin Film Thermocouple Positions on Dual Notched Shear (DNS) Specimens

Specimen I.D.	Material	Loading Rate	Inner Thermocouple Position T(i) X (mm) [in]	Inner Thermocouple Position T(i) Y (mm) [in]	Outer Thermocouple Position T(o) X (mm) [in]	Outer Thermocouple Position T(o) Y (mm) [in]
GOA-11	DQ Steel	Quasi-Static	(0.660) [0.026]	(0.711) [0.028]	---	---
FKS-6	Q&T Steel	Quasi-Static	(0.711) [0.028]	(0.762) [0.030]	---	---
GOA-10	DQ Steel	Dynamic	(0.711) [0.028]	(0.660) [0.026]	(1.676) [0.066]	(0.660) [0.026]
FKS-4	Q&T Steel	Dynamic	(0.635) [0.025]	(0.711) [0.028]	(1.702) [0.067]	(0.610) [0.024]
FKS-8	Q&T Steel	Dynamic	(0.610) [0.024]	(0.635) [0.025]	(2.032) [0.080]	(0.635) [0.025]
GOA-7	DQ Steel	Impact	(0.356) [0.014]	(0.559) [0.022]	(1.880) [0.074]	(0.559) [0.022]
GOA-8	DQ Steel	Impact	(0.940) [0.037]	(0.711) [0.028]	(2.032) [0.080]	(0.711) [0.028]
GOA-9	DQ Steel	Impact	(0.914) [0.036]	(0.660) [0.026]	(2.134) [0.084]	(0.508) [0.020]
FKS-3	Q&T Steel	Impact	(0.940) [0.037]	(0.711) [0.028]	(2.159) [0.085]	(0.711) [0.028]
FKS-5	Q&T Steel	Impact	(0.864) [0.034]	(0.635) [0.025]	(2.108) [0.083]	(0.635) [0.025]
FKS-2	Q&T Steel	Impact	(0.864) [0.034]	(1.016) [0.040]	(2.007) [0.079]	(0.686) [0.027]

X = Distance From the Fracture Surface (Figure 5)
Y = Distance Ahead of The Fatigue Crack Tip (Figure 5)

Table 7 - Results of Dual Notched Shear Specimen Tests of Quenched and Tempered (Q&T) and Direct Quenched (DQ) Steels at Quasi-Static and Dynamic Loading Rates

Specimen I.D.	Displacement Rate (mm/sec) [in/sec]	Maximum Load (kN) [lbs]	Time to Maximum Load	Maximum Displacement (mm) [in]	Delta T(i) Maximum (^{o}C) [^{o}F]	Delta T(o) Maximum (^{o}C) [^{o}F]	Energy Absorbed (J) [in-lbs]	Energy Area (J/mm^2) [$in\text{-}lbs/in^2$]
GOA-11	(0.010) [0.0004]	(56.3) [12,650]	197s	(0.762) [0.030]	(1.22) [2.2]	--- ---	(36.6) [324]	(0.460) [2630]
FKS-6	(0.012) [0.0005]	(49.6) [11,150]	140s	(0.711) [0.028]	(0.67) [1.2]	--- ---	(29.8) [264]	(0.384) [2196]
GOA-10	(30.5) [1.2]	(74.3) [16,706]	34.8ms "	(0.813) [0.032]	(14 @ 100ms) [26 @ 100ms]	(6 @ 160ms) [10 @ 160ms]	(54.1) [479]	(0.685) [3913]
FKS-4	(38.1) [1.5]	(59.5) [13,378]	22.5ms "	(0.762) [0.030]	(17 @ 90ms) [30 @ 90ms]	(4 @ 160ms) [7 @ 160ms]	(38.6) [342]	(0.483) [2763]
FKS-8	(33.0) [1.3]	(57) [12,815]	27.4ms "	(0.813) [0.032]	(9 @ 140ms) [16 @ 140ms]	(7 @ 220ms) [12 @ 220ms]	(36.1) [320]	(0.453) [2589]

Table 8 - Results of Dual Notched Shear Specimen Tests of Quenched and Tempered (Q&T) Direct Quenched (DQ) Steels at Impact Loading Rate

Specimen I.D.	Displacement Rate (mm/sec) [in/sec]	Maximum Load (kN) [lbs]	Time to Maximum Load (ms)	Maximum Displacement (mm) [in]	Delta T(i) Maximum (^{o}C) [^{o}F]	Delta T(o) Maximum (^{o}C) [^{o}F]	Energy Absorbed (J) [in-lbs]	Energy Area (J/mm^2) [in-lbs/in^2]
GOA-7	(559) [22]	(76.9) [17,302]	2.4 "	(0.559) [0.022]	(16 @ 20ms) [28 @ 20ms]	(6 @ 100ms) [10 @ 100ms]	(35.3) [312]	(0.454) [2587]
GOA-8	(508) [20]	(75.7) [17,012]	2.4 "	(0.762) [0.030]	(19 @ 40ms) [34 @ 40ms]	(8 @ 110ms) [14 @ 110ms]	(48.8) [432]	(0.605) [3484]
GOA-9	(203) [8]	(86.2) [19,368]	2.7 "	(0.305) [0.012]	(12 @ 35ms) [21 @ 35ms]	(4 @ 140ms) [7 @ 140ms]	(19.1) [169]	(0.266) [1520]
FKS-3	(508) [20]	(84.5) [18,992]	2.7 "	(0.559) [0.022]	--- ---	--- ---	(39.7) [351]	(0.477) [2721]
FKS-5	(686) [27]	(82.8) [18,616]	2.6 "	(0.584) [0.023]	(18 @ 70ms) [32 @ 70ms]	(5 @ 160ms) [8 @ 160ms]	(38.9) [344]	(0.489) [2792]
FKS-2	(914) [36]	(86.5) [19,453]	2.7 "	(0.686) [0.027]	(30 @ 60ms) [54 @ 60ms]	(12 @ 160ms) [22 @ 160ms]	(47.2) [418]	(0.585) [3344]

Table 9 - Shear Zone Widths, Volumes, Strains and Strain Rates for DNS Specimens (Thermocouple (Side A) Fracture Surfaces)

Specimen I.D.	Material	Shear Zone Width (mm)	Shear Zone Width (in)	Shear Zone Volume (mm^3)	Shear Zone Volume (in^3)	Shear Strain at Maximum Displacement	Shear Strain Rate
GOA-11	DQ Steel	0.194	0.0076	7.70	0.000470	3.9	0.052
FKS-6	Q&T Steel	0.237	0.0093	9.24	0.000564	3.0	0.051
GOA-10	DQ Steel	0.161	0.0063	6.39	0.000390	5.0	189
FKS-4	Q&T Steel	0.177	0.0070	7.03	0.000429	4.3	215
FKS-8	Q&T Steel	0.153	0.0060	6.17	0.000376	5.3	216
GOA-7	DQ Steel	0.109	0.0043	4.30	0.000263	5.1	5128
GOA-8	DQ Steel	0.142	0.0056	5.72	0.000349	5.4	3577
GOA-9	DQ Steel	0.110	0.0043	3.94	0.000240	2.8	1845
FKS-3	Q&T Steel	0.127	0.0050	5.36	0.000327	4.4	4000
FKS-5	Q&T Steel	0.109	0.0043	4.28	0.000261	5.4	6294
FKS-2	Q&T Steel	0.111	0.0044	4.47	0.000273	6.2	8234

Table 10 - Shear Zone Widths, Volumes, Strains and Strain Rates for DNS Specimens (Side B Fracture Surfaces)

Specimen I.D.	Material	Shear Zone Width (mm)	Shear Zone Width (in)	Shear Zone Volume (mm^3)	Shear Zone Volume (in^3)	Shear Strain at Maximum Displacement	Shear Strain Rate
GOA-11	DQ Steel	0.262	0.0103	10.45	0.000638	2.9	0.038
FKS-6	Q&T Steel	0.214	0.0084	8.23	0.000503	3.3	0.056
GOA-10	DQ Steel	0.163	0.0064	6.42	0.000392	5.0	187
FKS-4	Q&T Steel	0.189	0.0074	7.65	0.000467	4.0	202
FKS-8	Q&T Steel	0.208	0.0082	8.21	0.000501	3.9	159
GOA-7	DQ Steel	0.155	0.0061	5.93	0.000362	3.6	3606
GOA-8	DQ Steel	0.147	0.0058	5.88	0.000359	5.2	3456
GOA-9	DQ Steel	0.107	0.0042	3.85	0.000235	2.9	1897
FKS-3	Q&T Steel	0.132	0.0052	5.44	0.000332	4.2	3848
FKS-5	Q&T Steel	0.106	0.0042	4.27	0.000261	5.5	6472
FKS-2	Q&T Steel	0.115	0.0045	4.63	0.000283	6.0	7948

Table 11 - Additional Deformed Volumes Associated With Bending Deformation in Dual Notched Shear (DNS) Specimens

Specimen	Material	Loading Rate	Volume Associated With Side A (mm^3)	Volume Associated With Side A (in^3)	Volume Associated With Side B (mm^3)	Volume Associated With Side B (in^3)
GOA-11	DQ Steel	Quasi-Static	6.70	0.00041	7.29	0.00044
FKS-6	Q&T Steel	Quasi-Static	2.60	0.00016	5.70	0.00035
GOA-10	DQ Steel	Dynamic	5.30	0.00032	5.10	0.00031
FKS-4	Q&T Steel	Dynamic	3.20	0.00020	3.40	0.00021
FKS-8	Q&T Steel	Dynamic	3.70	0.00023	2.30	0.00014
GOA-7	DQ Steel	Impact	0.55	0.00003	6.20	0.00038
GOA-8	DQ Steel	Impact	1.45	0.00009	3.60	0.00022
GOA-9	DQ Steel	Impact	0.40	0.00002	6.20	0.00038
FKS-3	Q&T Steel	Impact	4.30	0.00026	1.50	0.00009
FKS-5	Q&T Steel	Impact	2.10	0.00013	3.30	0.00020
FKS-2	Q&T Steel	Impact	2.65	0.00016	2.90	0.00018

Table 12 - "Y" Dimension of Bending Deformation in Central Section of Dual Notched Shear (DNS) Specimens (Figures 28-33, A Side Fracture Surfaces)

Specimen	Material	Loading Rate	"Y" Dimension of Bending Deformation (mm)	(in)
GOA-11	DQ Steel	Quasi-static	0.63	0.2469
FKS-6	Q&T Steel	Quasi-static	0.32	0.1272
GOA-10	DQ Steel	Dynamic	0.72	0.2843
FKS-4	Q&T Steel	Dynamic	0.48	0.1870
FKS-8	Q&T Steel	Dynamic	0.59	0.2319
GOA-7	DQ Steel	Impact	0.13	0.0524
GOA-8	DQ Steel	Impact	0.13	0.0516
GOA-9	DQ Steel	Impact	0.11	0.0449
FKS-3	Q&T Steel	Impact	0.68	0.2693
FKS-5	Q&T Steel	Impact	0.40	0.1571
FKS-2	Q&T Steel	Impact	0.39	0.1531

Table 13 - Dual Notched Shear (DNS) Specimen Shear Zone Energy Densities and Temperatures Calculated from Absorbed Energy for Thermocouple Side (Side A) Shear Zones

Specimen I.D.	Material	Total Energy for Specimen (J)	Total Energy for Specimen (in-lbs)	Energy Associated with Side A Zone (J)	Energy Associated with Side A Zone (in-lbs)	Energy/Total Deformed Volume (J/mm^3)	Energy/Total Deformed Volume ($in\text{-}lbs/in^3$)	Estimated Maximum Temperature in Shear Zone (^oC)	Estimated Maximum Temperature in Shear Zone (^oF)
GOA-11	DQ Steel	36.6	324	14.0	146	0.972	165700	264	506
FKS-6	Q&T Steel	29.8	264	14.2	119	1.196	163971	324	615
GOA-10	DQ Steel	54.1	479	24.2	215	2.075	303554	562	1044
FKS-4	Q&T Steel	38.6	342	16.6	154	1.627	244520	441	826
FKS-8	Q&T Steel	36.1	320	13.6	144	1.383	237161	375	707
GOA-7	DQ Steel	35.3	312	15.7	141	3.194	472303	865	1590
GOA-8	DQ Steel	48.8	432	23.2	194	3.211	442531	870	1598
GOA-9	DQ Steel	19.1	169	8.7	76	2.005	286713	543	1010
FKS-3	Q&T Steel	39.7	351	17.7	158	1.834	269244	497	927
FKS-5	Q&T Steel	38.9	344	17.5	155	2.748	395908	745	1373
FKS-2	Q&T Steel	47.2	418	20.9	188	2.908	434186	788	1450

Table 14 - Estimates of Shear Zone Temperatures From Thermocouple Measurements at Inner Location (Side A Shear Zones)

Specimen	Material	Loading Rate	Initial Temperature (°C)	Initial Temperature (°F)	Delta T(i) Maximum (°C)	Delta T(i) Maximum (°F)	Time From Maximum Load to Delta T(i) Maximum (s)	Distance From Shear Zone* (mm)	Distance From Shear Zone* (in)	Estimated Maximum Temp. in Shear Zone (°C)	Estimated Maximum Temp. in Shear Zone (°F)
GOA-10	DQ Steel	Dynamic	28	82	14	26	0.065	0.6730	0.2650	60	140
FKS-4	Q&T Steel	Dynamic	28	82	17	30	0.068	0.5970	0.2350	62	144
FKS-8	Q&T Steel	Dynamic	28	82	9	16	0.113	0.5530	0.2177	42	108
GOA-7	DQ Steel	Impact	24	76	16	28	0.017	0.3260	0.1283	59	138
GOA-8	DQ Steel	Impact	24	76	19	34	0.037	0.8450	0.3327	120	248
GOA-9	DQ Steel	Impact	24	76	12	21	0.032	0.8380	0.3299	95	203
FKS-3	Q&T Steel	Impact	---	---	---	---	---	---	---	---	---
FKS-5	Q&T Steel	Impact	23	73	18	32	0.067	0.8070	0.3177	73	163
FKS-2	Q&T Steel	Impact	23	73	30	54	0.057	0.8260	0.3252	121	250

* - Distance From Thermocouple Location to Edge of Shear Zone as Determined From Metallographic Examination

Table 15 - Calculation of Thermal Diffusivity/Rate Parameter (V*) for Dual Notched Shear (DNS) Specimens - [Sung and Achenbach, 1987]

Specimen	Material	Loading Rate	V Displacement Rate (mm/sec)	V Displacement Rate (in/sec)	L Characteristic Length Shear Zone Width (mm)	L Characteristic Length Shear Zone Width (in)	V* (L/2k)V
GOA-10	DQ Steel	Dynamic	31	1.2	0.1610	0.0634	0.21
FKS-4	Q&T Steel	Dynamic	38	1.5	0.1770	0.0697	0.29
FKS-8	Q&T Steel	Dynamic	33	1.3	0.1530	0.0602	0.22
GOA-7	DQ Steel	Impact	559	22	0.1090	0.0429	2.62
GOA-8	DQ Steel	Impact	508	20	0.1420	0.0559	3.10
GOA-9	DQ Steel	Impact	203	8	0.1100	0.0433	0.96
FKS-3	Q&T Steel	Impact	508	20	0.1270	0.0500	2.77
FKS-5	Q&T Steel	Impact	686	27	0.1090	0.0429	3.21
FKS-2	Q&T Steel	Impact	914	36	0.1110	0.0437	4.35

Table 16 - Results of Microhardness Tests on Metallographic Sections Through Dual Notched Shear (DNS) Specimens

Specimen	Material	Loading Rate	Average Hardness* Bulk (HV)	Average Hardness* Shear Zone (HV)
GOA-11	DQ Steel	Quasi-Static	317	330
FKS-6	Q&T Steel	Quasi-Static	346	354
GOA-10	DQ Steel	Dynamic	338	378
FKS-4	Q&T Steel	Dynamic	310	346
GOA-8	DQ Steel	Impact	338	454 (Deformed) 477 (Microvoid)
FKS-2	Q&T Steel	Impact	310	361

* - Average of 5 Values, 10 g Scale Used

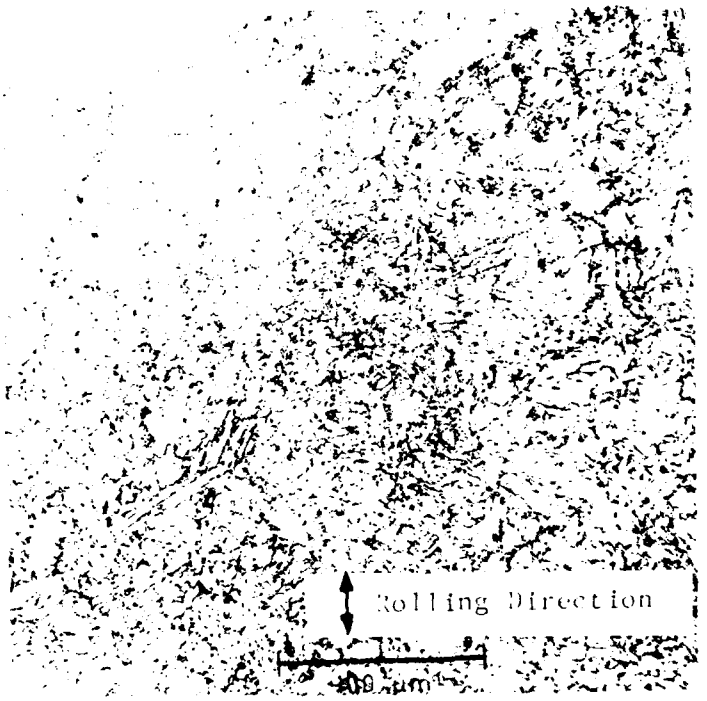

Figure 1 - Microstructure of Q&T Steel (2% Nital Etch)

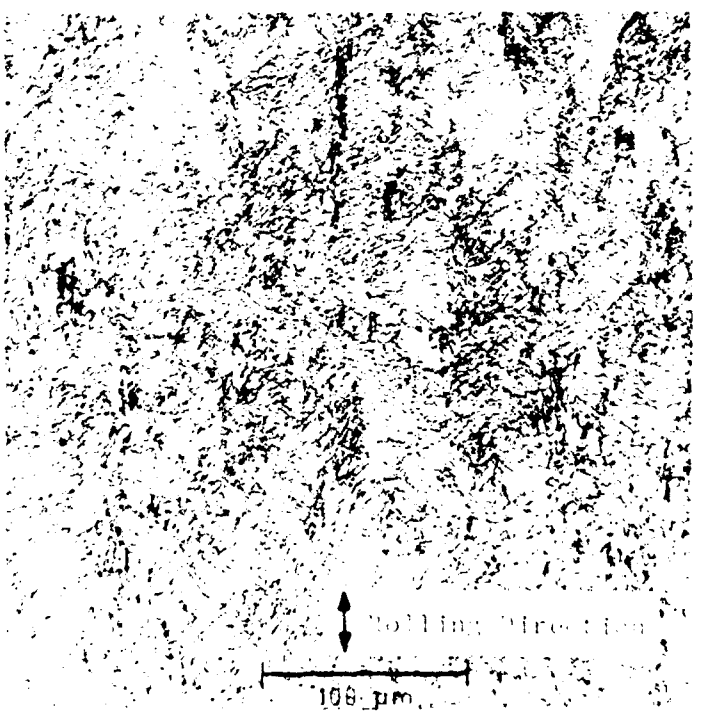

Figure 2 - Microstructure of DQ Steel (2% Nital Etch)

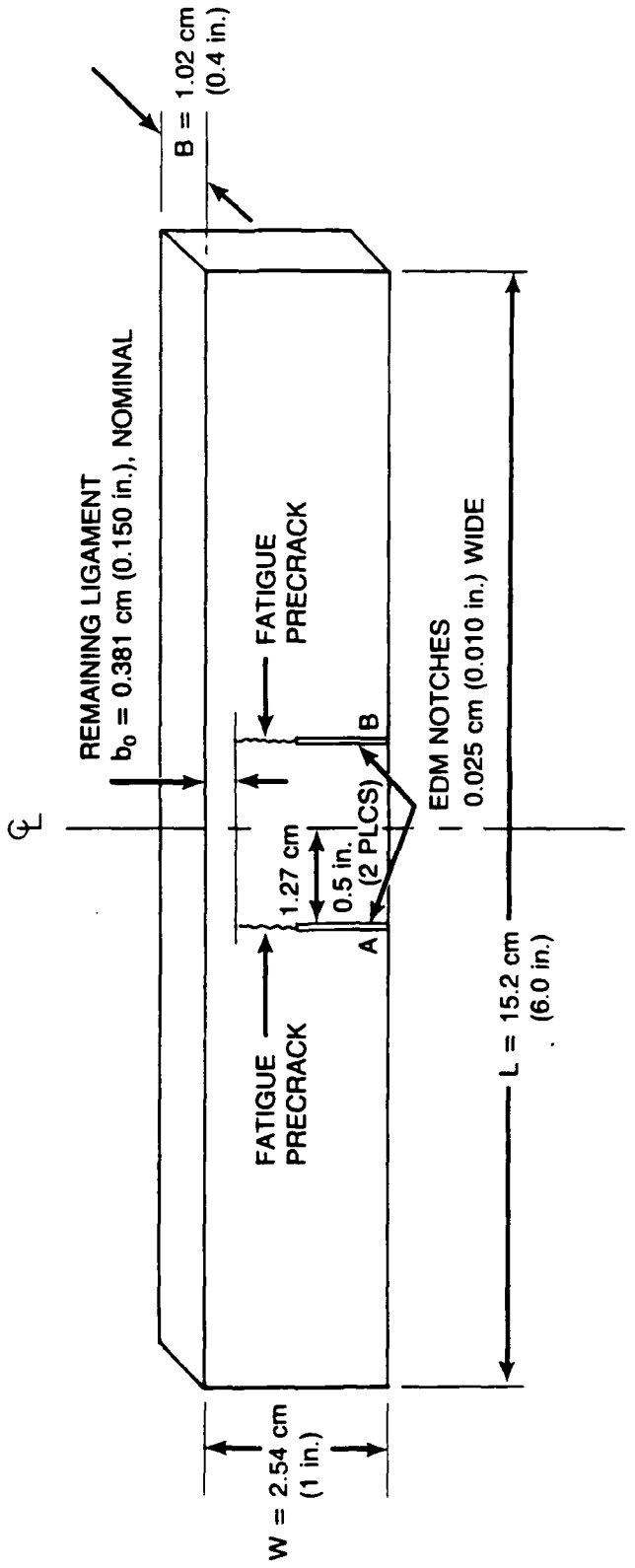

Figure 3 - Dual Notched Shear (DNS) Specimen.

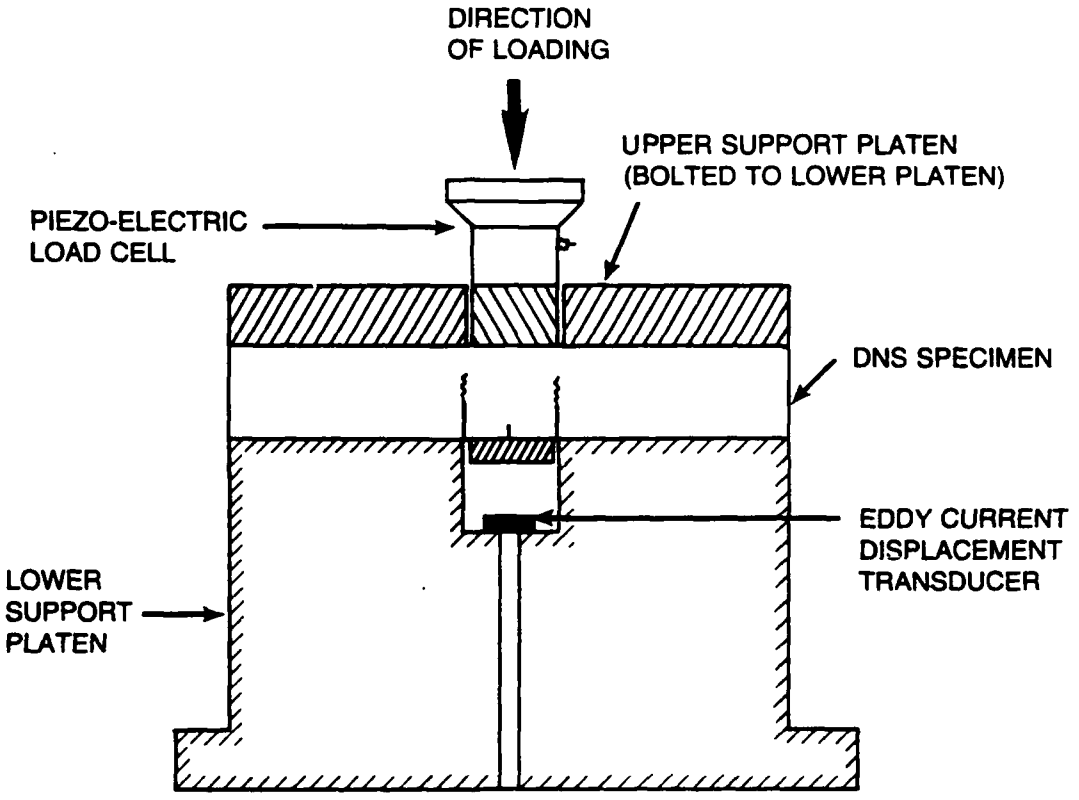

Figure 4 - Schematic of DNS Loading Apparatus.

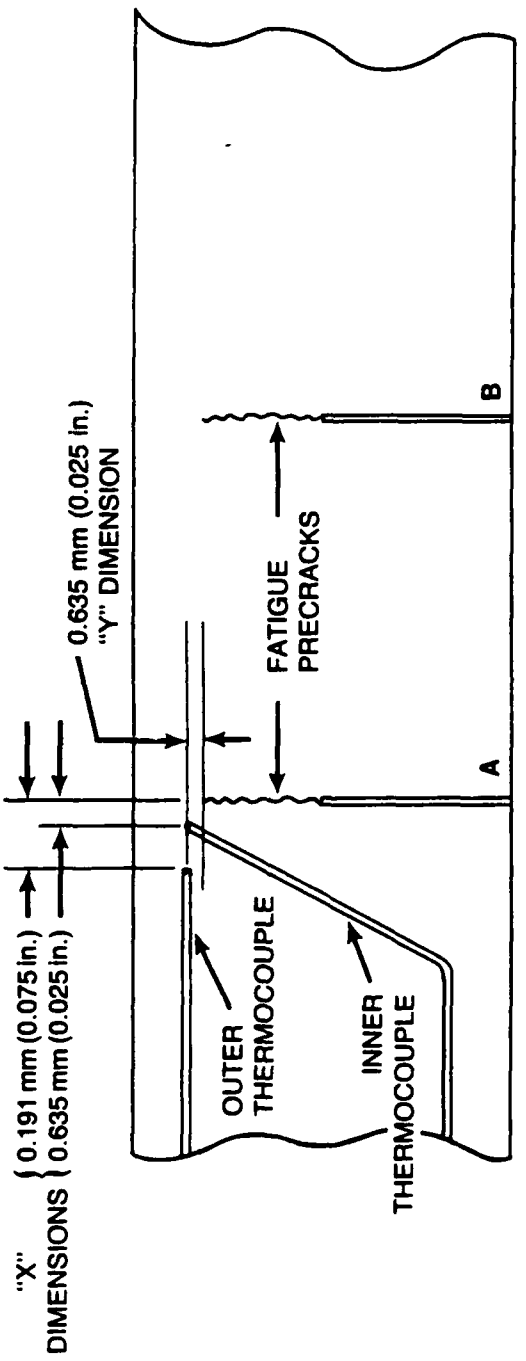

Figure 5 - Nominal Positions of Thin-Film Thermocouples on DNS Specimen.

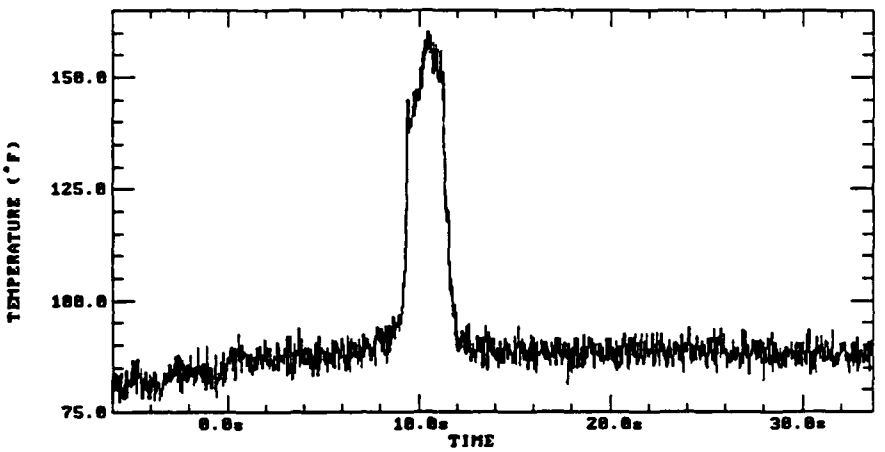

Figure 6 - Response of Thin Film Thermocouple to Point Heat Source

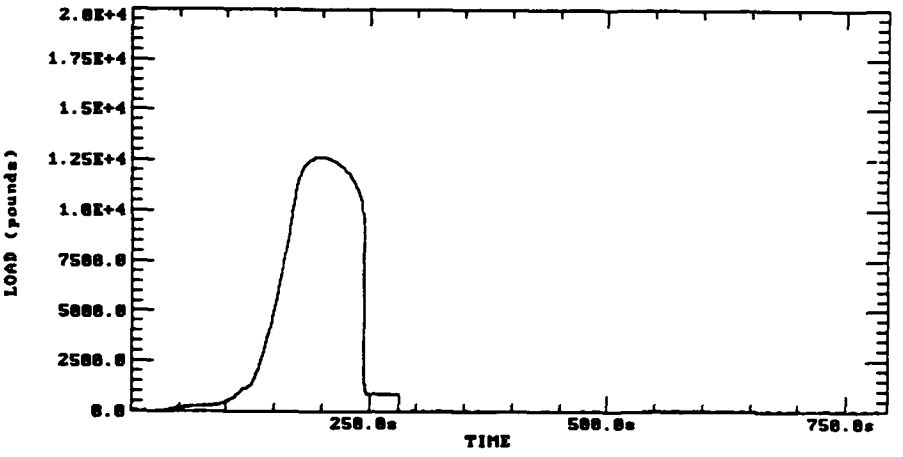

Figure 7 - Load vs. Time Record for DQ Steel Specimen GOA-11, Quasi-Static Rate

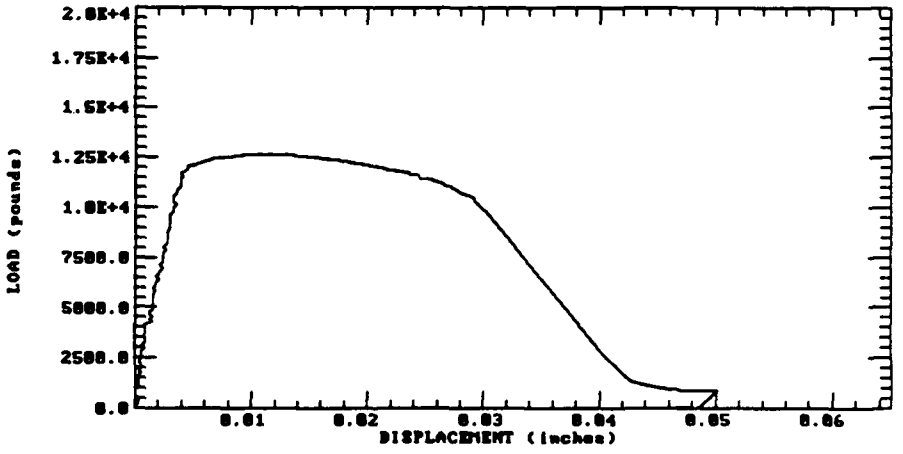

Figure 8 - Load vs. Displacement Record for DQ Steel Specimen GOA-11, Quasi-Static Rate

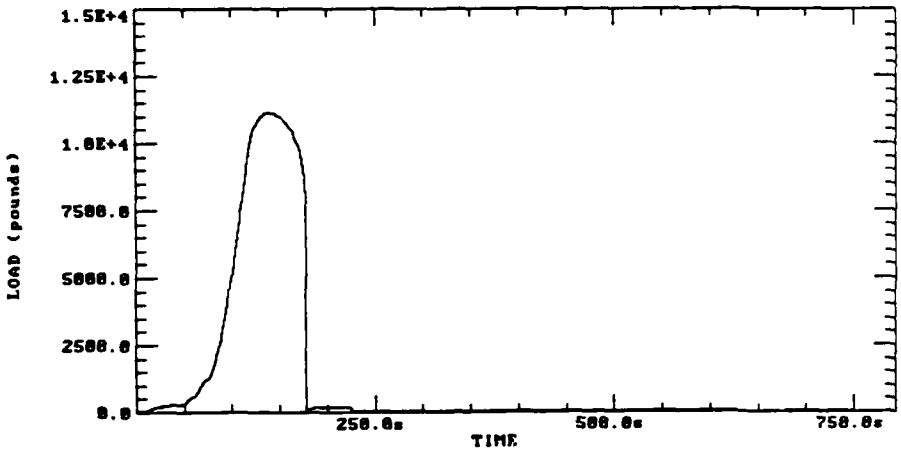

Figure 9 - Load vs. Time Record for Q&T steel Specimen FKS-6, Quasi-Static Rate

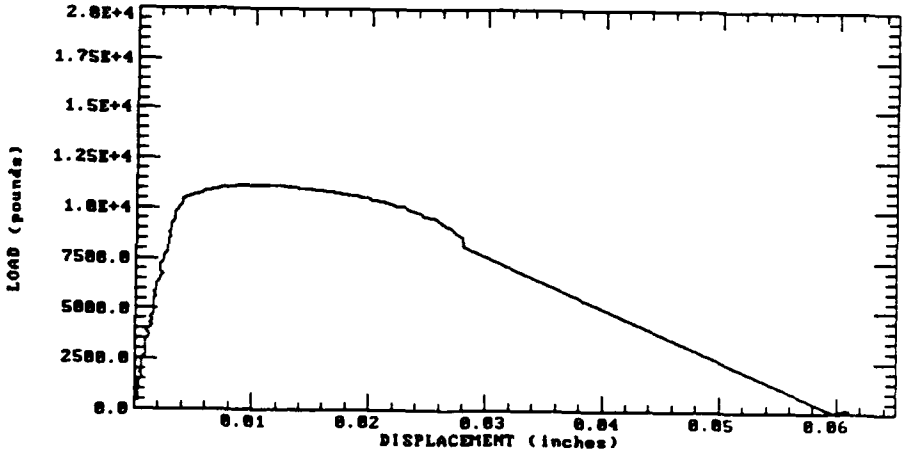

Figure 10 - Load vs. Displacement Record for Q&T Steel Specimen FKS-6, Quasi-Static Rate

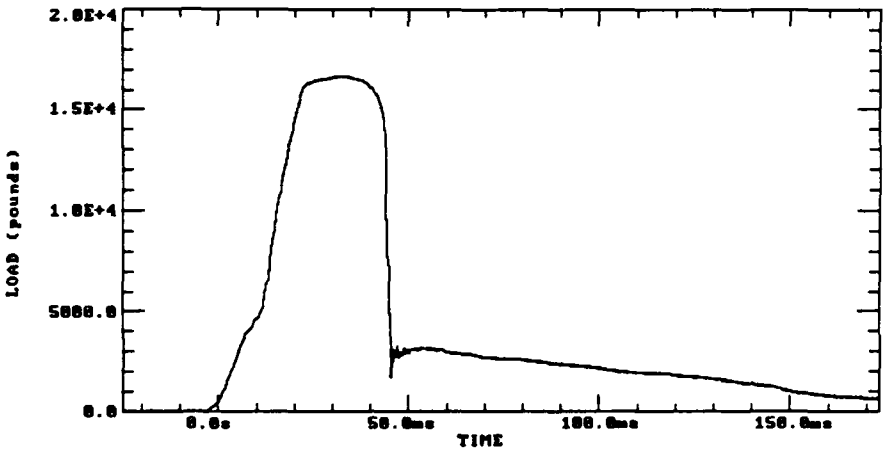

Figure 11 - Load vs. Time Record for DQ Steel Specimen GOA-10, Dynamic Rate

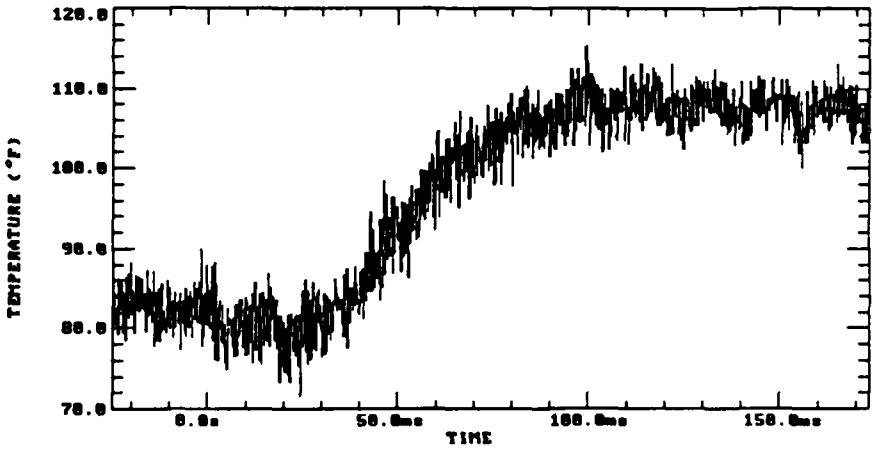

Figure 12 - Temperature vs. Time Recorded at Inner Thermocouple Location for DQ Steel Specimen GOA-10, Dynamic Rate

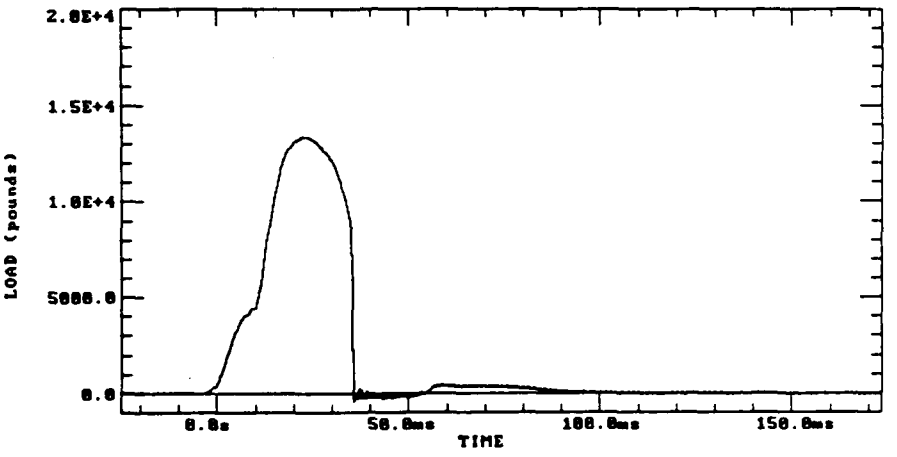

Figure 13 - Load vs. Time Record for Q&T Steel Specimen FKS-4, Dynamic Rate

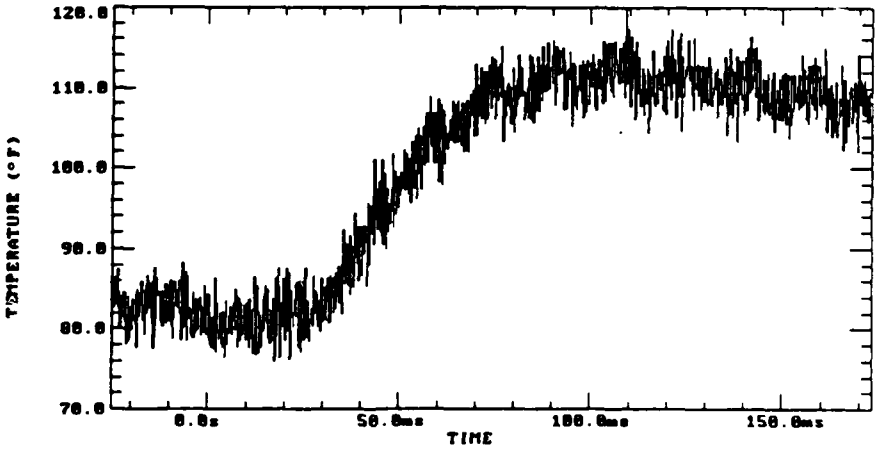

Figure 14 - Temperature vs. Time Recorded at Inner Thermocouple Location for Q&T Steel Specimen FKS-4, Dynamic Rate

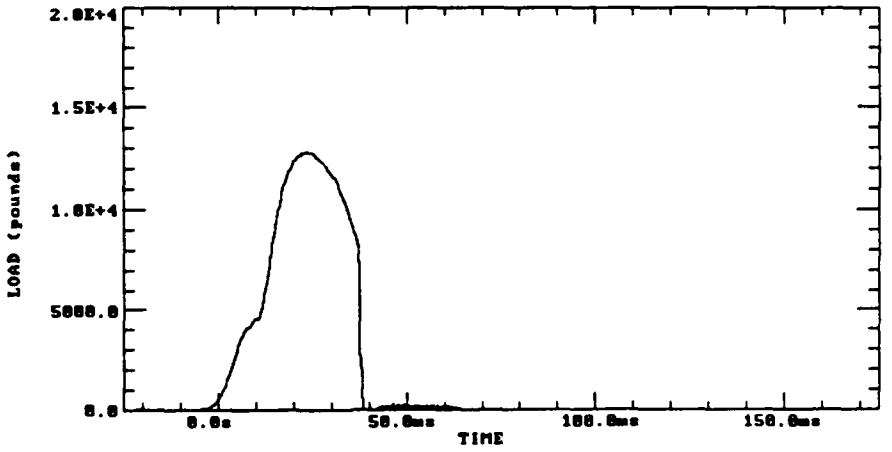

Figure 15 - Load vs. Time Record for Q&T Steel Specimen FKS-8, Dynamic Rate

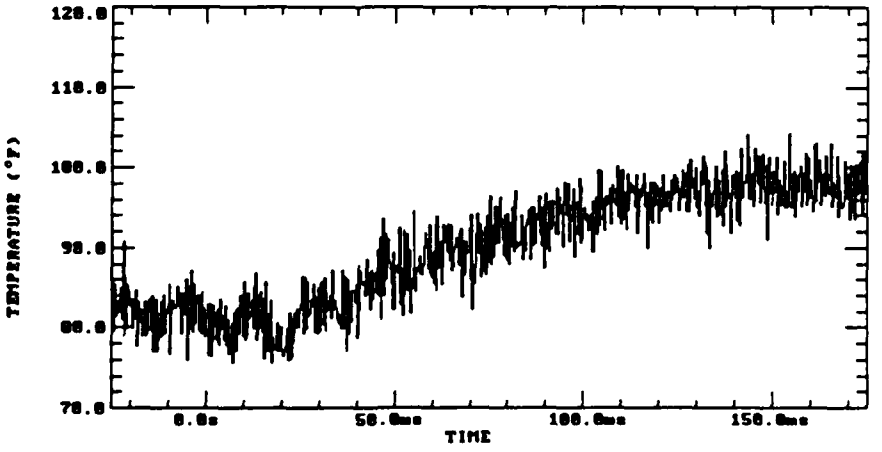

Figure 16 - Temperature vs. Time Recorded at Inner Thermocouple Location for Q&T Steel Specimen FKS-8, Dynamic Rate

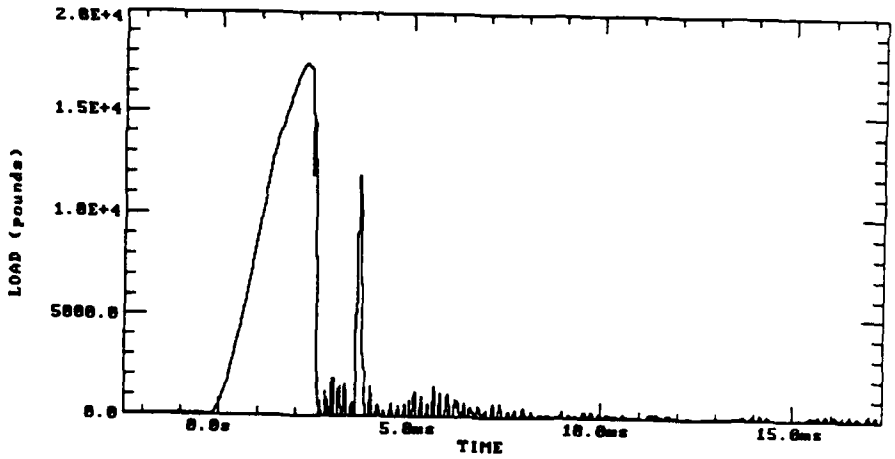

Figure 17 - Load vs. Time Record for DQ Steel Specimen GOA-7, Impact Rate

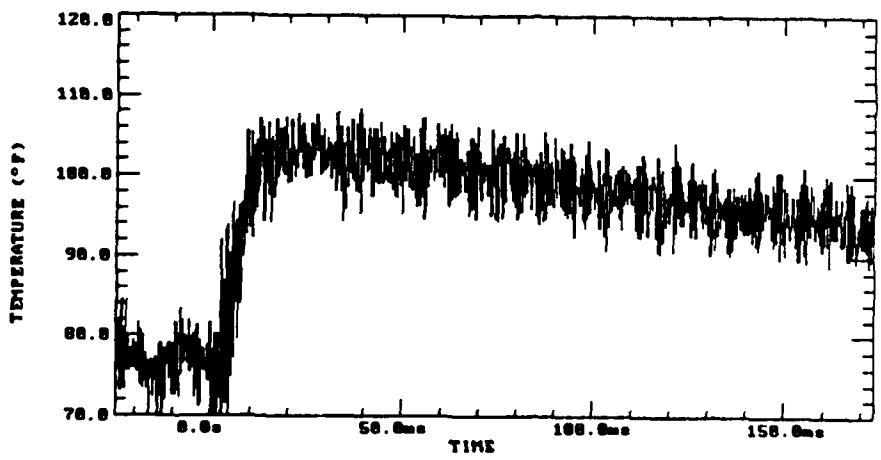

Figure 18 - Temperature vs. Time Recorded at Inner Thermocouple Location for DQ Steel Specimen GOA-7, Impact Rate

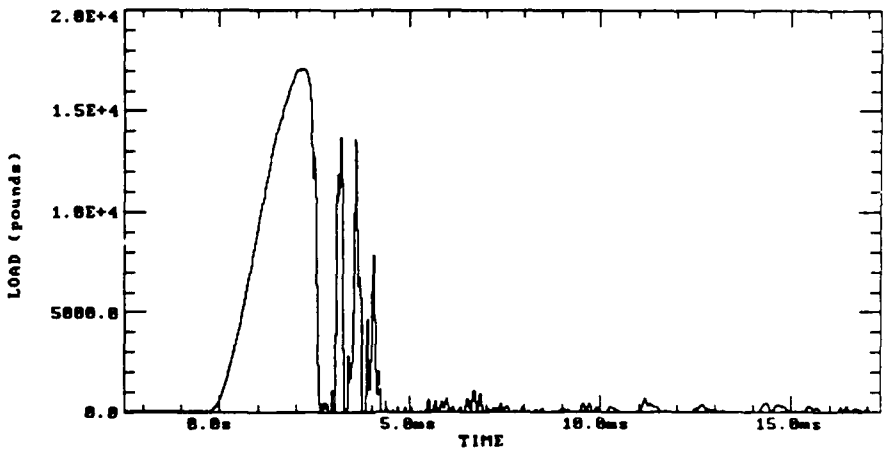

Figure 19 - Load vs. Time Record for DQ Steel Specimen GOA-8, Impact Rate

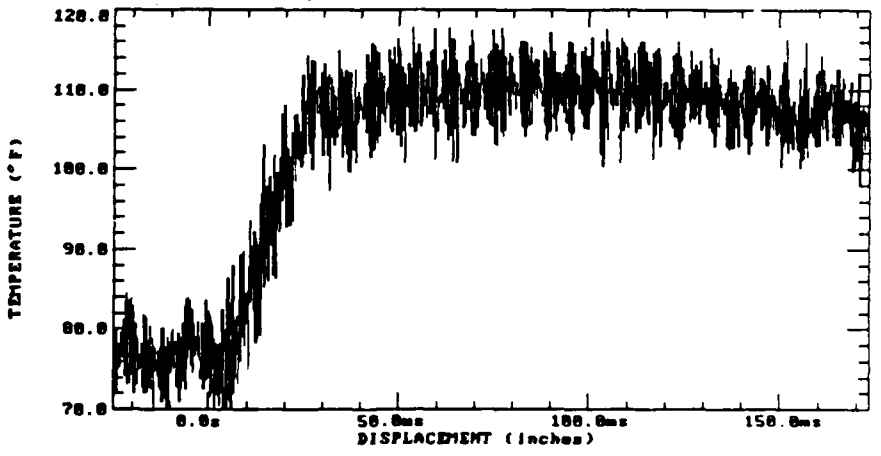

Figure 20 - Temperature vs. Time Recorded at Inner Thermocouple Location for DQ Steel Specimen GOA-8, Impact Rate

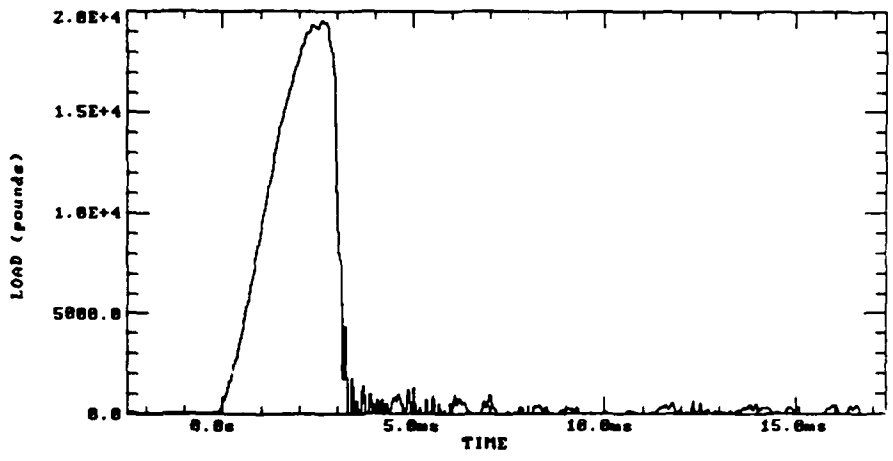

Figure 21 - Load vs. Time Record for DQ Steel Specimen GOA-9, Impact Rate

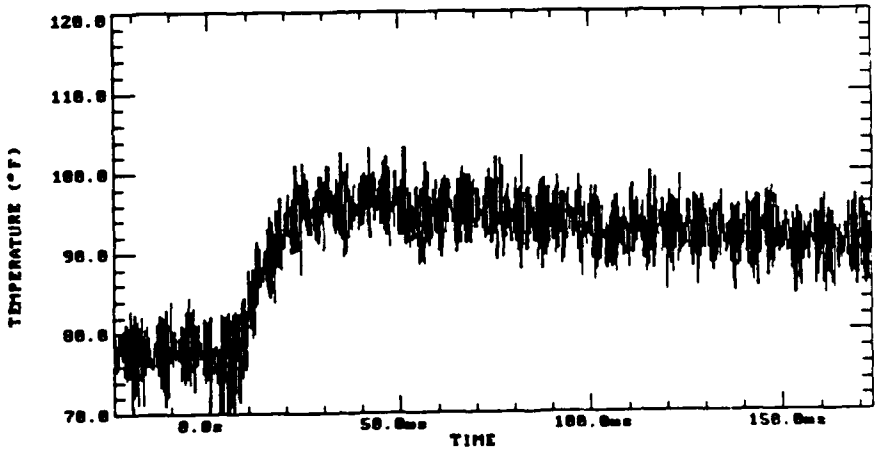

Figure 22 - Temperature vs. Time Recorded at Inner Thermocouple Location for DQ Steel Specimen GOA-9, Impact Rate

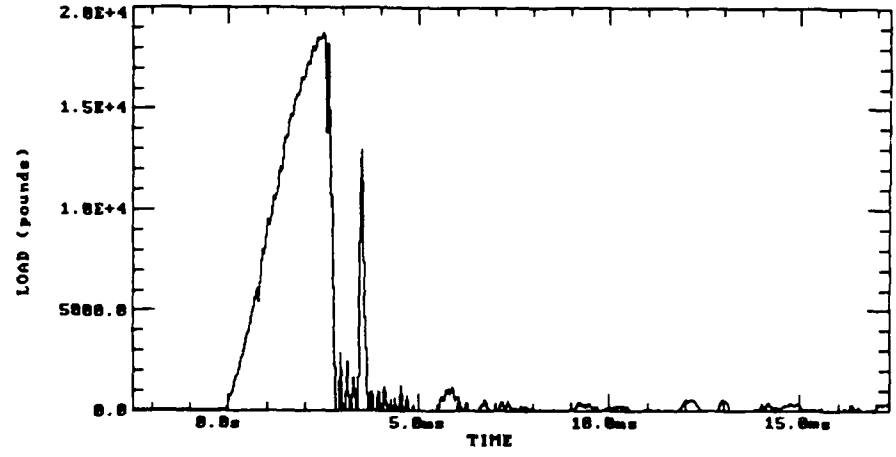

Figure 23 - Load vs. Time Record for Q&T Steel Specimen FKS-5, Impact Rate

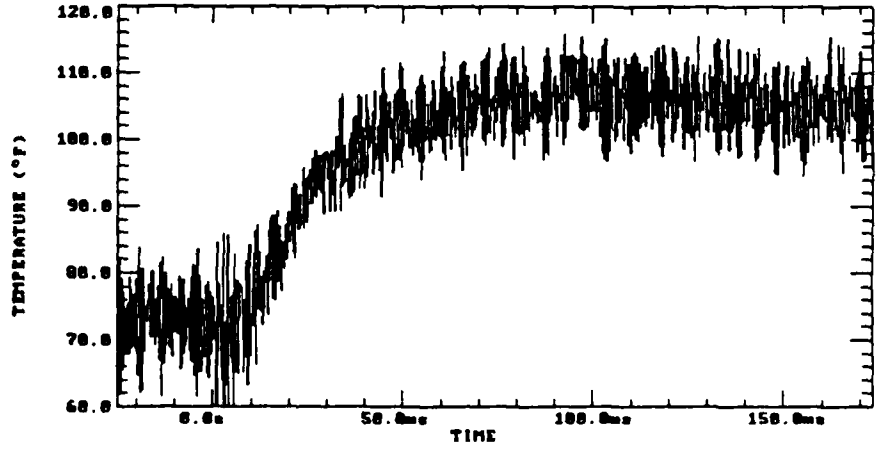

Figure 24 - Temperature vs. Time Recorded at Inner Thermocouple Location for Q&T Steel Specimen FKS-5, Impact Rate

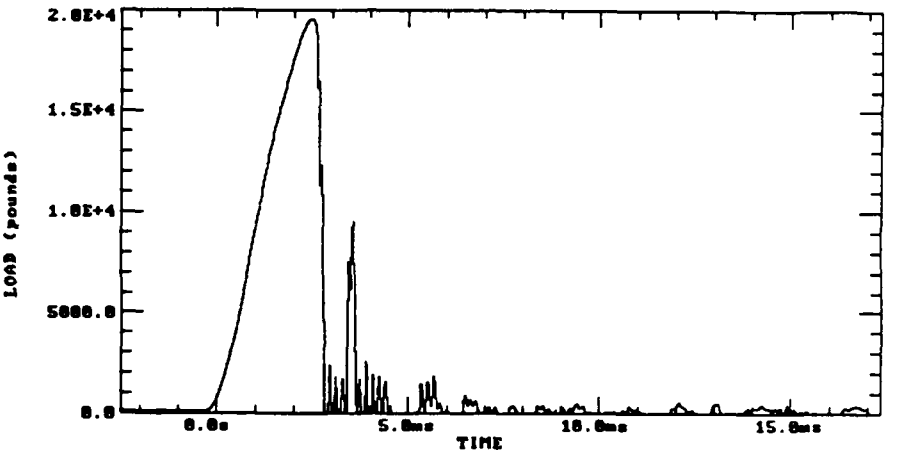

Figure 25 - Load vs. Time Record for Q&T Steel Specimen FKS-2, Impact Rate

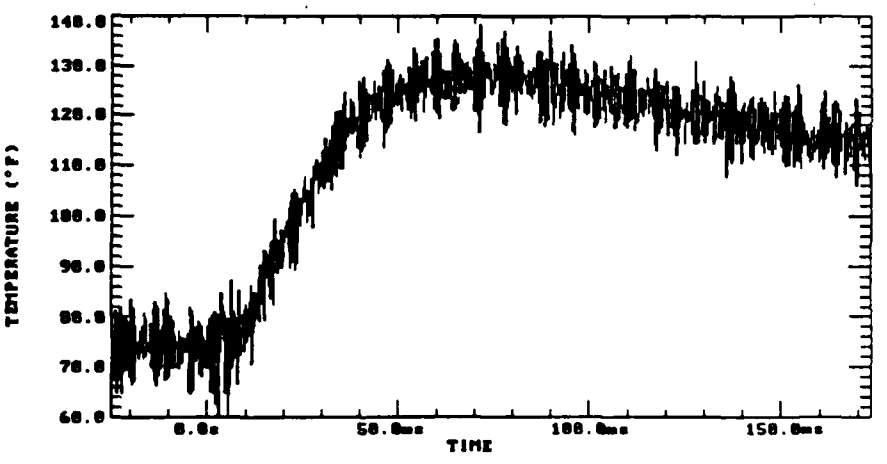

Figure 26 - Temperature vs. Time Recorded at Inner Thermocouple Location for Q&T Steel Specimen FKS-2, Impact Rate

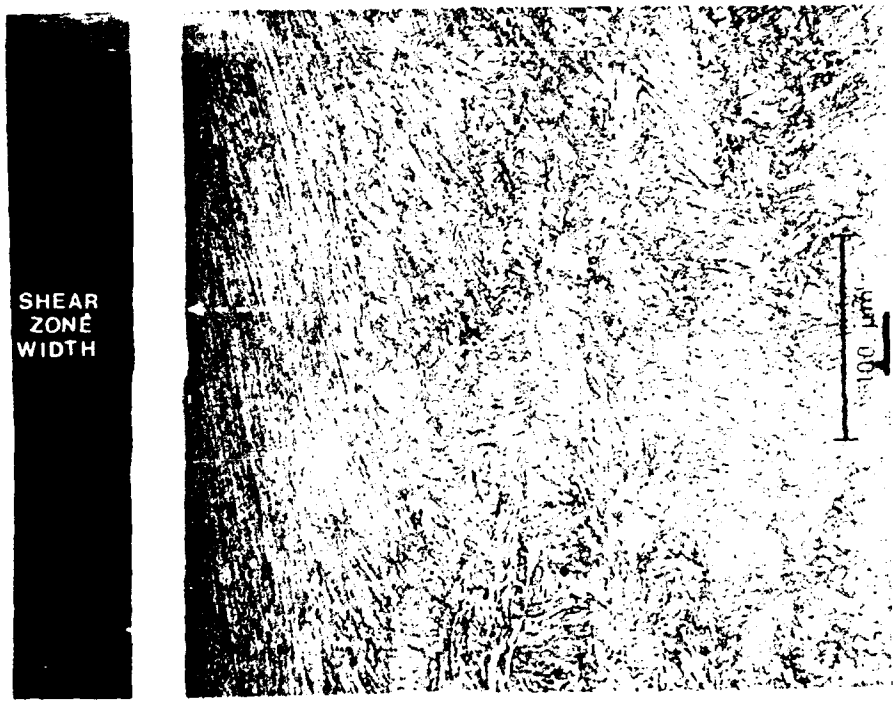

Figure 27 - Fracture Surface Profile of DQ Steel Specimen GOA-9, Showing Shear Zone Adjacent to Fracture Surface

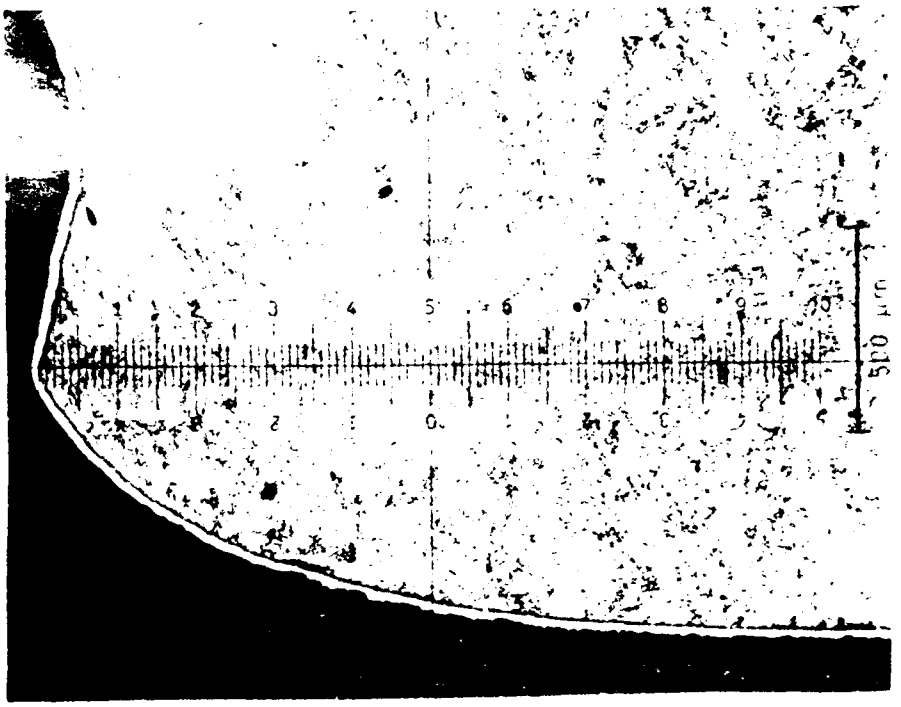

Figure 28 - Bending Deformation in Central Section of DQ Steel Specimen GOA-11 (Quasi-Static, Side A)

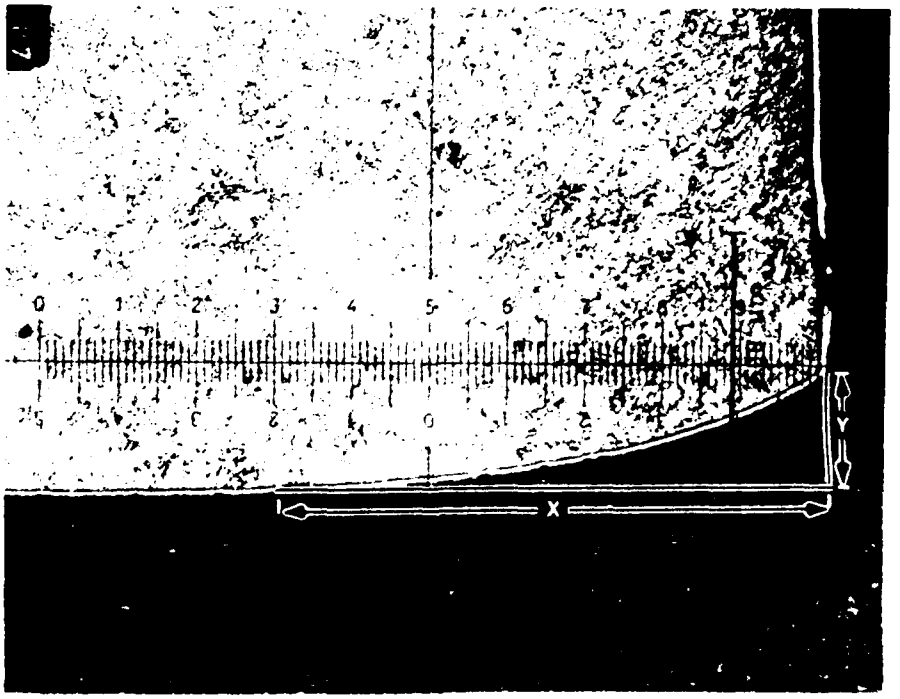

Figure 29 - Bending Deformation in Central Section of Q&T Steel Specimen FES-6 (Quasi-Static, Side A)

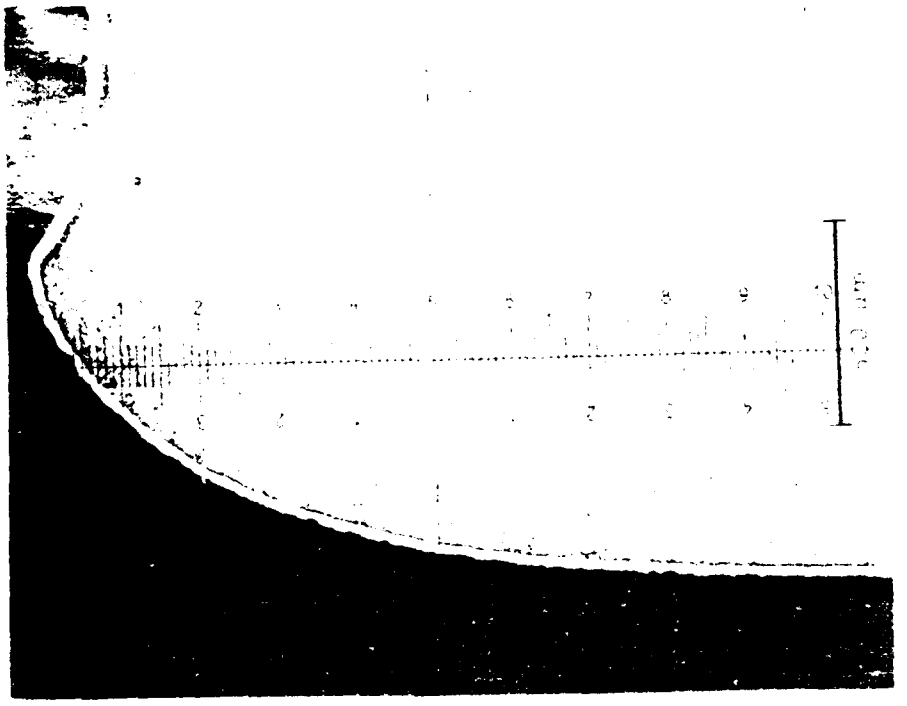

Figure 30 - Bending Deformation in Central Section of DQ Steel Specimen GOA-10 (Dynamic, Side A)

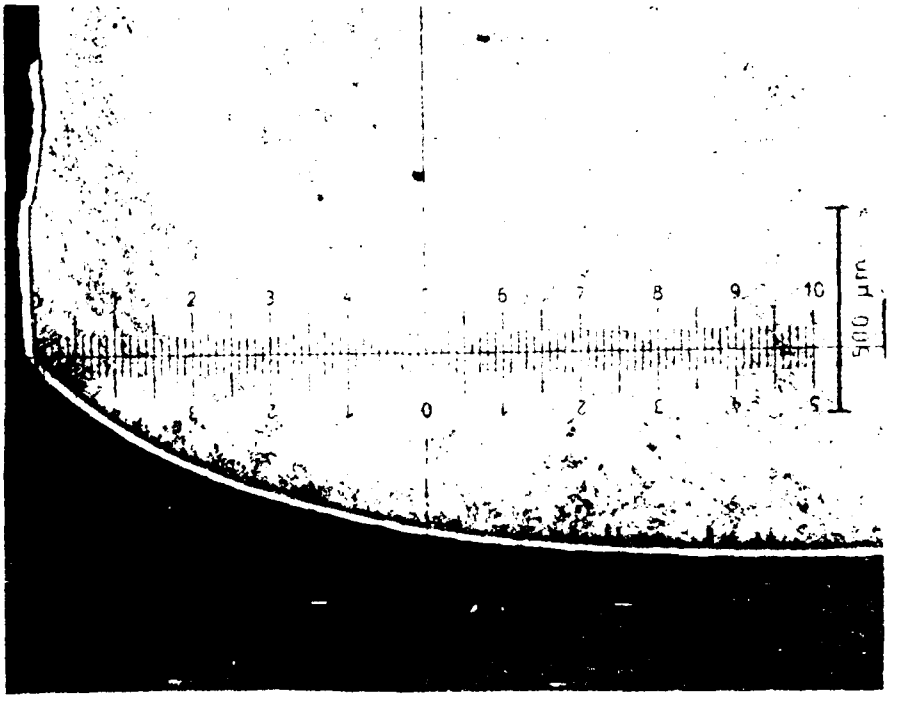

Bending Deformation in Central Section of DQ Steel Specimen GOA-11 (Dynamic, Side A)

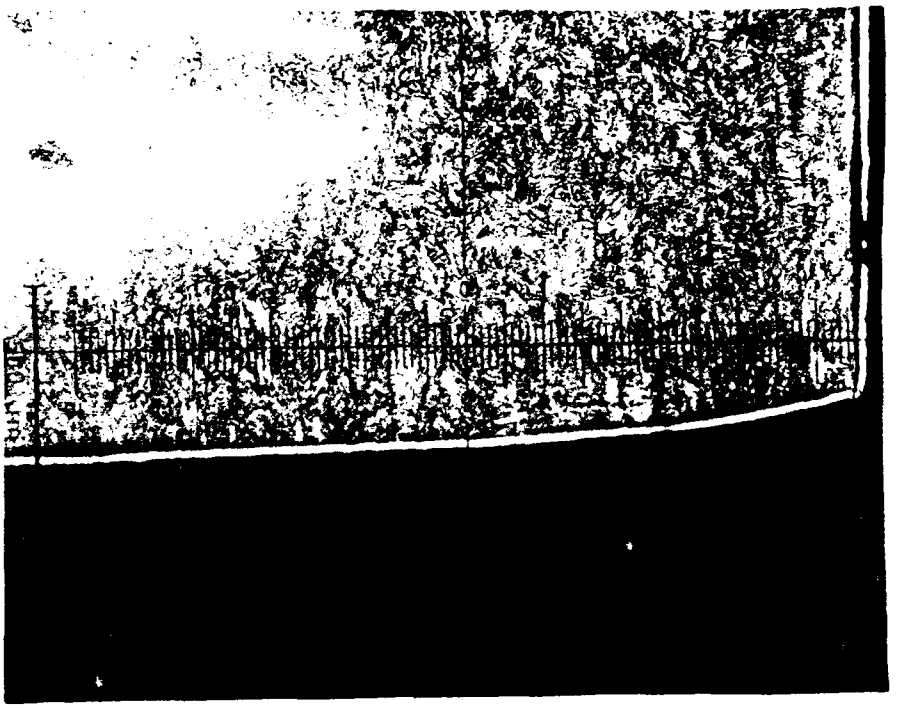

Figure 32 - Bending Deformation in Central Section of DQ Steel Specimen GOA-8 (Impact, Side A)

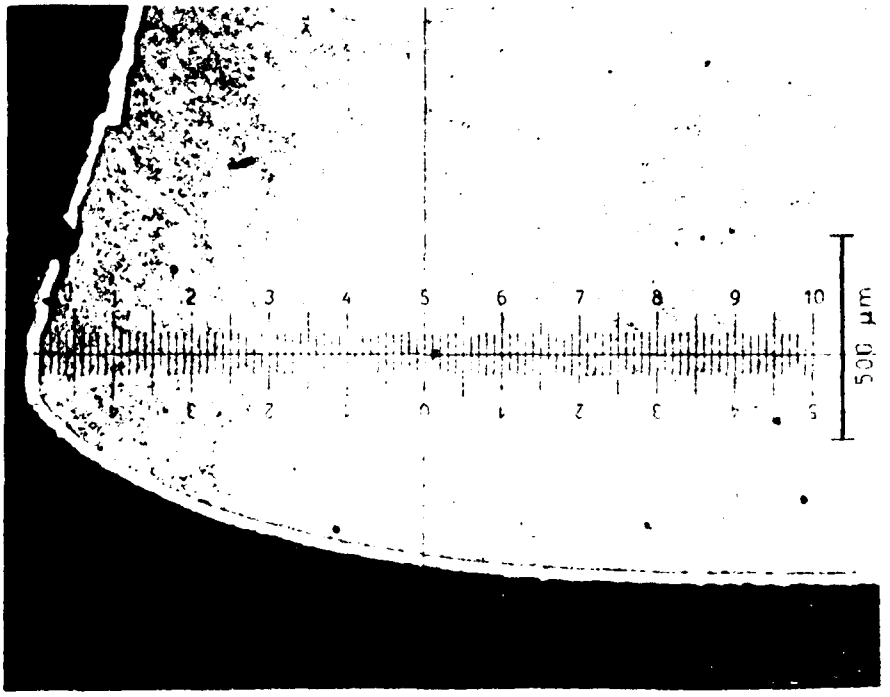

Figure 33 - Bending Deformation in Central Section of Q&T Steel Specimen FKS-2 (Impact, Side A)

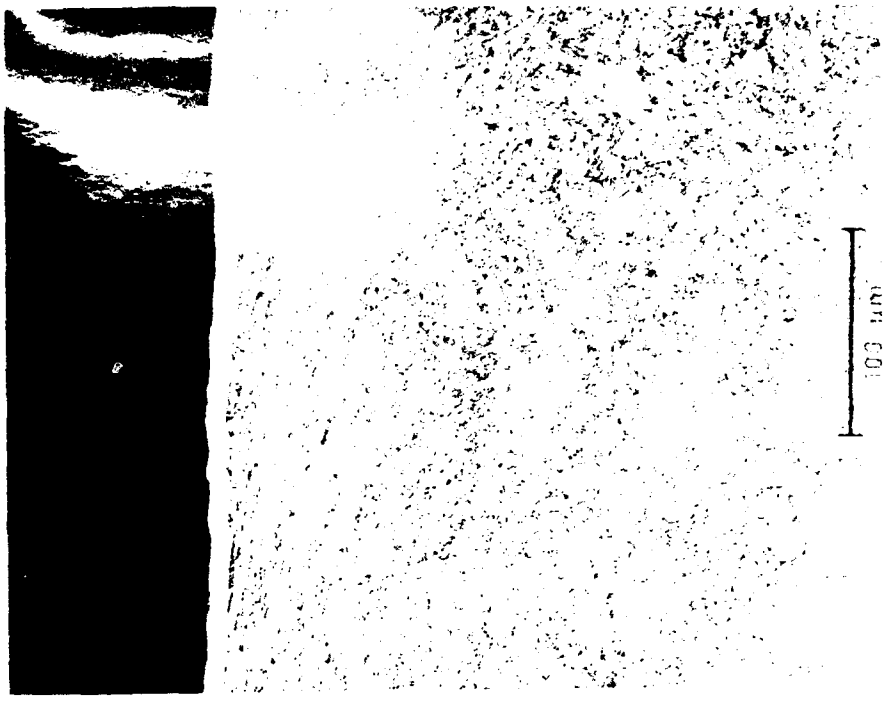

Figure 34 - Fracture Surface Profile of Q&T Steel Specimen FKS-2 (Impact), Showing Shear Zone Adjacent to Fracture Surface

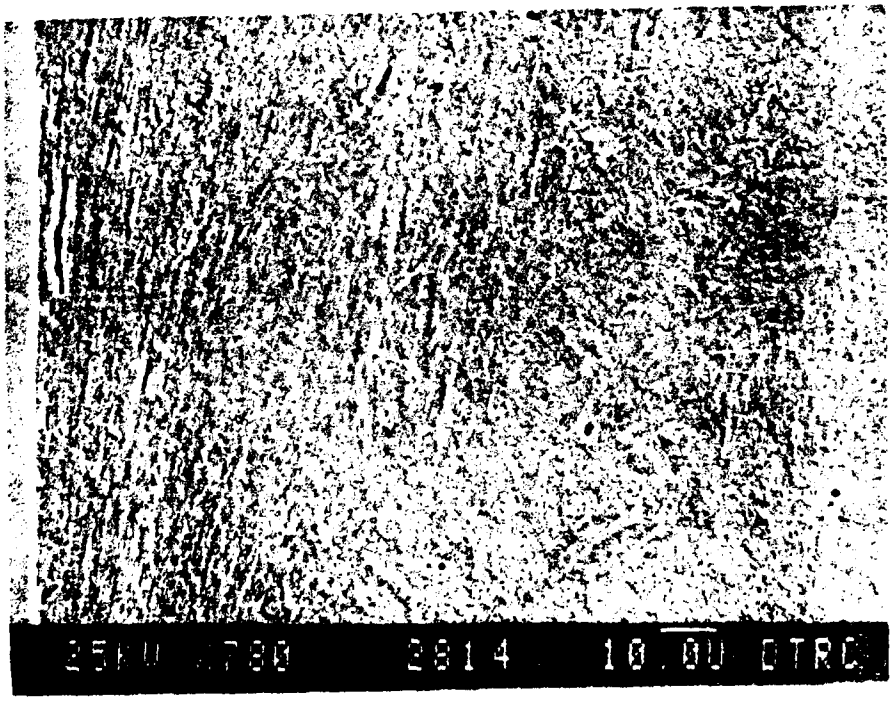

Figure 35 - SEM Micrograph of Fracture Profile of Q&T Steel Specimen FKS-2 (Impact), Showing Microvoids Below the Fracture Surface

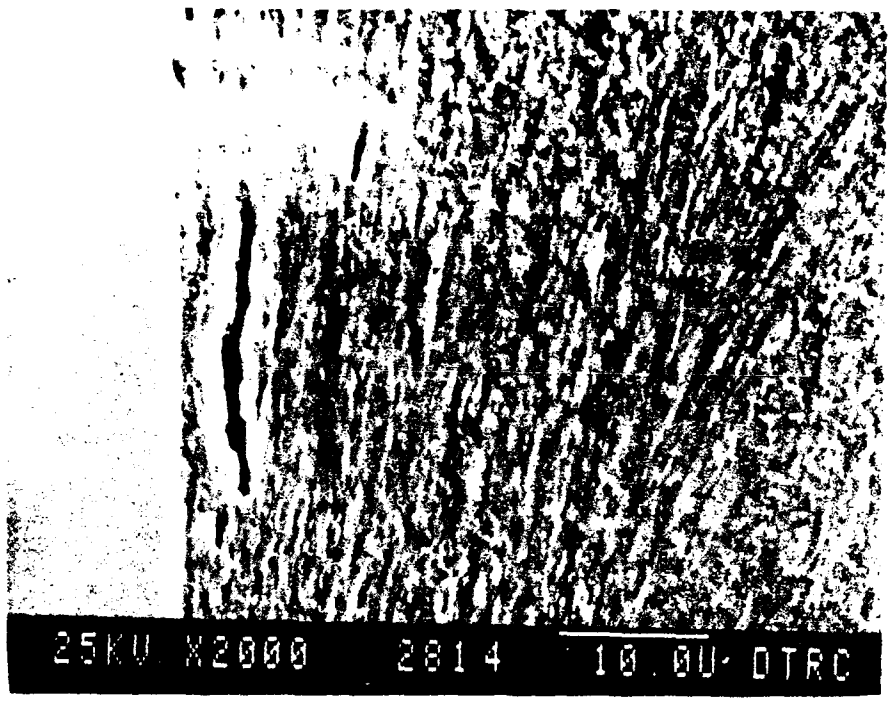

Figure 36 - SEM Micrograph of Fracture Profile of Q&T Steel Specimen FKS-2 (Impact), Showing Enlargement of Microvoid Region in Figure 35.

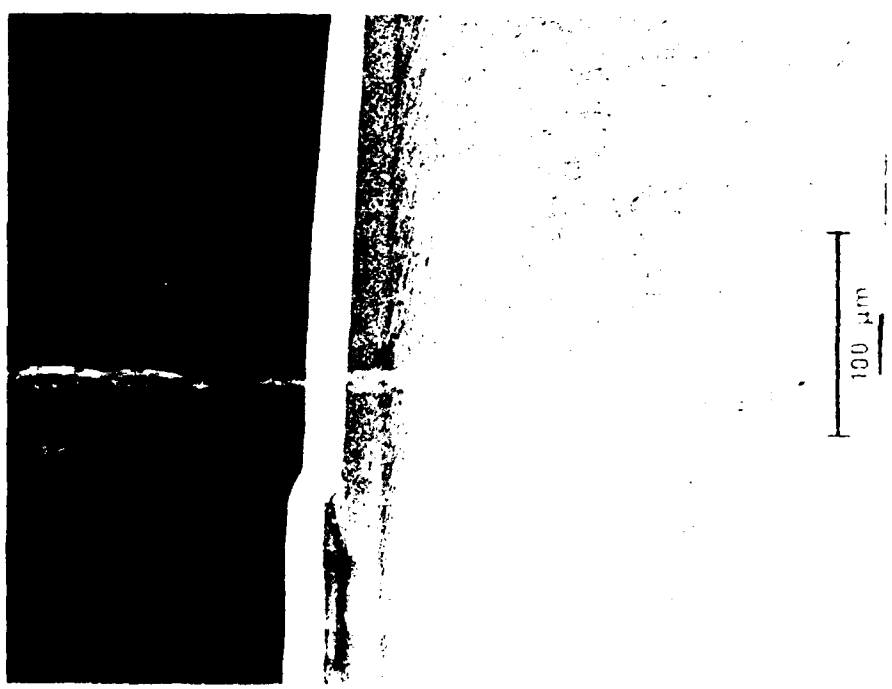

Figure 37 - Fracture Surface Profile of DQ Steel Specimen "A-2" (Impact), Showing Dark Etching Zone Adjacent to the Fracture Surface.

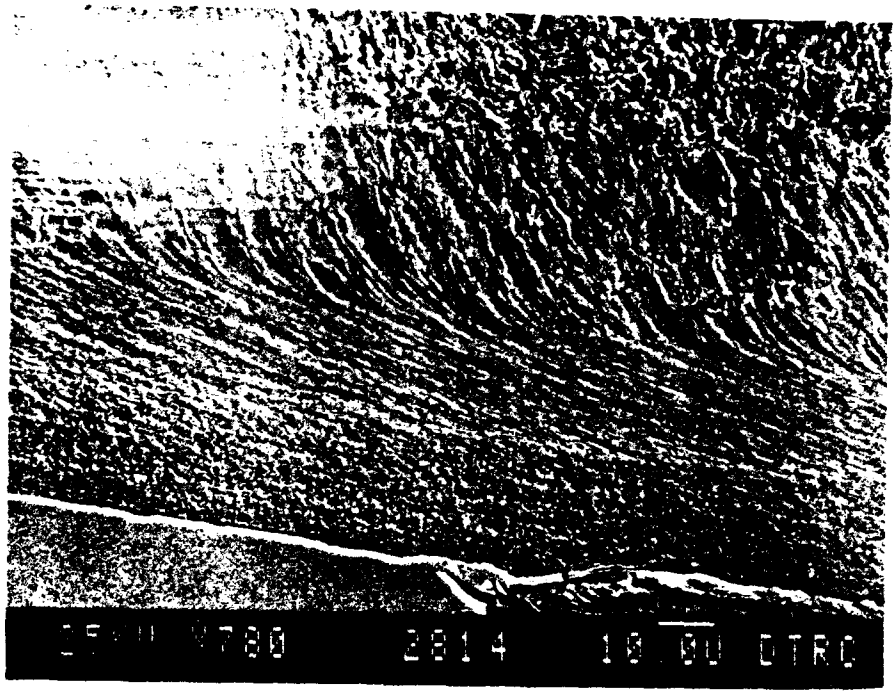

Figure 38 - SEM Micrograph of Fracture Profile of DQ Steel Specimen GOA-8 (Impact), Showing Microvoids Adjacent to the Fracture Surface and Deformed Shear Zone

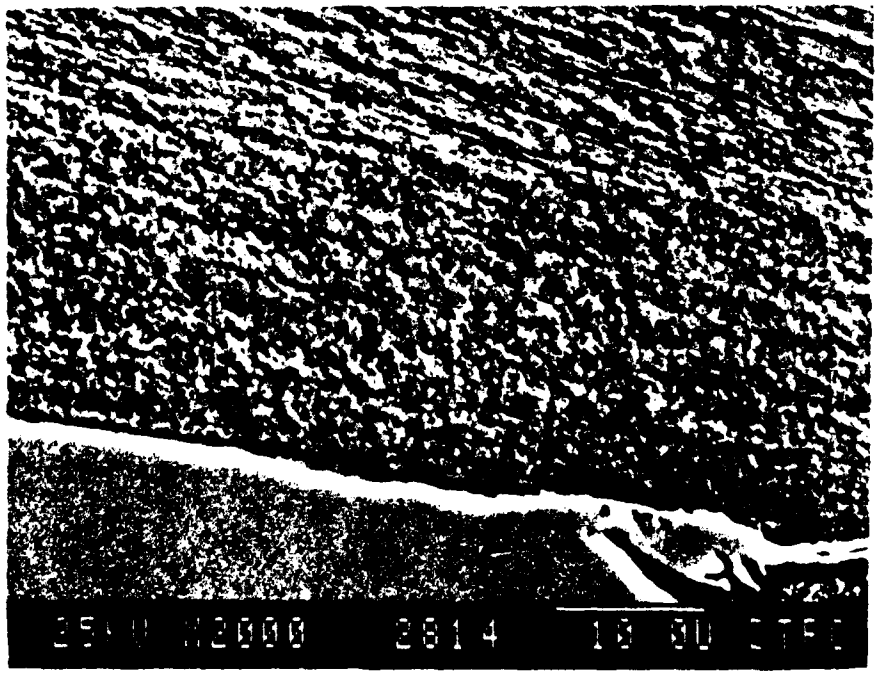

Figure 39 - Fracture Surface Profile of DQ Steel Specimen GOA-8 (Impact), Showing Enlargement of Microvoid Region From Figure 38.

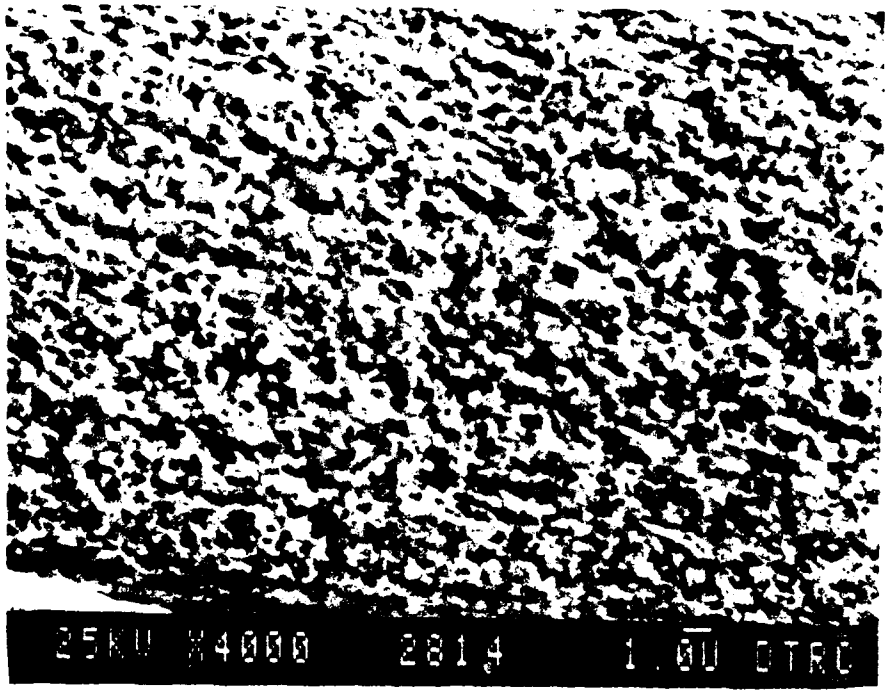

Figure 40 - Fracture Surface Profile of DQ Steel Specimen C[illegible]-8 (Impact), Showing Further Enlargement of Microvoid Regi[illegible] from Figures 37 and 38.

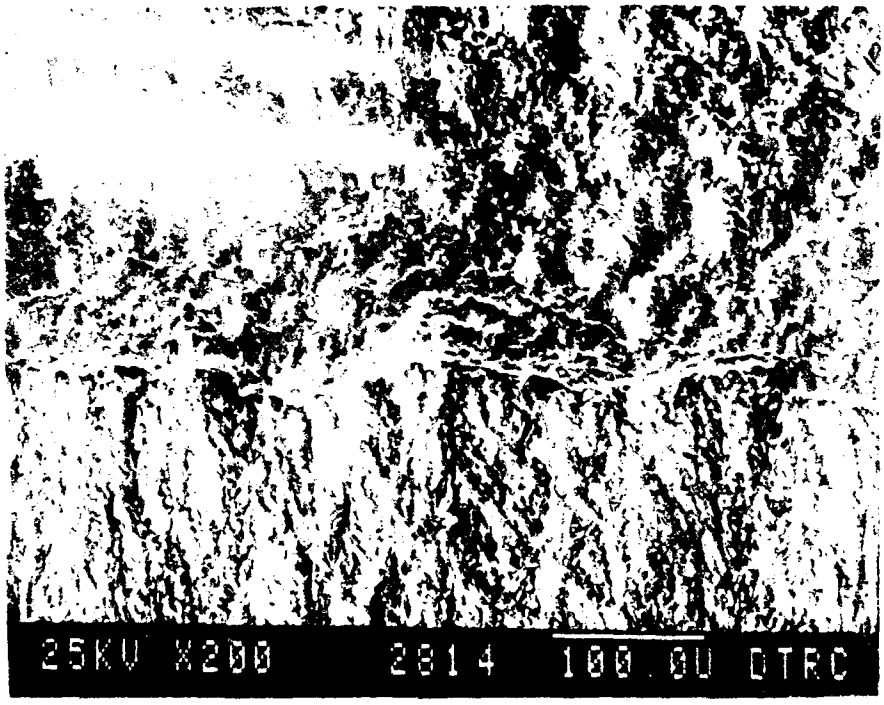

Figure 41 - SEM Fractograph of DQ Steel Specimen GOA-11 (Quasi-Static) Showing Fatigue Precrack/Shear Fracture Interface

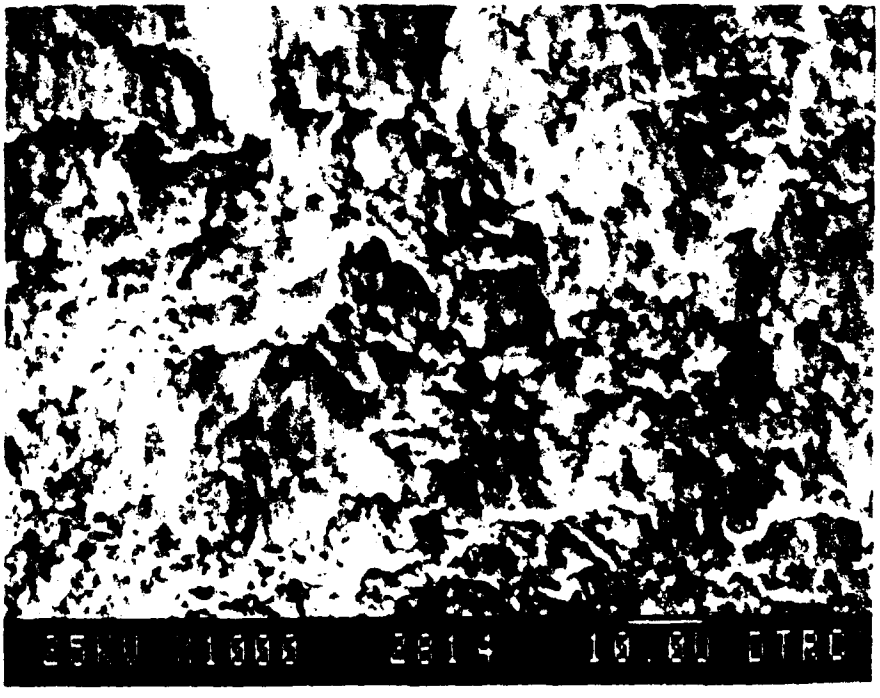

Figure 42 - SEM Fractograph of DQ Steel Specimen GOA-11 (Quasi-Static) Showing Shear Fracture Region Immediately Ahead of Fatigue Precrack

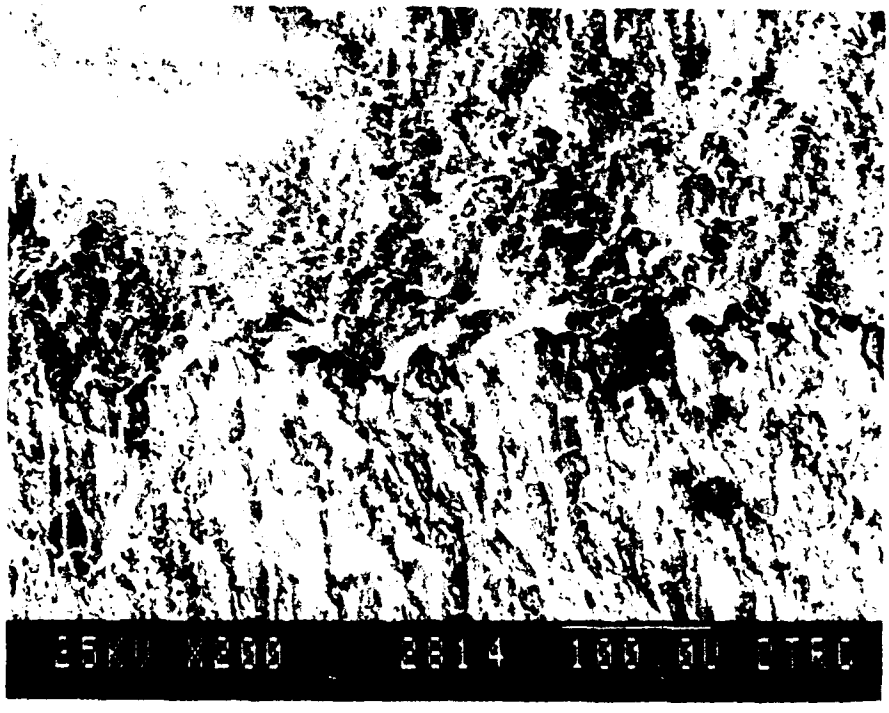

Figure 43 - SEM Fractograph of Q&T Steel Specimen FKS-6 (Quasi-Static) Showing Fatigue Precrack/Shear Fracture Interface

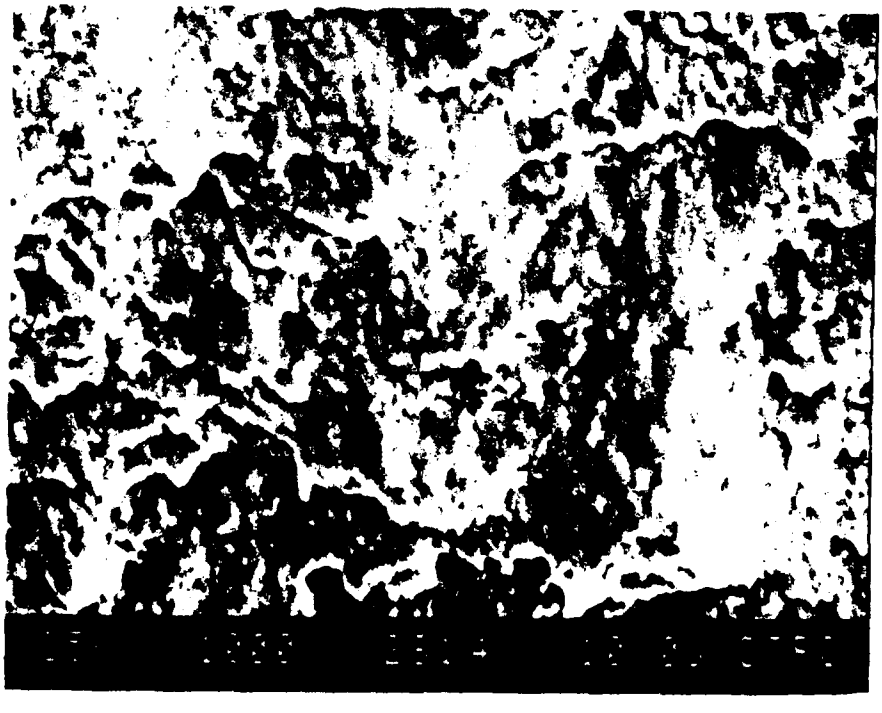

Figure 44 - SEM Fractograph of Q&T Steel Specimen FFS-6 (Quasi-Static) Showing Shear Fracture Region Immediately Ahead of the Precrack

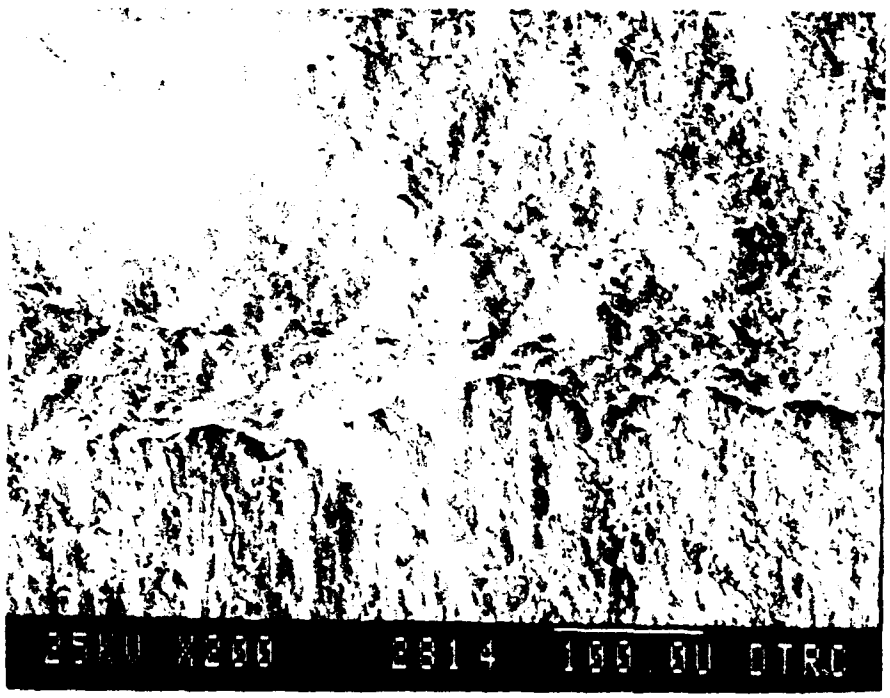

Figure 45 - SEM Fractograph of DQ Steel Specimen 60A-10 (Dynamic) Showing Fatigue Precrack/Shear Fracture Interface

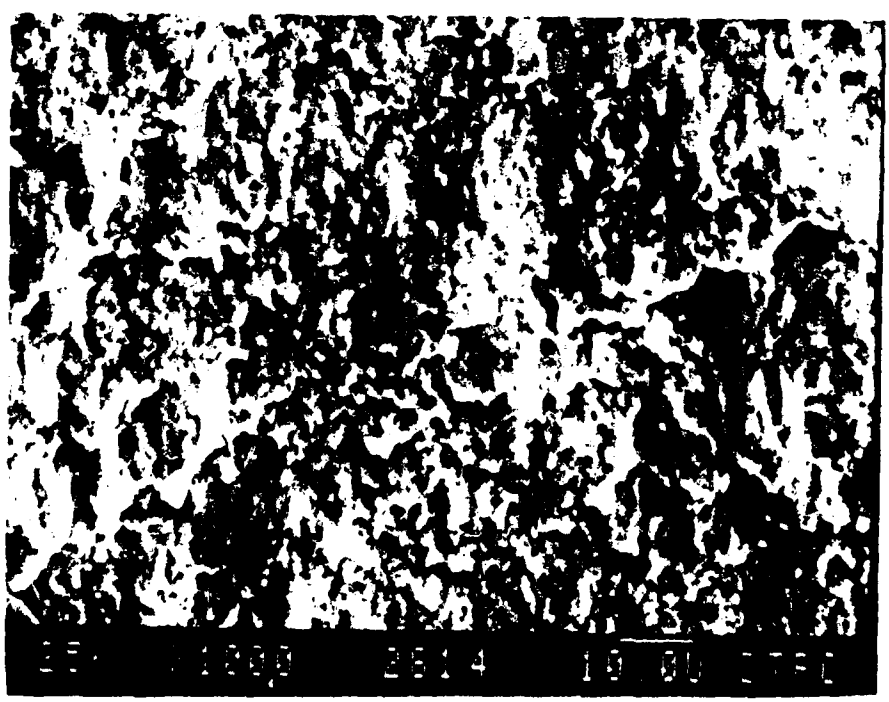

Figure 46 - SEM Fractograph of DQ Steel Specimen 60A-10 (Dynamic), Showing Shear Fracture Region Immediately Ahead of the Precrack

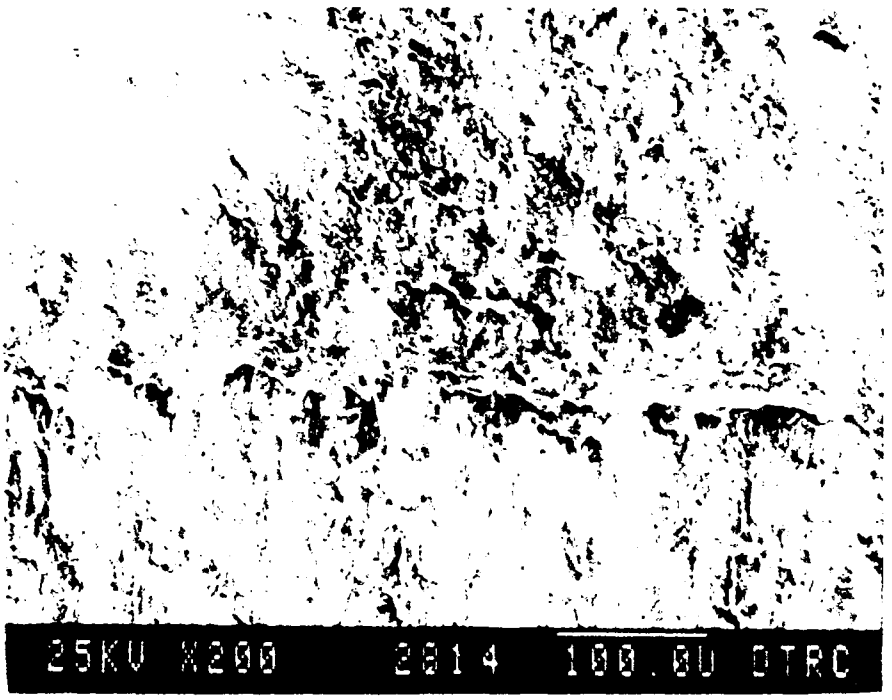

Figure 47 - SEM Fractograph of Q&T Steel Specimen FKS-4 (Dynamic), Showing Fatigue Precrack, Shear Fracture Interface

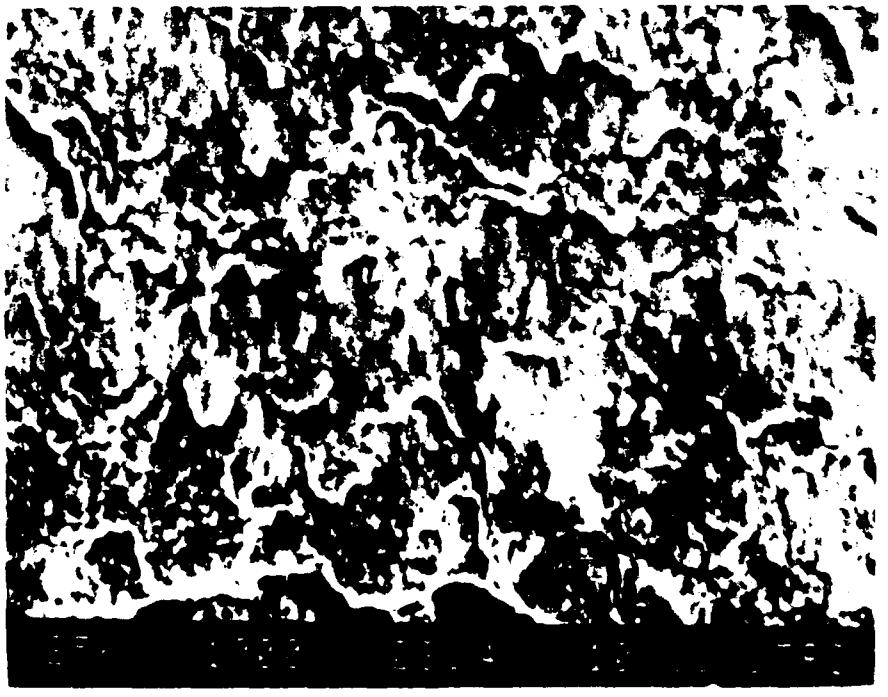

Figure 48 - SEM Fractograph of Q&T Steel Specimen FKS-4 (Dynamic), Showing Shear Fracture Region Immediately Ahead of the Precrack

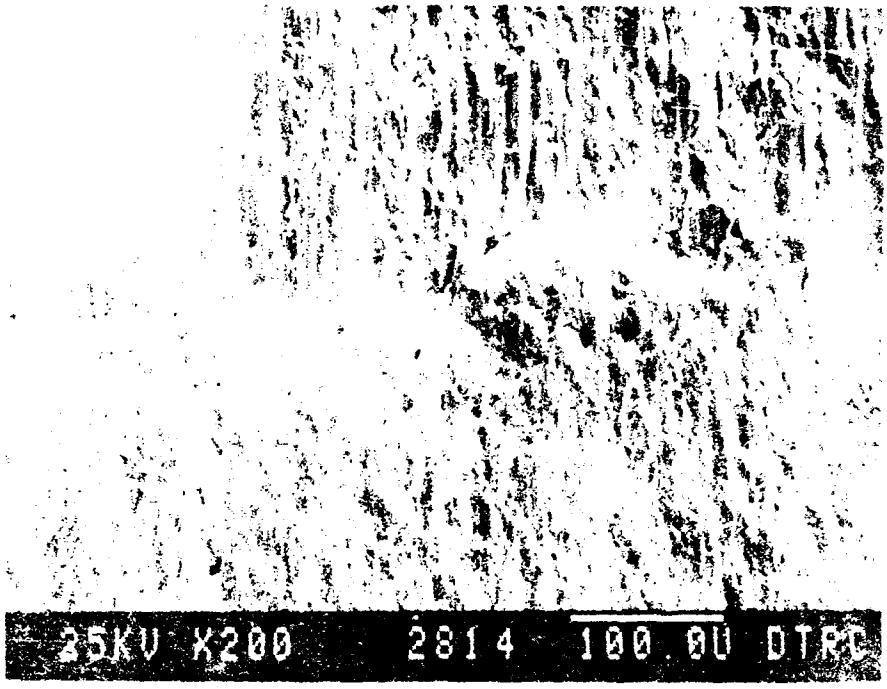
25KV X200 2814 100.0U DTRC

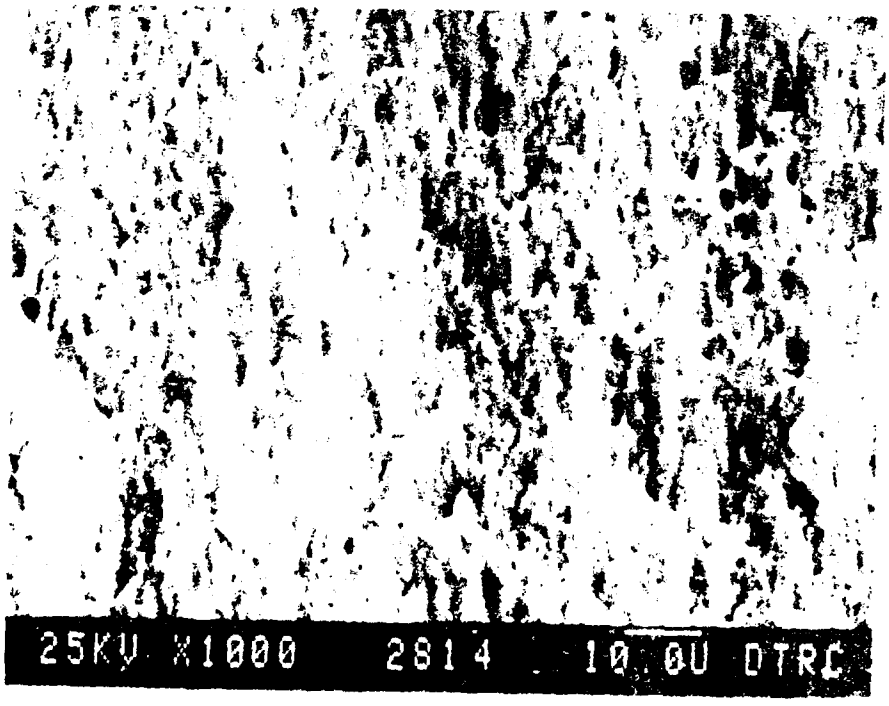
25KV X1000 2814 10.0U DTRC

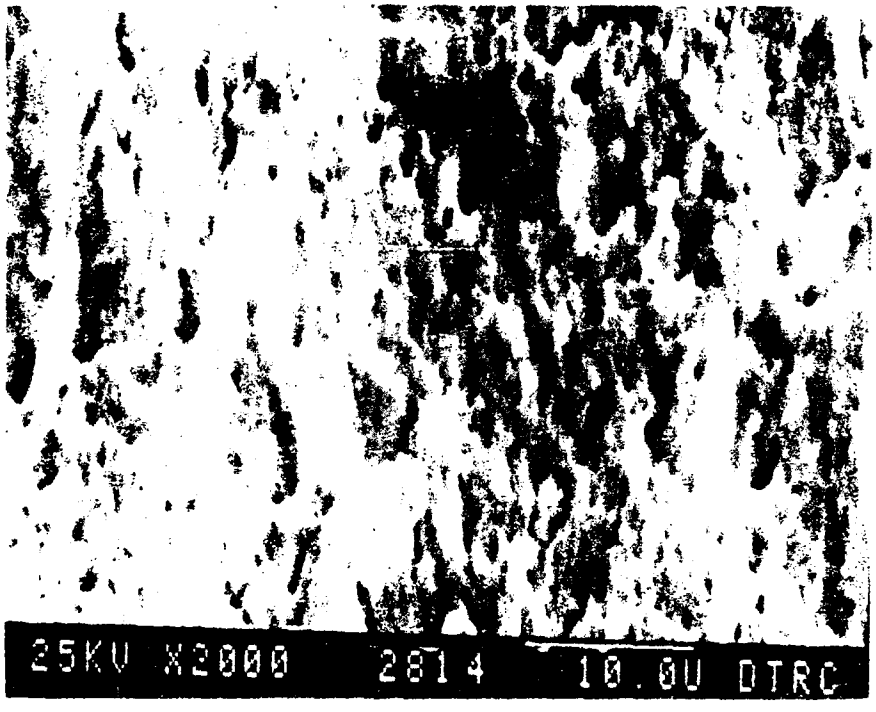

[illegible] SEM Fractographs of D6 Steel Specimens [illegible]
[illegible] Showing Development of Shear Fracture Lips
[illegible] in Figure 4.

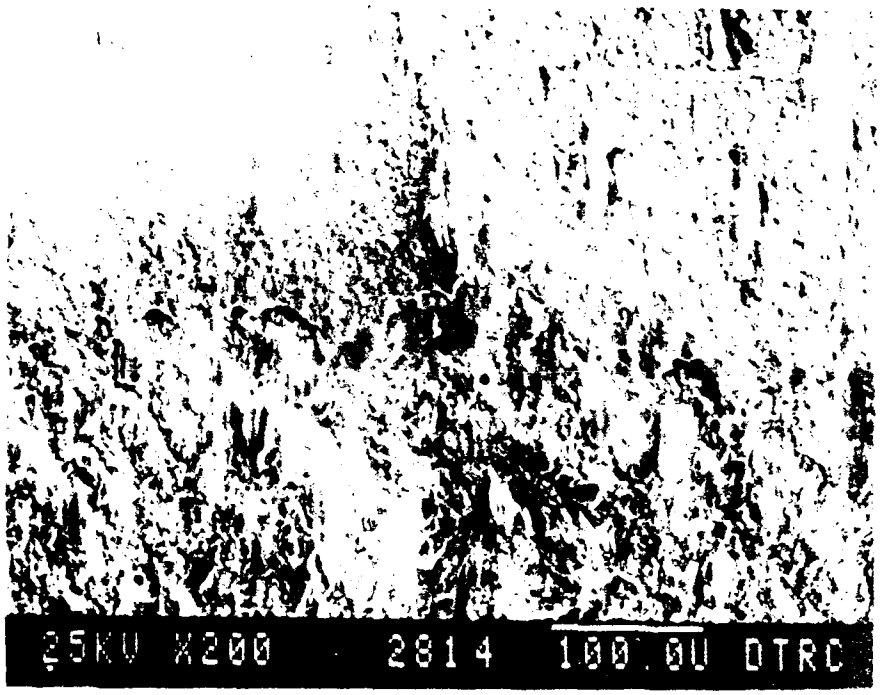

Figure 52 - SEM Fractograph of Q&T Steel Specimen FES-7 (Impact), Showing Fatigue Precrack/Shear Fracture Interface

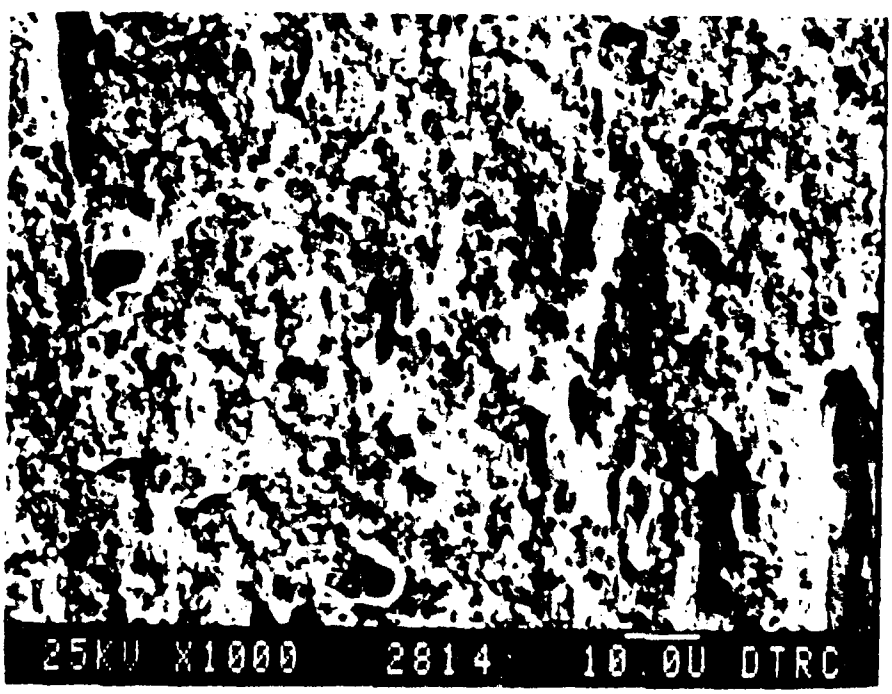

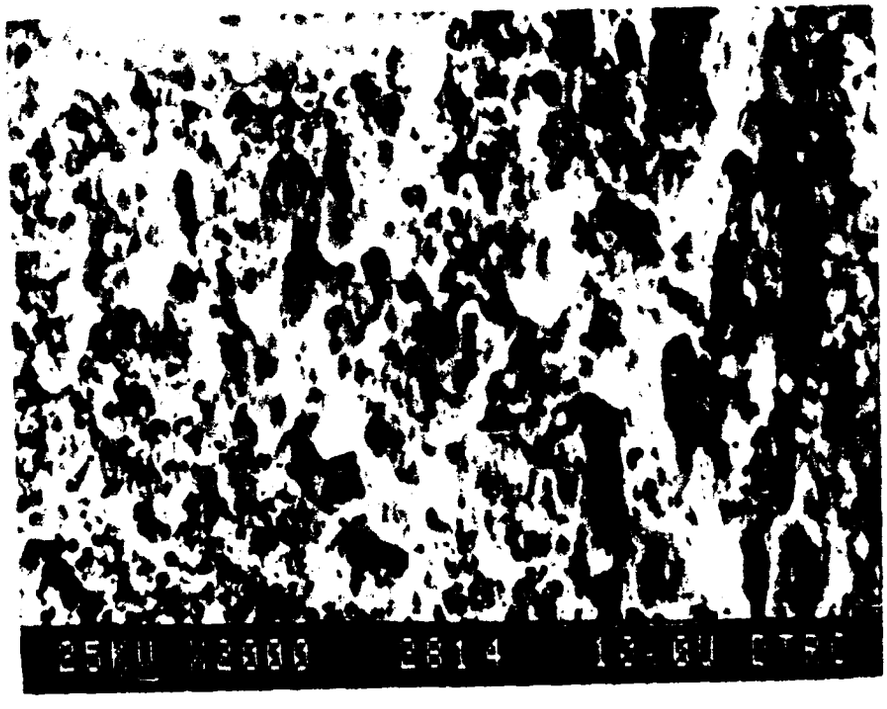

Figure [illegible] - SEM Fractograph of Q&T Steel Specimen FKS-2
Inset [illegible] Showing Enlargement of Shear Fracture Region Shown in
Figure [illegible].

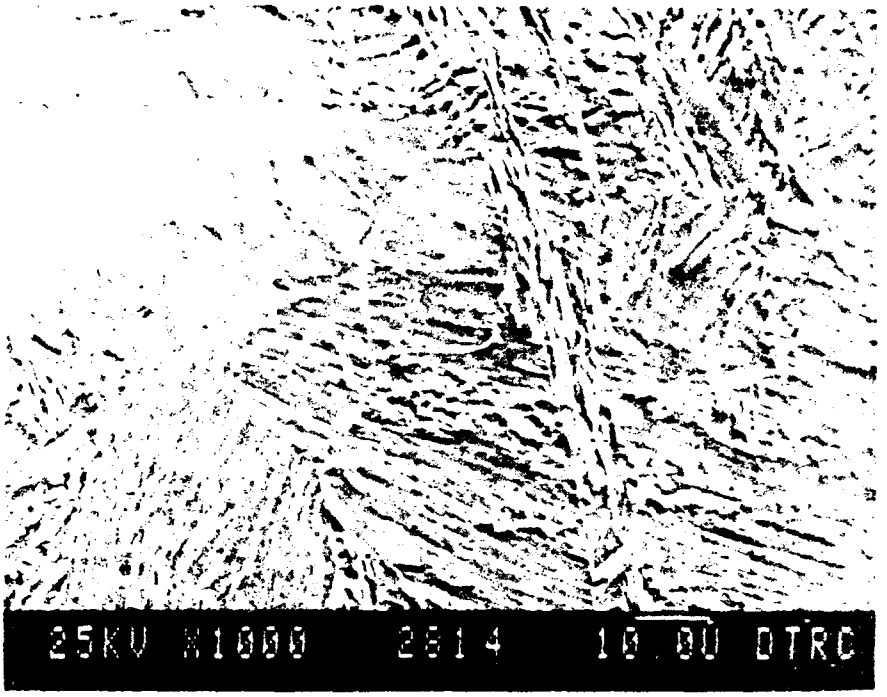

Figure 55 - SEM Micrograph of DQ Steel Microstructure

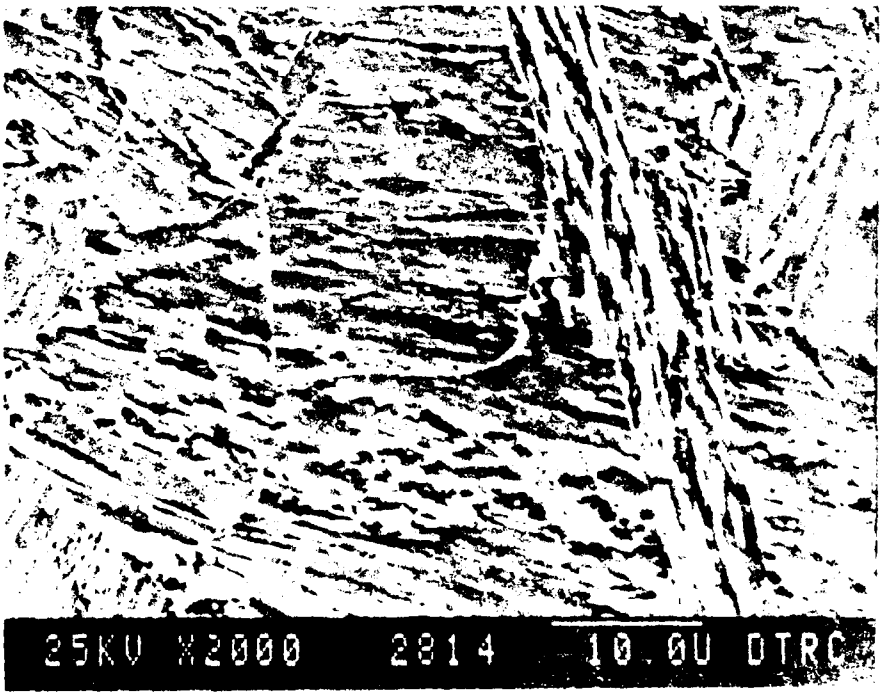

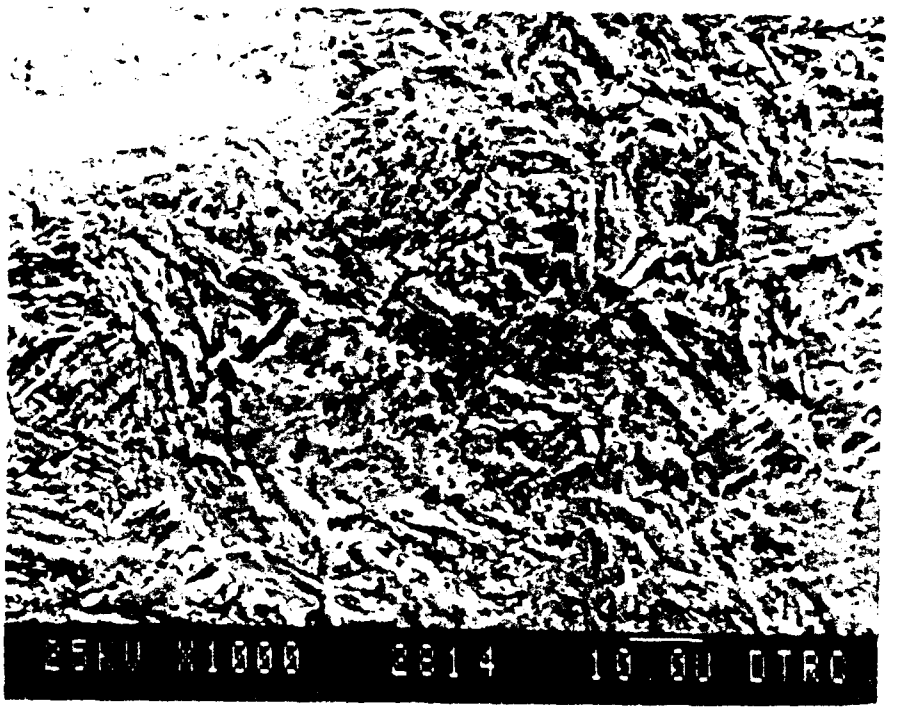

Figure [illegible] - SEM Micrograph of CST Steel Microstructure

Figure [illegible] - SEM Micrograph of CST Steel Microstructure [illegible] of Region Shown in Figure [illegible]

INITIAL DISTRIBUTION

OUTSIDE CENTER

Copies

12	DTIC

CENTER DISTRIBUTION

1	011.5	Caplan
1	28	Wacker
1	2801	Crisci
1	2803	Cavallaro
1	2803	Hardy
1	281	Gudas
4	2814	Montemarano
10	2814	Hackett
1	2814	Kirk
1	2814	R. Link
1	522.1	TIC
1	5231	Office Services